NEW HUMANIZED MOUSE MODEL (DRAGA: HLA-A2. HLA-DR4.RAG1KO.IL2RγCKO.NOD) TO GENERATE AND TEST THERAPEUTIC HUMAN ANTI-FLU MONOCLONAL ANTIBODIES

by

Mirian Irma Mendoza

Dissertation submitted to the Faculty of the

Department of Molecular and Cell Biology Graduate Program of the

Uniformed Services University of the Health Sciences

In partial fulfillment of the requirements for the degree of

Doctor of Philosophy 2017

FINAL EXAMINATION/PRIVATE DEFENSE FOR THE DEGREE OF DOCTOR OF PHILOSOPHY IN THE MOLECULAR AND CELL BIOLOGY GRADUATE PROGRAM

Name of Student: Mirian Irma Mendoza

Date of Examination: Wednesday, December 6, 2017
Time: 3:00 pm
Place: A2011

DECISION OF EXAMINATION COMMITTEE MEMBERS:

	PASS	FAIL
Dr. Gabriela Dveksler DEPARTMENT OF PATHOLOGY Committee Chairperson	✓	
Dr. Teodor-Doru Brumeanu DEPARTMENT OF MEDICINE Dissertation Advisor	✓	
Dr. Andrew Snow DEPARTMENT OF PHARMACOLOGY Committee Member	✓	
Dr. Kathleen Pratt DEPARTMENT OF MEDICINE Committee Member	✓	
Dr. Sofia Casares NMRC Committee Member	✓	
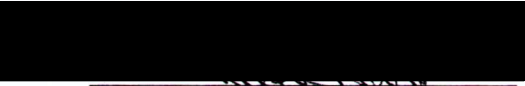
Gregory P. Mueller, Ph.D., Associate Dean || www.usuhs.mil/graded || graduateprogram@usuhs.edu
Toll Free: 800-772-1747 || Commercial: 301-295-3913 / 9474 || DSN: 295-9474 || Fax: 301-295-6772

ii

APPROVAL OF THE DOCTORAL DISSERTATION IN THE MOLECULAR AND CELL BIOLOGY GRADUATE PROGRAM

Title of Dissertation: "New humanized mouse model (DRAGA: HLA-A2.HLA-DR4.Rag1KO.IL2RγcKO.NOD) to generate and test therapeutic human anti-flu monoclonal antibodies"

Name of Candidate: Mirian Irma Mendoza
Doctor of Philosophy
December 6, 2017

DISSERTATION AND ABSTRACT APPROVED:

DATE:

4/1/18

Dr. Gabriela Dveksler
DEPARTMENT OF PATHOLOGY
Committee Chairperson

4/2/18

Dr. Teodor-Doru Brumeanu
DEPARTMENT OF MEDICINE
Dissertation Advisor

4/3/18

Dr. Andrew Snow
DEPARTMENT OF PHARMACOLOGY
Committee Member

4/2/18

Dr. Kathleen Pratt
DEPARTMENT OF MEDICINE
Committee Member

4/2/18

Dr. Sofia Casares
NMRC
Committee Member

The author hereby certifies that the use of any copyrighted material in the thesis manuscript entitled:

"New humanized mouse model (DRAGA: HLA-A2. HLA-DR4.Rag1KO.IL2RγcKO.NOD) to generate and test therapeutic human anti-flu monoclonal antibodies"

is appropriately acknowledged and, beyond brief excerpts, is with the permission of the copyright owner.

Mirian Irma Mendoza
MOLECULAR CELL BIOLOGY PROGRAM/DEPARTMENT OF MEDICINE
Uniformed Services University
December 6, 2017

ABSTRACT

Title of Dissertation: **"New humanized mouse model (DRAGA: HLA-A2. HLA-DR4.Rag1KO.IL2RγcKO.NOD) to generate and test therapeutic human anti-flu monoclonal antibodies"**

Author: **Mirian Mendoza, Ph.D., 2017**

Uniformed Services University of the Health Sciences,

4301Jones Bridge Rd, Bethesda, MD 20814

Thesis directed by: **Teodor-Doru Brumeanu, M.D., Professor**

Department of Medicine

Uniformed Services University of the Health Sciences

4301 Jones Bridge Rd, Bethesda, MD 20814

ABSTRACT:

Over the past century, four different influenza pandemics have occurred resulting in numerous fatalities around the globe. Given the uncertainties of a new influenza virus, new preventive measurements and treatments need to be developed. Antibody-based therapy has been effectively used before to treat infectious diseases, including respiratory syncytial virus infection. Neutralizing antibodies play an important role in protection from influenza virus infection by recognizing its major surface glycoprotein: hemagglutinin (HA). The recently developed DRAGA (HLA-DR4.RagKO.IL2RγcKO.A2.NOD) mouse model expresses the human MHC class I molecule HLA-A2 in combination with the human MHC class II molecule HLA-DR4. DRAGA mice can produce all immunoglobulin subtypes and elicit high titers of specific human antibodies against an infectious agent. The aim of this work is to generate and test the efficacy of neutralizing hu-mAbs targeting a conserved HA region using DRAGA mice. First, we establish

a new model of human influenza infection. Second, we generate human monoclonal antibodies targeting influenza virus using DRAGA mice as a new source for hu-mAb development and generation. Third, we assess the therapeutic potential of a human anti-influenza monoclonal antibody, 16D11, in a DRAGA mouse model of infection. We show that DRAGA mice can sustain influenza infection by RT-qPCR and manifest clinical symptoms of infection such as weight loss. Next, we demonstrate that a single dose of anti-flu hu-mAb can significantly delay the lethality of influenza virus in DRAGA mice infected with PR8/A/34 influenza virus. By generating anti-flu hu-mAbs specific to one or more influenza strains, we provide evidence that hu-mAbs generated from humanized mice can be used as a new generation of therapeutics designed to neutralize influenza infection.

ACKNOWLEDGMENTS

DEDICATION

I dedicate this dissertation to my beloved grandfather Eusebio Temistocles Ura, whose devotion to his grandchildren has given him the vigor to live beyond ninety-five spring seasons.

TABLE OF CONTENTS

LIST OF ABBREVIATIONS

AID: activation induced cytidine deaminase enzyme

BCR: B cell receptor

C57BL/6: C57 black 6 mouse; common inbred strain of laboratory mouse

CDR: complementary-determining region

DAPI: 4′,6-Diaminodino-2-phenylindole

FACS: fluorescence-activated cell sorting

FITC: Fluorescein isothiocyanate

Foxp3: Forkhead Box P3; a transcriptional regulator important for development and inhibitory

        function of regulatory T-cells (Treg)

GM-CSF: Granulocyte macrophage colony stimulating factor

HA: hemagglutinin protein from influenza virus

H & E: hematoxylin and eosin staining

HLA-A2.1: human leukocyte antigen-A*0201

HLA-DR4: human leukocyte antigen-DR*0401

HSC: Hematopoietic stem cells

HV: hypervariable region

Ig: Immunoglobuling; Ab

iRBC: infected red blood cell

K6H6: hybridoma: B lymphocyte; somatic cell hybrid

IL-2Rγc: interleukin-2 (IL-2) receptor gamma chain

KO: knock out

LAIV: live attenuated vaccine

mAbs: monoclonal antibodies

MHC: (major histocompatibility complex): group of genes that encode for surface proteins of
        cells that help the immune system recognize foreign substance

NA: neuraminidase protein from influenza virus

NOD: non-obese diabetic mouse

NP: nucleoprotein

PA: acidic protein from influenza virus

PB1: polymerase basic protein 1 from influenza virus

PB2: polymerase basic protein 2 from influenza virus

Prdck: Protein Kinase, DNA-Activated, Catalytic Polypeptide; involved in DNA double strand
        break repair and recombination

RAG 1: recombination-activating protein 1

RT-qPCR: real-time reverse transcription polymerase chain reaction

SCID: severe combined immunodeficiency

SA: Sialic acid bonds

TIV: trivalent inactivated influenza vaccine

TD: thymus-dependent antigens

TI: thymus-independent antigens

T1D: Type 1 diabetes, autoimmune diabetes.

Tregs: T regulatory cells

VH: variable heavy chain of immunoglobulin

VL: variable light chain of immunoglobulin

Chapter 1:
DISSERTATION INTRODUCTION

1.1: Influenza

Influenza, commonly known as the "flu", is an acute, contagious, respiratory febrile illness caused by infection with influenza type A or B viruses. The most common symptoms are fever, malaise, and cough. It is usually a self-limited febrile illness, but it can also cause consequential sequelae such as pneumonia, bronchitis, sinus and ear infections. Severe complications of influenza can result in hospitalization or death. People at high risk of developing influenza-related complications include children younger than five years of age (especially children younger than two), adults sixty-five years of age and older, pregnant women, and patients with immunosuppression (e.g. HIV/AIDS or cancer patients) [1,2]

Influenza viruses belong to the family *Orthomyxoviridae* and are classified based on major antigenic differences into influenza virus types A, B, C, and D. All four virus classes have a segmented genome of negative sense single-stranded RNA (ssRNA) (Figure 1). There are eight discreet nucleocapsid segments within the virion genome of types A and B. Each nucleocapsid is composed of a single segment of genomic RNA associated with viral nucleoprotein (NP), and one end is bound with three polymerase proteins, basic polymerase 1 (PB1), basic polymerase 2 (PB2) and acidic protein (PA)[2]. These eight nucleocapsids can undergo reassortment, combining two or more influenza viruses of the same or different subtypes, and co-infect a single cell and exchange RNA segments to form a genetically novel virus[3]. Influenza viruses are enveloped viruses with spherical or filamentous forms ranging from 80 to 120 nm. Two of the genomic segments encode the surface envelope glycoproteins known to contain antigenic sites: hemagglutinin (HA) and neuraminidase (NA) spikes. HA binds to sialic acid receptors and is responsible for mediating entry of the virus into cells. NA is a viral enzyme that catalyzes the removal of terminal sialic acids, allowing new virions to bud from

infected cells. Each HA trimeric spike is a protein domain composed of three HA polypeptides. The HA polypeptide is initially synthesized as a monomer (HA_0) then cleaved by proteases into the globular head HA_1 and stem HA_2 domains (or subunits). To date, 16 HA and 9 NA subtypes have been described in influenza A viruses[2].

Outbreaks of influenza are unpredictable and can occur with varying severity. For example, attack rates may be as high as 10-40% of the general population over a 5-6 week period[1,2]. Seasonal epidemics result in morbidity and mortality, and when the virus spreads globally, infecting a large proportion of the human population, what was an influenza epidemic becomes pandemic. There have been recurrent epidemics of febrile respiratory diseases every 1 to 3 years for at least the past 400 years [2] and four pandemics have occurred since 1918[4]. The most deadly

Figure 1: Structure of an influenza A virus virion.

Figure modified from Nelson M. and Holmes E., 2007. Copyright by Springer Nature publishing group. Reprinted with permission.

pandemic, also known as the Spanish flu, occurred in 1918-1919 and caused an estimated 50 million deaths[4]. The most recent pandemic occurred in 2009, causing between 151,700 and 575,400 deaths, raising concerns about future pandemics, preparedness and response.

Alterations to the antigen structure of HA and NA external glycoproteins are referred to as antigenic drift or antigenic shift. Antigenic drift refers to the continual evasion of host immunity by minor antigenic changes that occur frequently with HA or NA of the virus. Gradual accumulation of amino acid mutations has been frequently seen in the antigenic sites of the HA molecule. On the other hand, antigenic shift refers to the formation of a new influenza virus subtype with new combinations of HA and NA antigens to which the human population lacks immunity. Re-assortment of influenza virus results in an antigenic shift of the virus giving rise to the severe influenza pandemics[3].

1.2: Animal models of influenza infection

Animal models for influenza research are essential to better understand how host and viral factors contribute to disease and transmission outcomes of influenza infection in humans[5]. In addition, animal models of influenza infection are used to assess the effectiveness of intervention methods such as vaccination to prevent or reduce influenza morbidity and mortality in humans. Several factors must be considered in selecting an animal for influenza research. First, the animal must be susceptible to infection and support replication of the virus. Second, the animal must present clinical signs of infection such as weight loss, lethargy, raised body temperature (pyrexia), or histopathological changes in tissues collected from the nasopharynges or lung[5]. Improvement of these manifestations of infection when the animal received an investigational drug, therapeutic or vaccine will suggest the efficacy of the antiviral treatment.

Studies involving the use of animals as models of infection for influenza have exploited mice, ferrets, nonhuman primates, guinea pigs, cats, and dogs. To understand influenza transmission to humans, researchers have used domestic poultry and pigs as intermediate hosts.

However, safety precautions must be taken when working with these two types of animal models since influenza infection can occur during occupational exposure. Another aspect to be considered during the selection process is whether adaptation of the human influenza strains to animal models is necessary, as seen with mice; other animal models like ferrets and guinea pigs do not require adaption of human influenza strains. When a mouse strain is paired with its appropriate influenza virus strain, signs of disease include huddling, ruffled fur, lethargy, weight loss, and death (euthanasia as a humane endpoint). Assessment of lungs from infected mice reveal lung lesions characteristic of pneumonia, such as pulmonary edema and inflammatory infiltrates[5]. Of these parameters, the most commonly used to evaluate influenza pathogenicity in mice are weight loss and mortality.

Since the 1930s, ferrets have been used to mimic human influenza infection without prior adaption to the species. Like humans, viral replication and tissue damage are manifested primarily in the upper respiratory tract. Furthermore, ferrets display symptoms including fever, nasal discharge, lethargy, weakness, weight loss, and the hallmark feature, sneezing[5]. The main disadvantage of using ferrets as animal models for influenza infection are the complex husbandry requirements, expense, and size, all of which limit their use for influenza research[5].

Since not all animal models mimic human influenza infection, a new emphasis has been placed on developing *in vivo* models for the analysis of human immune response during influenza infection.

1.3: Limitations to prevention methods of influenza infection

The antigenic evolution of influenza highlights the threat of future emerging pandemics that might be highly pathogenic, equaling or even exceeding the high morbidity and mortality

seen in 1918[1-3]. Two main interventional tools available to reduce and control a future pandemic are vaccination and antiviral drugs. However, according to the CDC, recent studies have shown that vaccination can reduce the risk of infection by 40%-60% among the overall population during seasons in which the vaccine influenza strain matches to the circulating influenza strain[6]. On the other hand, antiviral medication such as adamantines or M2 inhibitors and neuraminidase inhibitors are associated with toxicities, rapid emergence of drug-resistant strains, and are not effective against influenza B viruses due to their structurally different M2 channel[7-10]. Therefore, during a pandemic, these prevention strategies are no guarantee for success given the uncertainties of the novel virus. Additionally, current influenza vaccines used in the U.S. rely on growing flu virus in chicken eggs. During a pandemic, it becomes difficult to accelerate vaccine production since this process is dependent on a large supply of fertile chickens, chicken eggs, and efficient growth of the virus in the eggs. The outbreak of H1N1 proved that new vaccine technologies have to be developed to meet the public health need[11].

Despite the variation in vaccine effectiveness, vaccination remains the best method of prevention and control of influenza infections. It normally elicits a potent neutralizing antibody response against one of the major viral surface glycoproteins, HA, which directly neutralizes virus infectivity. Most vaccines are trivalent, containing representative HAs from two influenza A strains and one influenza B strain. In the last couple of years, the FDA has approved the administration of quadrivalent influenza vaccines containing two influenza A strains and two influenza B strains. Most recently the FDA approved the administration of recombinant HA proteins as flu vaccines which do not require egg-grown vaccine virus thus eliminating the need for chicken eggs during the production process[12]. Current trivalent and quadrivalent vaccines contain killed influenza viruses and induce a protective serum antibody response but a poor cell-

mediated response. On the other hand, the live attenuated vaccine (LAIV), containing live

attenuated viruses, induces both humoral and cellular immune responses. However, due to the

poor or low effectiveness of LAIV during the 2013–14 and 2015–16 seasons, the CDC does not

recommend its administration for the 2017-2018 season[13]. As new strains of influenza virus

emerge, new formulations of the vaccine have to be generated and this can be expected to occur

annually[12]. Given the inevitability of a new pathogenic strain of influenza, possibly resistant to

antiviral medications such as oseltamivir and zanamivir, and the lack of a heterovariant vaccine,

alternative treatment strategies for influenza are necessary. Immunotherapy with monoclonal

antibodies could be a new alternative to treat viral diseases such as the influenza infection.

1.4: Immunoglobulins

The main function of B cells is to produce antibodies that contribute to immunity against

any pathogen present in the extracellular spaces of different organs. The humoral immune

response is initiated when B cells are activated by either thymus-dependent (TD) or thymus-

independent (TI) antigens. Protective antibody responses to protein antigens derived from

pathogenic microbes (e.g. viruses) typically require antigen-specific T cell help (i.e. TD). First,

the B cell must bind the antigen through its B-cell receptor (BCR) to signal the interior of the

cell. Then, the bound antigen is internalized, processed and returned to the surface as peptides

bound to MHC class II molecules. A $CD4^+$ helper T cell that recognizes these specific peptide-

MHC class II complexes through its T-cell receptor will engage the B cell and form a T:B cell

conjugate. This interaction can induce the B cell to differentiate into antibody-producing plasma

cells in response to helper T cell-derived signals (e.g. CD40L, cytokines). This process is

accomplished when activated B cells migrate from lymphoid follicles into germinal centers

(GCs), specialized compartments for affinity maturation of antibodies. Within the GC, B cells will continue to proliferate as they undergo somatic hypermutation and class switching, culminating in the selection of B cells expressing high-affinity antibodies for effective humoral immune responses. GC B cells can ultimately differentiate into either long-lived antibody secreting plasma cells whose sole function is to secrete high-affinity class switched antibodies, or memory B cells, whose function is to generate an accelerated and more robust antibody-mediated immune response upon re-infection[14].

Antibodies are said to neutralize the pathogen when they cover up the sites on a pathogen's surface necessary for growth and replication [15]. Neutralizing antibodies developed during the primary immune response to influenza viruses are important for future immunity to these viruses. This property is based on the abilities of the neutralizing antibody to coat the virus, inhibit its attachment to human cells, and successfully prevent infection[15]

Antibodies are considered specific when they bind to only one antigen or to a very small number of different substances (e.g. phosphorylcholine or vitamin K_1). When a B cell clone undergoes development, it is committed to produce immunoglobulins of much different specificity. Before it has encountered an antigen, a mature B cell only expresses membrane bound immunoglobulins IgM and IgD, where IgM serves as the cell receptor for the antigen. When the antigen binds to IgM the B cell becomes stimulated to undergo diversification through a process known as somatic hypermutation, which introduces point mutations through the variable (V) regions of the heavy-chain and light-chain genes[15]. Somatic hypermutation gives rise to B cells bearing mutant immunoglobulin molecules on their surface with substitutions in the antigen-binding site increasing their affinity for the antigen. During the course of the adaptive immune response, somatic hypermutation results in affinity maturation by increasing

the affinity of the antigen-binding sites of antibodies for the antigen[15]. Antibody diversification

through SHM relies on point mutations introduced in V genes of both heavy and light chains by

the activation-induced cytidine deaminase (AID) enzyme. AID is a cytosine deaminase that

enzymatically converts cytosine to uracil in the immunoglobulin genes of the V region. Further

DNA recombination of immunoglobulins through a process known as isotype switching, enables

the rearranged V-region coding sequence to be used with other heavy-chain C genes to produce

IgG, IgA, or IgE antibodies. Class switching does not affect the antigen binding site, but it does

affect the effector functions of the antibodies. B cells will then proliferate and differentiate into

plasma cells, which will secrete antibodies with the same specificity as that of the membrane

bound immunoglobulin[15].

Antibodies are composed of polypeptides built from a basic unit of four polypeptide

chains, in which each chain holds a variable and constant region. Each unit consists of two

identical heavy chains and identical light chains assembling the structure into a Y letter shape.

Both heavy and light chains have an amino-terminal variable region that differs in amino acid

sequence from one immunoglobulin to the next, and a constant region that is very similar in

amino acid sequence between immunoglobulins. The variable domains in the heavy chain (VH)

and in the light chain (VL) together form the antigen binding site. Differences of amino acid

sequences concentrated within the V domains of both light and heavy chains are called

hypervariable regions (HV). Hypervariable regions are also known as complementary-

determining regions CDR1, CDR2, and CDR3. CDRs contribute much of the antigen specificity

of the antigen-binding site located at the tip of each arm of the antibody molecules[15]. CDR3 of

the heavy chain has been shown to be a determinant of antibody specificity and holds the highest

degree of diversity in both sequence and length[16]

Immunoglobulins are classified based on structural differences in the constant region of the molecule and different effector functions[15]. In humans, IgG is further subdivided into four subclasses (IgG1, IgG2, IgG3, and IgG4), while IgA is subdivided into two subclasses (IgA1 and IgA2). The light chains have only two isotypes or classes termed kappa and lambda. No functional difference has been found between antibodies that have lambda chains in comparison to those that have kappa chains. Both heavy and light chains have an amino-terminal variable region that differs in amino acid sequence from one immunoglobulin to the next, and a constant region that is very similar in amino acid sequence between immunoglobulins[15]. Each of the five classes of immunoglobulins has distinct physical and functional properties. IgM is the first class of immunoglobulin produced in response to activation of a B cell. IgM antibodies secreted by B cells are pentamers with a high molecular weight of 970 kDa. The pentameric structure of IgM also increases its avidity for antigens before its affinity increases through the process of affinity maturation. The four IgG isotypes generated during an immune response are mainly found in the bloodstream and in the extracellular spaces of tissues[15]. IgA isotypes can also be found in the bloodstream, but their main role is defending the mucosal surfaces lining the gut and respiratory tract. IgE is involved in defense against parasitic infections, and in allergic reactions. IgD is a surface immunoglobulin found in mature B cells, and its biological role is unknown. The IgG class is the most stable with a serum half-life of 20 days, while IgM and IgA have a serum half-life of 10 and 6 days, respectively. Both IgE and IgD are the least stable since their serum half-life is 2 to 3 days[15].

IgG is the principal class of antibody in the blood and extracellular fluids, as well as a key player of humoral immune responses. IgG is known for its efficiency in opsonization, activation of the complement system, and neutralization of pathogens. While IgM has a lower

affinity for its antigen, its efficient activation of the complement system is important in controlling infections. Furthermore, Skountzou et al, demonstrated that IgM antibodies conferred complete protection against a lethal dose of influenza virus 600 days post-primary infection, and that IgM antibodies in the presence of complement can neutralize influenza virus just as efficiently as IgG antibodies[17]. This study demonstrated that virus-specific IgM titers are an important correlate of protection against influenza viruses[17].

Antibodies produced in response to a foreign antigen are valuable for many biological purposes, including passive immunization for treatment of infectious diseases (see below).

1.5: Monoclonal antibodies (mAbs)

Antibody-based (serum) therapies were recognized a century ago to be useful in treating infectious diseases[18]. In the early 20th century, serum was used to treat bacterial infections caused by *Corynebacterium diphtheriae*, *Streptococcus pneumoniae, Neisseria meningitides*, and *Clostridium tetanai[18]*. Serum therapy continued to be used until the mid-1930s, but was abandoned with the introduction of antimicrobial therapy. However, by the 1970s, with the introduction of hybridoma technology[18], antibody therapy was reawakened. Kohler and Milstein developed a technique to immortalize plasma cells and produce monoclonal antibodies by immortalizing the growth of a clonal population of cells secreting homogenous antibodies[19]. An antibody-secreting cell is isolated and then fused with a myeloma cell, a type of B cell tumor. This hybrid can be maintained *in vitro* and will continue to secrete antibodies with a defined specificity[20]. Myeloma cells provide the correct genes to continue cell division in culture, while the antibody secreting cells provide the functional immunoglobulin genes. For the first time it

became feasible to produce large quantities of an immunoglobulin of a defined specificity and of

a single isotype *in vitro*. Advancement in the technology of human mAb development has

established several methods for human antibody generation such as (1) immortalization and

hybridization of antigen-specific human B cells, (2) generation of chimeric and humanized

antibody from mouse Ab by genetic engineering, (3) acquisition of antigen-specific human B

cells by the phage display method, and (4) development of transgenic mice (e.g. humanized

mice) for production of human mAbs[21]. However, when mAbs were first introduced as
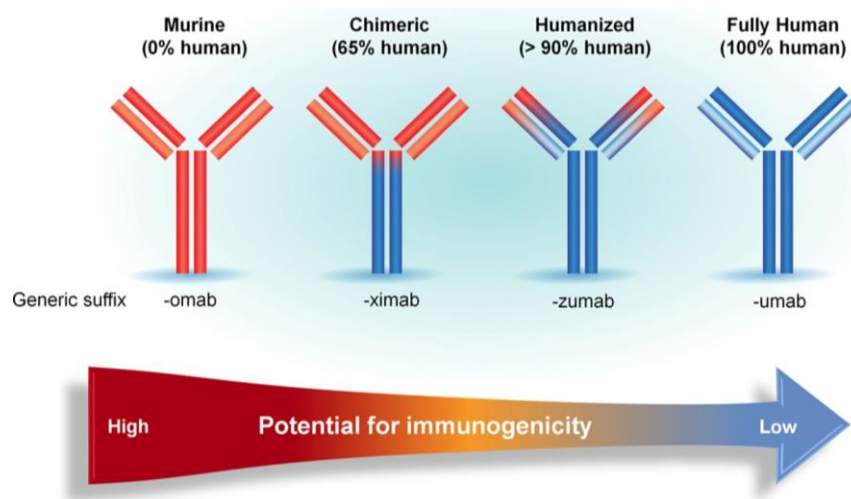
therapeutics, they were initially of mouse origin. Major advances have been made to humanize them and subsequently produce fully human antibodies (Fig. 2).

Monoclonal antibodies (mAbs) are classified according to their sequence source. There are murine only mAbs, chimeric

Figure 2: Humanization of therapeutic antibodies has reduced their immunogenicity.

Figure modified from Foltz et al 2013.
Copyright by Wolters Kluwer Health, Inc. publishing group.
Reprinted with permission.

(murine variable regions and human constant regions), humanized (human with murine CDRs)

mAbs, and fully human mAbs (Fig. 2). There has been a dramatic reduction in the use of

chimeric and humanized mAbs since the 2000s, and a substantial increase in the use of human

mAbs. Murine mAbs, e.g. muromonab-CD3, were of limited use clinically because humans

generated antibodies specific for the constant regions of the mouse antibody after the first

treatment[15]. A solution to this problem was the development of chimeric monoclonal antibodies

such as rituximab. However, it was discovered that 40% of chimeric antibodies induced anti-

mAb antibody responses *in vivo*. The next approach to reducing the anti-mAb immune response

was to humanize the monoclonal antibodies by genetic engineering. With this new approach,

only 9% of the humanized mAbs induced an anti-mAb immune response. Furthermore,

humanization of mAbs can be difficult considering the limited homology between the mouse

variable regions of the heavy and light chains and the human variable regions. This process

requires several rounds of engineering and maturation to reach a potent mAb[22]. Thus, generating

fully human monoclonal antibodies (hu-mAbs) that avoid eliciting an immune response without

sacrificing functionality would be useful.

Currently, the use of monoclonal antibodies for the treatment of viral diseases such as

hepatitis and respiratory syncytial virus infection has been established[23]. Therefore, we can

hypothesize that monoclonal antibodies have the potential to be used alone for the treatment of

infection with influenza virus strains resistant to current antivirals, or in combination with

antivirals to treat patients with severe infections[24].

Employing humanized mice harboring a human immune response with the capacity to

generate human antibodies against an antigen is becoming an attractive new source for the

generation of therapeutic human antibodies.

1.6: Humanized mouse models for immune investigation

Experimental studies in rodents elucidated a better understanding of many biological

processes in humans. Immunodeficient mouse models have been very important in the

advancement of human transplantation for cancer treatment, regenerative medicine, and therapeutic development[25]. Currently, three platforms (NOG, NSG and BRG) of mouse strains are used to recapitulate the human immune system engrafted in mice[26].

The development of immunodeficient mice for humanized models began with the discoveries of nude mice in 1962, and of severe combined immunodeficiency (SCID) mice in 1983[18,27]. McCune et al. transplanted fetal liver and thymus to introduce human T and B cells into SCID mice, termed SCID-hu mice, to develop a humanized mouse model. However, the engraftment rate of human cells in this model was low[28]. Then, the $Prkdc^{scid}$ gene was introduced into the non-obese diabetic (NOD) mouse strain to generate NOD-scid mice, which have been shown to support the differentiation of human hematopoietic stem cells (HSC)[29]. These mice were used extensively until the development of NOD/Shi- scid IL2rγ null (NOG) and BALB/cA-Rag2^{null}Il2rγ^{null} (BRG) mice. Ito et al. generated the NOG mice by knocking out IL-2Rγ in mice and crossing this strain with NOD-scid mice[25]. Moreover, Ito et al. developed the BRG mice by inactivating the IL2-Rγ from BALB/cA-Rag2^{null}. In 2005, Shultz et al. developed the NOD/LtSz-Prkdc^{scid} Il2rgtm1Wjl/J (NSG) mice by crossing NOD/LtJ-scid females with B6-IL2Rγnull males[30]. The NSG mouse model is similar to the NOG mouse model. Common characteristics between the NOG, NSG, and BRG models is the deficiency in T, B and natural killer (NK) cells due to the inactivation of the $Prkdc$ gene (SCID)/Rag gene and the $Il2rg$ gene. Transfer of mature human PBMCs or of HSCs are two techniques used to generate humanized mice. HSC transfer, rather than PBMC transfer, has been shown to result in better differentiation of hematopoietic cells and is more efficient in NOG/NSG/BRG mice[29].

There are four different types of engraftment techniques for the development of a functional human immune system in the three types of immunodeficient mouse models. Of these

four (Hu-PBL-SCID, Hu-SRC-SCID, SCID-hu, BLT), the bone marrow, liver, thymus (BLT) mouse has been able to develop a complete human immune system in which T cells are HLA restricted and higher levels of total human hematopoietic stem cell engraftment are achieved. However, the responses to vaccination or virus infection are predominately limited to IgM antibody production with little IgG antibody generation. An additional disadvantage is that surgical expertise is required to co-implant the human fetal liver, thymus fragments and bone marrow cells[26].

These limitations are due, in part, to differences between mice and humans in growth factors and cytokines required for hematopoietic and immune system development, and the presence of mouse MHC molecules instead of human HLA molecules. This suggested that the requirement of human HLA expression in the mouse host must be a crucial factor for a better human immune system mouse model[26]. Continued development provides models with increased levels of human immune system engraftment and reconstitution, as well as improvement in functional activity.

Humanized mice can therefore become versatile tools for development of new therapeutics, and to study the interaction of influenza virus infection with the human immune system.

1.7: DRAG or DRAGA mice as models of the human immune system

Generating fully human monoclonal antibodies from transgenic mice would allow researchers to discover epitopes of an infectious agent necessary to elicit a potent immune response in a model that most closely resembles the human immune system.   Transgenic mouse
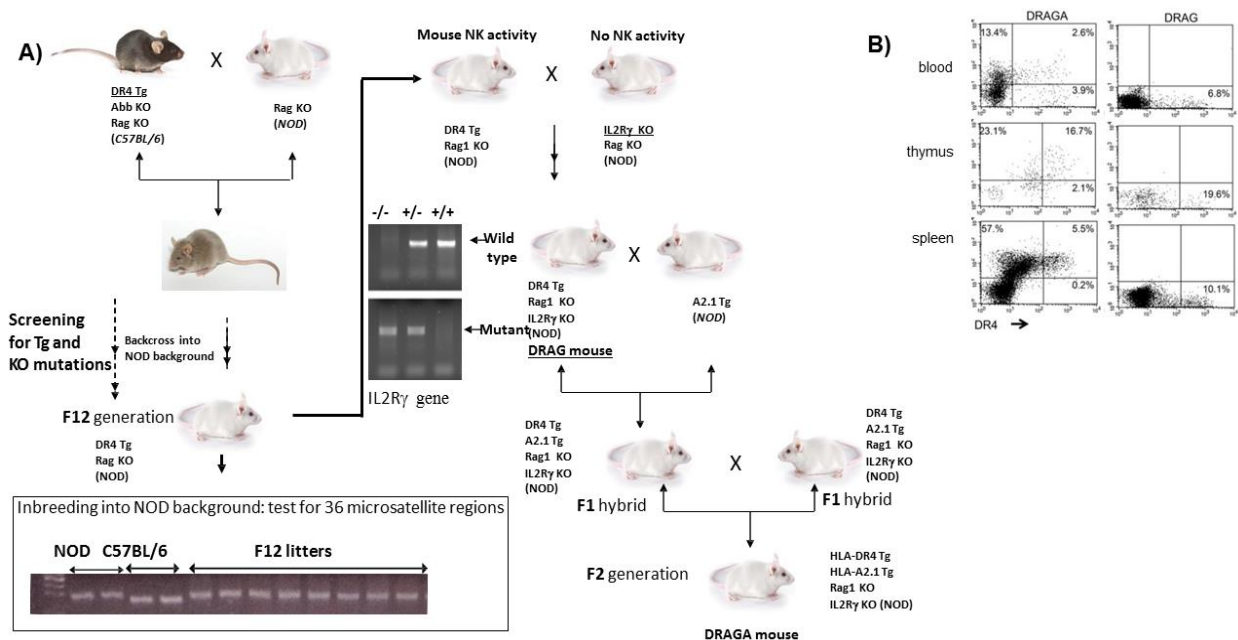
Figure 3: Development of humanized mouse strain DRAG or DRAGA. (**A**) Colony expansion of founder mice to generate NRG DRAG and DRAGA mouse model. (**B**) FACS analysis of blood, thymus and spleen of naïve (non-HSC infused) DRAGA and DRAG mice stained with HLA-A2 and HLA-DR4 Abs.

models could also serve as a new source to isolate hu-mAbs for therapeutic purposes, including

high affinity IgG. Additionally, humanized mice able to mimic the human immune system could

be used as new models of infection for agents such as bacteria, viruses and parasites. In

collaboration with Dr. Casares, our lab developed a new strain of humanized mice

RagKO.IL2RγcKO.NOD expressing the MHC class II molecule HLA-DR*0401, termed the

DRAG mouse[31]. DRAG (HLA-DR*0401.RagKO.IL2RγcKO.NOD) mice represent an "NRG"

animal model with chimeric human-mouse class II transgenes encoding the HLA class II antigen

binding domain molecule (Fig. 3). DRAG mice develop a high rate of human T and B cell

reconstitution upon infusion of $CD34^+$ HLA-DR-0401 matched HSC from umbilical cord blood

(Fig 4). T cell reconstitution is higher in DRAG mice, since 14 out of 15 (93.3%) DRAG mice

developed human T cells after 25 weeks post-HSC infusion in comparison to 4 out of 11 (36.4%)

control mice (RagKO.IL2RγcKO.NOD lacking expression of HLA-DR4).   In the thymus of

DRAG mice human thymocyte cell development was promoted, and there was a considerably

higher number of human CD45^{+} cells than in control mice, with the majority being CD4^{+} CD8^{+}

double positive, followed by CD4^{+} single positive and CD8^{+} single positive. The spleen of

DRAG mice has also been shown to contain mature human T cells, in which there was 23.8% of

CD4^{+} T cells and 5.0% of CD8^{+} T cells[31].

It has been shown that IL2RγcKO NOD and BALB/c mice infused with HSC have

functional impairment of human T cells since they responded weakly to stimulation with anti-

human CD3/CD28 antibodies or PMA/ionomycin[32]. On the other hand, T cells from DRAG

mice responded vigorously to CD3/CD28 or PMA/ionomycin stimulation and in response

secreted high levels of human cytokines, demonstrating that the expression of HLA-DR4

molecules rescued the function of human T cells. In addition, depletion of CD4^{+} or CD8^{+} T cells
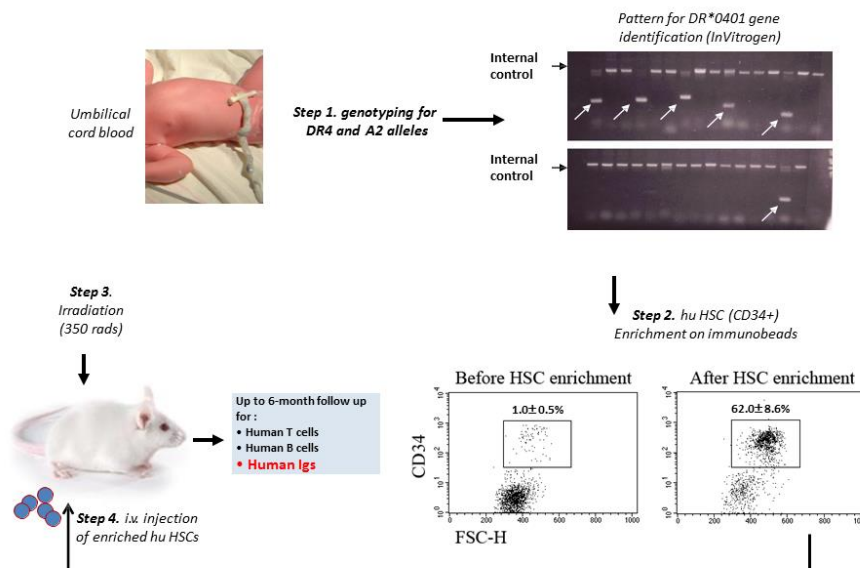
Figure 4: Reconstitution of DRAGA mice with HSCs

from splenic cells reduced secretion of IL-2 and IFNγ[31]. Furthermore, FACS analysis of blood from DRAG and control mice using an anti-human CD19 marker showed that the rate of B-cell reconstitution in 14 of 15 mice (93.3%) was similar to 9 of 11 (81.8%) control mice (RagKO.IL2RγcKO.NOD lacking expression of HLA-DR4). Thus, the expression of HLA-DR4 molecules in DRAG mice did not significantly improve reconstitution of human B cells in peripheral blood or in spleens of control mice.

DRAG mice have also been shown to allow human immunoglobulin isotype switching (IgM, IgG, IgA, IgE)[31] with IgG2 being the most prevalent in plasma, and in the absence of immunization. Furthermore, it was demonstrated that human B cells from DRAG mice elicit a specific humoral immune response when immunized with TT (anti-tetanus toxin) vaccine. The TT vaccine elicited high titers of anti-TT IgG antibodies as measured by ELISA 14 days later[31].

An additional distinctive feature of the DRAG mouse model is the reconstitution of CD4^{+} T follicular helper cells (TFH). A recent study demonstrated that DRAG mice have a high frequency of TFHs. This subtype of CD4^{+} T cells is known to play a major role in the induction of protective immunity against infectious agents and is required for maturation of B cells in germinal centers[33].

After development of the DRAG mice, Dr. Casares' group introduced an MHC class I molecule in addition to the MHC class II molecule to enhance the mouse's human immune system and potentially study CD8^{+} T cell responses. Previous studies demonstrated that HLA-A2 transgenic immunodeficient *Il2rg*-null mice developed an HLA-A2-restricted human CD8^{+} T cell response to infectious agents. Infection with EBV led to the development of HLA-A2-restricted human CD8^{+} T cell responses and protective CD4^{+} and CD8^{+} T cell-mediated

immunity[34,35]. Thus, the DRAG mouse model was further refined into the recently developed

DRAGA (HLA-DR4.RagKO.IL2RγcKO.A2.NOD) (Fig. 3 and Fig. 4) mouse model expressing

MHC class I molecule HLA-A2 in combination with human MHC class II molecule HLA-DR4.

Co-expression of HLA-A2 and HLA-DR4 in DRAGA mice did not result in differences in the

ability of these mice to develop human T and B cells, to reconstitute cytokine-secreting CD4$^+$ T

and CD8$^+$ T cells, or to undergo immunoglobulin class switching [36]. Interestingly, upon

immunization with GIL peptide derived from the influenza A virus matrix protein, encapsulated

in liposomes, the frequency and cytotoxicity of antigen-specific CD8$^+$ T cells in DRAGA mice

was significantly higher than in NRG mice expressing HLA-A2 molecules[36].

To date, DRAG mice have been used to assess susceptibility to infection with HIV virus,

Zika virus (ZIKV), and *Plasmodium falciparum* species[33,37-39]. Specifically, Yi et al,

demonstrated the protective efficacy of a targeted DNA vaccine against ZIKV infection in the

humanized mouse model DRAG[38].

In terms of using our current humanized mouse model to develop mAbs, our lab has

been able to generate hu-mAbs using the DRAG or DRAGA mouse models against other

infectious agents such as *Plasmodium falciparum* and Ebola virus. DRAG mice immunized with

irradiated sporozoites produced the first known hu-mAb directed against sporozoite's

Circumsporozoite protein (CSP) using a humanized mouse model. The second infectious agent

used to determine if DRAGA mice can generate specific anti-infectious hu-mAbs was a

conjugate composed of Ebola virus (EBOV) recombinant proteins: glycoprotein (GP) and matrix

protein VP40. These findings will soon be published, demonstrating the ability of DRAGA to

develop antibodies with potential for therapeutic administration against infectious agents.

In summary, DRAG/DRAGA represent new mouse models to study human T and B cell development and function response to infectious pathogens, vaccine development, and generation of human monoclonal antibodies for prophylactic and/or therapeutic use.

1.8 Humanized mice and influenza research

To our knowledge, in addition to Dr. Majji's assessment of influenza derived peptide immunization, only five other research studies have used humanized mice as animal models for influenza research[36]. Each study has assessed the effectiveness of humanized mice in influenza research at different levels, and with different types of humanized mice. For example, Yu et al. used the NOD/SCID $\beta2m^{-/-}$ immunodeficient mice transplanted with human CD34$^+$ hematopoietic progenitor cells (HPCs) to assess and evaluate *in vivo* function of human APCs in response to influenza virus vaccines[40]. They demonstrated that their humanized mice model can mount antigen-specific recall CD8$^+$ T-cell immunity on vaccination with seasonal trivalent influenza vaccines (i.e., live attenuated influenza virus [LAIV] vaccine and inactivated influenza virus [TIV] vaccine). The study by Wada et al. proved the usefulness of NOJ mice (NOD/SCID/Jak3$^{-/-}$) reconstituted with human PBMCs in evaluating the immunogenicity of influenza vaccines by recapitulating a comparative immunogenicity of influenza vaccines as observed in humans[41]. Their mouse model appears to be useful for human vaccine studies, since it can mimic the human recall responses to protein-based influenza vaccines, making it a suitable model for use in preclinical trials.   Subsequently, Yu et al. used autologous T cells isolated from the donors of mobilized HSCs to engraft onto Hu-SRC NOD-*scid β2m^null* mice and assess the infection and human immune response produced against the LAIV[42]. Willinger et al. assessed the importance of macrophages in early viral responses using a humanized mouse

model. Their BRG model, injected with human IL-3 and GM-CSF, increased myeloid engraftment within the lung and led to increased innate responses to influenza virus infection[43]. Lastly, Yi et al. showed that the treatment of NSG Hu-SRC-SCID mice with macrophage colony-stimulating factor (M-CSF) decreased viral transcript levels early after infection and was associated with abrupt increase of inflammatory cytokines IL-6 and TNF after 48 hours post infection[44]. In summary, these studies have contributed to the understanding of the usefulness of humanized mice for influenza research, yet questions remain on the effectiveness of humanized mice in assessing influenza vaccines or therapeutics.   Only a couple of types of humanized mice have been used to assess human immune response to influenza, and none of the studies used humanized mice as a model to assess anti-flu therapeutics. Furthermore, only two of these studies assessed the ability of humanized mice to sustain influenza infection, indicating that more studies are necessary to examine the advantages and disadvantages of using humanized mice as an animal model to study influenza vaccine effectiveness as well as influenza infection.

In the past decade several labs have developed neutralizing antibodies against influenza[45-47]. It has been demonstrated that most of these antibodies show cross-reactivity against different strains within a subtype, group or even between different groups. However, the majority of these antibodies are mouse monoclonal antibodies, and only a couple of labs have generated human monoclonal antibodies against influenza[45-49]. For example, human monoclonal antibodies were obtained from memory B cells of a 2009 pandemic H1N1 influenza vaccine recipient[50]. In this study, most of the fully human antibodies showed neutralizing activity against the HA protein but not the HA1 fragment. Their work also suggested that the antibody response was primarily targeting the HA2 stem region.

To date, human monoclonal antibodies produced from humanized mice against influenza have not been reported. Thus, we propose that DRAGA mice can be a new source of human monoclonal antibody generation. This contribution could be significant during an epidemic or pandemic period of influenza infection. A synthetic peptide-based vaccine has the potential to elicit antibodies against a known region of the hemagglutinin protein. If this region is conserved among several influenza strains, we can generate a region-specific yet broadly neutralizing antibody response. MAbs generated against a conserved region of influenza virus have been previously shown to provide protection against distinct viral subtypes[51,52]. Thus, we expect that hu-mAbs generated against a peptide conserved in several influenzas strains could provide protection against a single or more strains of virus prophylactically and therapeutically. In comparison to other mAbs (chimeric or humanized), hu-mAbs are expected to be less immunogenic, have a longer half-life in humans, and be more effective since less engineering troubleshooting would be required for their generation. In addition, administering a preparation of hu-mAbs as therapeutics could be beneficial, especially for patients unable to receive a flu vaccine because they are in high risk groups or have egg allergies. The ultimate universal therapy would provide protection against various influenza strains without the side effects of conventional flu vaccines.

DRAGA mice could also be used as a tool for the development of influenza vaccines able to induce a broad and long-lasting immunity. By testing the ability of DRAG/DRAGA mice to generate hu-mAbs against a conserved epitope, we will test the methodology of using humanized mice for influenza vaccine development.

1.9: Aim and Hypotheses

The primary objective of this dissertation was to assess the ability of a newly generated, humanized mouse (DRAGA mouse: HLA-DR*0401.HLA-A*0201.RagKO.IL2RγcKO.NOD) as a model of influenza infection. Our secondary objective was to use DRAGA mouse as a tool to first generate, and then test human anti-influenza monoclonal antibodies (hu-mAbs) for their potential therapeutic effect against influenza infection. These objectives were accomplished by addressing the following aims:

1. **Establish a new model of human influenza infection.**

   As noted above, DRAGA or DRAG mice have been previously shown to model infection with HIV virus, Zika virus, and malaria (*Plasmodium falciparum* species) parasite. Since the murine immune response to infection with influenza does not fully mimic the human immune response, *we hypothesized that DRAGA mice can resemble the human immune response to influenza infection.*

2. **Generate human monoclonal antibodies targeting influenza virus in DRAGA mice.**

   It has been previously demonstrated that DRAGA or DRAG mice are able to generate specific antibodies to malaria (*Plasmodium falciparum* species) and Zika virus. Thus, *we hypothesized that DRAGA mice can be used as a tool to develop human monoclonal antibody therapeutics against influenza infection.*

3. **Assess the therapeutic potential of human anti-influenza monoclonal antibodies in DRAGA mouse model of infection.**

   A large body of evidence stresses the generation of murine and humanized antibodies that can cross-neutralize influenza heterotypes in *in vitro* and *in vivo* assays. Herein, *we*

23

hypothesized that our newly generated humanized DRAGA mouse model for influenza infection can be potentially used to assess the therapeutic effect of human anti-influenza antibodies.

Chapter 2:
MANUSCRIPT

Generation and testing anti-influenza human monoclonal antibodies in a new humanized mouse model (DRAGA: HLA-A2. HLA-DR4. Rag1 KO. IL-2Rγc KO. NOD)

Published as: Mirian Mendoza[1], Angela Ballesteros[2],Qi Qiu[1], Luis Pow Sang[1], Soumya Shashikumar[3], Sofia Casardes[1,3], and Teodor-D. Brumeanu[1]*.

[1]*Uniformed Services University of the Health Sciences, Department of Medicine, Division of Immunology, Bethesda, MD 20814, U.S.A;* [2]*National Institute of Neurological disorders and Stroke, Molecular Physiology and Biophysics Section,, Bethesda, MD 20892,* [3]*Naval Medical Research Center/Walter Reed Army Institute of Research, US Military Malaria Vaccine Development, Silver Spring, MD 20910, U.S.A.*

* Corresponding author

Email address: teodor-doru.brumeanu@usuhs.edu (T-D.B)

2.1: Abstract

Pandemic outbreaks of influenza type A viruses have resulted in numerous fatalities around the globe. Since the conventional influenza vaccines (CIV) provide less than 20% protection for individuals with a weak immune system, it has been considered that broadly cross-neutralizing antibodies may provide better protection. Herein, we showed that a recently generated humanized mouse (DRAGA mouse; HLA-A2. HLA-DR4. Rag1KO. IL-2Rγc KO. NOD) that lacks the murine immune system and expresses a functional human immune system can be used to generate cross-reactive, human anti-influenza monoclonal antibodies (hu-mAb). DRAGA mice were also found to be suitable for influenza virus infection, as it can clear a sub-lethal infection and sustain a lethal infection with PR8/A/34 influenza virus. The hu-mAbs were designed for targeting a human B-cell epitope (^{180}WGIHHPPNSKEQ QNLY^{195}) of hemagglutinin (HA) envelope protein of PR8/A/34 (H1N1) virus with high homology among seven influenza type A viruses. A single administration of $HA_{180\text{-}195}$ specific hu-mAb in PR8-infected DRAGA mice significantly delayed lethality by reducing lung damage. The results demonstrated that the DRAGA mouse is a suitable tool to (i) generate heterotype cross-reactive, anti-influenza human monoclonal antibodies, (ii) serve as a humanized mouse model for influenza infection, and (iii) assess the efficacy of anti-influenza antibody-based therapeutics for human use.

Keywords: Humanized mice, Human monoclonal antibodies, Human influenza infection model, Anti-flu antibody therapy.

2.2: Introduction

Influenza viruses are enveloped orthomyxoviruses with a segmented RNA genome of negative polarity containing eight segments that encode ten proteins in the case of type A and B viruses[53]. Hemagglutinin (HA) is the most abundant immunogenic envelope protein of influenza viruses, and plays a critical role in viral invasion of the lung epithelial cells[54,55]. Pandemic outbreaks of influenza type A viruses often rampage global health, resulting in numerous fatalities such as the 1918 Spanish pandemic that killed 20 million people across Europe and 50 million worldwide[56]. Influenza infections kill 30,000 people on average in a non-epidemic year in the USA alone, particularly those with weak immune systems like children, elderly, and immunocompromised individuals. In addition, seasonal mutations in the HA protein like those expected for the avian and swain influenza viruses may pose significant challenges to the immune system and design of conventional influenza vaccines (CIV). CIV formulations rely on viral strains detected in previous years that cannot optimally protect against unpredictable seasonal viral mutants. In addition, current CIV preparations cannot be administered in already infected individuals[57]. Attempts to design more versatile vaccines such as parental adjuvant-combined vaccines, non-parental vaccine with nasal or epidermal split product of whole virion, inactivated virion, DNA-based vaccines, live vaccine preparations using recombinant live viruses, or virus-vectored vaccines, all showed a limited protection in humans and animal models[58,59].

It has been recently considered that the use of broadly cross-neutralizing human specific Abs against multiple influenza virus strains could be a more efficient prophylactic/therapeutic approach to protect against mutated influenza viruses than the current CIV preparations[60-62]. The choice of cross-neutralizing antibodies over CIV is based on experiments in animal models

showing that the anti-viral HA antibody response is critical for protection against influenza infection. Thus, IgA and IgM Abs can efficiently clear the virus from the lungs in a primary infection, while the IgG Abs can inhibit viral replication in the lungs[63,64]. A number of murine monoclonal cross-neutralizing Abs have been generated, and their cross-protective effect was assessed in animal models of influenza infection[61,65-76]. However, the major caveat of murine Abs in humans is that repeated administrations lead to the induction of human anti-mouse antibodies (HAMA), which can significantly diminish or abolish their therapeutic efficacy[77-82], and in some cases could even lead to serious adverse effects like anaphylactic shock[83]. To minimize HAMA effects, genetic engineering approaches were aimed at "humanizing" murine antibodies or designing complementary immunomodulatory strategies. Although humanized Abs showed some therapeutic effect in some cancer and autoimmune diseases, a complete suppression of HAMA effects has not been achieved yet[84-90]. For this reason, "fully" human Abs are now considered the safest prophylactic or therapeutic approach for humans. "Fully" human anti-influenza monoclonal Abs (hu-mAbs) have been successfully generated from EBV-immortalized B cells collected from infected or vaccinated individuals. Their viral neutralization capacity was successfully tested in mouse models for influenza infections[47,91]. However, EBV-generated hu-mAbs lack known epitope specificities, which confine the design of a broadly cross-protective Ab preparation against influenza infection. In contrast, the use of humanized mice to generate "fully" humanized Abs with known target specificities likely offers a more versatile approach.

Several humanized mouse models engineered on SCID and NOD backgrounds permit different stages of human B-cell development, with inefficient progression of fully mature human B cells required for antibody production and immunoglobulin class switching[92-97].

However, depending on the mouse strain and method of reconstitution, several limitations still exist: transfer of T and B memory cells from the donor through PBMC infusion is either inefficient or leads to acute or chronic GVDH, interference of murine innate immunity, lack of class switching, poor HSC engraftment, and inefficient human T and/or B cell expansion and homeostasis[98]. To avoid some of these limitations, we developed two new NRG strains of humanized mice (DRAG mouse: HLA-DR*0401[+]/IL-2γc KO, RAG1 KO, NOD; and DRAGA mouse: HLA-DR*0401[+]/HLA-A2.1[+]/IL-2γc KO, RAG1 KO, NOD)[31,36] that can efficiently reconstitute a human immune system upon engraftment with HLA-matched human hematopoietic stem cells (HSC), and produce high numbers of functional human T cells, B cells, dendritic cells, and FOXP3^{+} T regulatory cells[31,36,37]. DRAG and DRAGA mice elicit specific, "fully" human Abs upon immunization with foreign antigens[31,37]. Herein, we used a conserved HA$_{180-195}$ epitope with shared homology among several strains of influenza virus (PR8-H1N1, WSN-H1N1, Adachi-H2N2, Aichi-H3N2, Memphis-H3N2, VN1194-H4N1, Hok67-H5N3, W213-H9N2, and Maryland-H13N6)[61] to immunize DRAGA mice and to ultimately generate cross-reactive hu-mAbs. By establishing DRAGA as a humanized mouse model for PR8 influenza infection, we were also able to assess the therapeutic effect of a cross-reactive hu-mAb.

2.3: Results

Selecting the immunogenic, human B-cell epitope as a target for cross-reactive hu-Abs.

Previous data showed HA amino acid homology among several influenza A heterotypes[61]. We have thus selected a homologous HA epitope shared by several influenza type A heterotypes ([180]WGIHHPPNSKEQQ NLY[195]) as a target for hu-mAbs. The $HA_{180-195}$ epitope of PR8/A/34-H1N1 influenza virus has high homology among 7 other influenza type A viruses: WSN-H1N1, Adachi-H3N2, Aichi-H3N2, Memphis-H3N2, VN1194-H5N1, Hokkaido 67-H5N3, and W213-H9N2. This epitope is located in the HA head and partially comprised by one of the four HA1 antigenic sites (Sb antigenic site[99]) (**Fig.1A**) as a surface exposed α-helix flanked by two β-sheets (**Fig.1B**). "De novo" modeling of the $HA_{180-195}$ epitope in solution using PEP-FOLD server[100,101] led to the prediction of a similar helicoid folding to that in HA protein of the PR8/A/34 and Hokkaido viruses, but not of Memphis virus (**Fig. 1C**). The "de novo" software can model peptide structures in solution based on the amino acid composition and peptide bond properties, and it does not use any template or already known structure to generate a homology model. In addition, the I-TASSER software that uses an already solved structure from database and relies on sequence homology[102-104] also predicted a similar 3D folding of $HA_{180-195}$ epitope in the HA1 protein of PR8/A/34 and Hokkaido viruses, but not of Memphis virus. This is consistent with a 100% homology of $HA_{180-195}$ epitope at the positions 181-186 in all studied virus strains except the Memphis virus, which suggests that these amino acid residues are critical for the $HA_{180-195}$ helicoidally and/or interaction with our hu-mAbs.

We next questioned whether the $HA_{180-195}$ stretch of amino acids is a human T-cell or B-cell epitope. For this, two DRAGA mice were injected in the foot pads with KLH-$HA_{180-195}$ conjugate and 2 weeks later boosted with the same conjugate. Two weeks after the boost, the splenic cells were incubated for 2 and 4 days with $HA_{180-195}$ synthetic peptide and the secretion of

31

T-cell cytokines was measured by Luminex. A lack of IL-2, IL-4, IL-5, IL-10, and IFN-γ secretion (data not shown) ruled out the possibility that the $HA_{180-195}$ epitope is a human T-cell epitope.

To find out if the $HA_{180-195}$ is a B-cell epitope able to induce specific hu-Abs in DRAGA mice, the $HA_{180-195}$ synthetic peptide was covalently coupled to the KLH protein and the conjugate was used to immunize DRAGA mice (described in materials and methods section). Two weeks after the boost with KLH-$HA_{180-195}$ conjugate, sera from immunized mice was measured by ELISA for human specific Abs using plates coated with BSA-$HA_{180-195}$ conjugate in parallel with plates coated with PR8 virus. As illustrated in **Figure 2A**, immunized DRAGA mice elicited human IgM and IgG antibodies to the $HA_{180-195}$ epitope, which demonstrated that the $HA_{180-195}$ peptide consensus is an immunogenic human B-cell epitope able to prime human B cells toward secretion of specific IgM and IgG Abs. These results, together with the finding of human AID master of immunoglobulin class switch in the spleen of naïve DRAGA mice and its up-regulated expression upon PR8 infection of DRAGA mice (**Fig. 2B**), demonstrated the ability of B cells to undergo immunoglobulin class switching.

Immunochemical and structural characteristics of HA$_{180-195}$-specific hu-mAbs

Several hybridoma clones secreting $HA_{180-195}$ specific hu-mAbs were generated upon fusion of splenic cells from KLH-$HA_{180-195}$-immunized DRAGA mice with K6/H6 myeloma cells. Hybridoma cells were cloned and sub-cloned, and further selected for stable, highly hu-Ig secreting clones specific for $HA_{180-195}$ epitope by ELISA-coated plates with PR8 virus or BSA-$HA_{180-195}$ conjugate. The majority of hybridoma clones (85%) were specific for the KLH protein carrier. Two hybridoma clones secreting $HA_{180-195}$ specific IgG hu-mAbs were detected during

ELISA screening, but did not survive, most likely because of loss of chromosomes during re-cloning. Among all specific hu-mAbs, 6 highly secreting, stable $HA_{180-195}$-specific IgM hybridoma clones (16D11, 6C2 clones #2 and #9, 3E10, and 10B2, 8D12) were selected for further characterization. IgM hu-mAbs were affinity purified from the cell culture supernatants of hybridoma cells on columns comprised of goat anti hu-IgM Abs covalently coupled to Sepharose CL-4B gel matrix. The results of ELISA isotyping of $HA_{180-195}$-specific hu-mAbs were confirmed by Western Blot (WB) as IgM/λ hu-mAbs (**Fig. 3**). The hybridoma clone 3E10 was found to secrete monomeric, soluble human κ-chains (**Fig. 3)** with no specificity for PR8 virus or $HA_{180-195}$ epitope according to ELISA and WB analysis (data not shown).

Affinity purified IgM hu-mAbs subjected to SDS-PAGE under denaturing and reducing conditions showed 2 major bands between 70-75 and 27-30 KDa corresponding to the heavy and light chains, respectively, of an IgM molecule (**Fig. 4A**). Both immunoelectrophoresis (**Fig. 4B**) and agarose electrophoresis in Titan gels (**Fig. 4C**) revealed the monoclonality and distinct electrophoretic mobility for each IgM hu-mAb. The molecular assembly of IgM hu-mAbs was determined by FPLC size exclusion chromatography under native conditions, which showed that all selected hu-mAbs were secreted by the hybridoma cells as pentamers (**Fig. 4D**). Together, these assays revealed that the four analyzed anti-$HA_{180-195}$ hu-mAbs were comprised of IgM/λ monoclonal pentamers with different electrophoretic mobility. The unique electrophoretic mobility of each of IgM hu-mAb suggested differences in their amino acid composition. To find out if this is the case, we next sequenced all four hu-mAbs. Indeed, sequencing analysis of the heavy and light chain CDRs showed several amino acid differences between 16D11, 8D12, 10B2, and 13C10 hu-mAbs (**Fig. 5**). The 8D12 hu-mAb showed a valine substituted for leucine in the signal peptide of heavy chain at the position 89 and in CDR1 of the light chain a valine

substituted for alanine at position 53, as well as an alanine substituted for glycine in the signal peptide of the light chain at position 111. The 13C10 hu-mAb had an arginine substituted for glycine in the frame 3 of the light chain at position 97. The 16D11 hu-mAb showed the highest amino acid diversity in the CDR3 of heavy chain. The CDR3 regions of 8A4 and 25-3 isotype controls (IgM/λ hu-mAb) were also quiet diverse when compared with 16D11 hu-mAb

Nucleotide sequence analysis of 16D11 VH and VL chains using the IMGT/V-QUEST algorithm[105,106] identified the variable (V), diversity (D) and joining (J) gene segments used to assemble its heavy and light chain. The VH chain of 16D11 hu-mAb used the V gene from IGHV3-23*01 or IGHV3-23D*01 germlines, and the J gene from germline IGHJ4*02. Based on the amino acid junction analysis, the germline IGHD2-21*02 was identified as the D gene to be in reading frame 3 (**Fig. 6A**). Same analysis identified the CDR3 VL region to belong to IGLV3-1*01 germline, and the J gene to IGLJ1*01 germline (**Fig. 6B**). The IMGT/V-QUEST tool also identified the framework and CDRs in the VL and VH chains by comparison with the closet genes and alleles. The length and sequence corresponding to each region of VH and VL chains are shown according to the IMNGT standardized nomenclature and IMGT unique numbering in a Collier de Perles representation[106] (**Figs. 6A** & **6B**). In addition, the homology model of 16D11 Fab containing the VL and VH chains revealed an $HA_{180-195}$ binding groove built mainly by the CDR3 of both VH and VL regions (**Fig. 6C**). As depicted in **Figure 6**D and **6E**, the surface exposed binding groove specific to $HA_{180-195}$ epitope was mainly made of sequestered non-charged and positively charged areas.

HA cross-reactivity and binding affinity of 16D11 hu-mAb

The homology of the $HA_{180-195}$ epitope among 7 influenza A strains (shown in fig.1A) led to the question as to what extend whether the 16D11 hu-mAb may cross-react with the HA

proteins of these virus strains. ELISA showed that 16D11 hu-mAb bound strongly to the PR8

virus, and cross-reacted with the rHA of PR8-H1N1, WSN-H1N1, Aichi-H3N2, Hokaido-H5N3,

and Vietnam-H5N1 viruses, but not of Memphis and Hong Kong viruses (**Fig. 7A**). The 8D12,

10B2, 13C10 hu-mAbs and the human sera (positive control) also bound to the PR8 virus and

cross-reacted in ELISA with the rHA of the same 5 virus strains recognized by 16D11 hu-mAb,

but not with the rHA of Memphis and Hong Kong viruses (data not shown).

We next measured the affinity and kinetics of the 16D11 interaction with rHA of PR8

and Hokkaido viruses (to which 16D11 and the other hu-mAbs showed the strongest binding in

ELISA, **Fig. 7A**), and the affinity and kinetics of the 16D11 interaction with rHA of Memphis

(to which none of the hu-mAbs antibody bound in ELISA). Control IgM/λ isotypes for the

kinetics and binding affinities included the 25-3 and 8A4 hu-mAbs generated in DRAGA mice

and lacking specificity for the rHA of all 7 investigated influenza virus strains (data not shown).

The affinity and kinetics parameters were measured by Surface Plasmon Resonance (SPR) in a

Biacore3000 instrument (see materials and methods section). We first compared the binding of

16D11 at 200 nM to the rHA of PR8, Hokkaido, and Memphis viruses. SPR revealed a direct and

strong interaction of 16D11 hu-mAb with the rHA of PR8 and Hokkaido viruses, but not of

Memphis virus (**Fig. 7B**). Thus, SPR sensograms confirmed the ELISA results showing the lack

of 16D11 cross-reactivity with the rHA of Memphis virus. The kinetics and affinity interactions

of 16D11 hu-mAb with the rHA of PR8 (**Fig. 7C**) and Hokkaido (**Fig. 7D**) viruses showed

similar ka, kd, and KD values. Both interactions were characterized by a fast association constant

(ka) of 22.4-25.8 x10^{+3} M-1 s-1, and slow dissociation (kd) constant of 4.39-3.32 x10^{-3} s-1 with

affinity binding in the nano molar range (199 and 130 nM, respectively). Based on the

dissociation rate, the half-life time for 16D11 hu-mAb/rHA-PR8 complex was 2.6 minutes and

3.5 minutes for 16D11hu-mAb/rHA-Hokkaido complex (**Table 1**). These data revealed similar kinetics and binding affinities for the interaction of 16D11 hu-mAb with rHA of Hokkaido and PR8 viruses, and confirmed the ELISA data showing its lack of cross-reactivity with the rHA of Memphis virus, and its cross-reactivity with the rHA of 5 influenza viruses.

Neutralization of PR8/A/34 influenza virus by HA$_{180-195}$-specific hu-mAbs

We next measured the neutralization capacity of HA$_{180-195}$-specific hu-mAbs against the PR8 virus by hemagglutination inhibition assay (HIA). The results depicted from **Table 2** show that 16D11 hu-mAb has the highest neutralization capacity at 12.5 μg/ml, as compared with 10B2 hu-mAb at 50 μg/ml, and 6C2 (clone #2) and 13C10 hu-mAbs at 100 μg/ml. The 25-3 hu-mAb isotype control show no neutralization activity against PR8A/34 virus up to 300 μg/ml. The positive control for this assay that neutralized PR8/A/4 virus at 1/160 dilution was a human repository sera (HRS) from an individual vaccinated with seasonal CIV.

Testing the murine xenogeneic response to 16D11 hu-mAb.

Xenogeneic immune responses to murine and "partially" humanized antibodies can significantly lower their therapeutic efficacy[77-83]. Herein, we questioned whether a xenogeneic system like a wild type mouse model for influenza infection would be the appropriate approach to test the potential therapeutic effect of 16D11 hu-mAb. We first measured the murine antibody response to 16D11 hu-mAb _vs_. its lifespan in the blood of BALB/c mice. For this, BALB/c mice were injected intraperitoneally (i.p.) once or twice with 600 μg of 16D11 hu-mAb and 9 days later the murine primary antibody response to 16D11 hu-mAb was measured by ELISA. Data

depicted in **Fig. 1SA** revealed a strong and early murine IgM anti-16D11 hu-mAb response, which may explain the 99.7 % loss of 16D11 in the BALB/c blood circulation. Some 1.8 μg and respectively 2 μg of remaining 16D11 hu-mAb were detected by ELISA in the sera of BALB/c mice, 9 days post injection (**Fig. 1SB**). In contrast, the same experiment carried out in DRAGA mice showed that 12% of 16D11 hu-mAb was still present in the blood circulation of DRAGA mice, 9 days after i.p. injection of 600 μg (not shown). This indicated that the lifespan of 16D11 hu-mAb in BALB/c mice was 40 times shorter than in DRAGA mice. To find out whether a significant loss of 16D11 hu-mAb in the BABL/c blood circulation may interfere with its therapeutic potential, PR8 lethally-infected BALB/c mice were i.p. injected with 600 μg of 16D11 hu-mAb 2 hours prior infection, and their body-weights was monitored every other 3rd day. Data in **Figure 2S** show no significant difference in the rate of body-weight loss between infected *vs*. infected and treated BALB/c mice during a 20 day period of follow up. Together, the results showing a strong murine antibody response against 16D11 hu-mAb *vs*. its significantly short lifespan in BALB/c blood circulation, as well as the lack of therapeutic effect of this antibody in PR8-infected BALB/c mice, strongly suggest that a xenogeneic murine response may have interfered with its potential anti-flu therapeutic effect.

Modeling the PR8 virus infection in DRAGA mice

To avoid possible murine xenogeneic interference with the *in vivo* effect of 16D11 hu-mAb, we thought that DRAGA mice having the murine immune system replaced with a functional human immune system would be an appropriate model for testing its anti-flu therapeutic effect. For this, we first investigated whether DRAGA mice are suitable for PR8 virus infection. The results in **Figure 8A** show that DRAGA mice (n=6) inoculated intranasally

(i.n.) with a sub-lethal dose (LD$_{25}$) of PR8 virus did not lose weight post-infection except for one

mouse with a 5% temporary loss while HA viral RNA was detected in the lungs. The HA viral

RNA was totally cleared between day 7 and 14 post-infection according to RT-qPCR (**Fig. 8B**),

and afterwards mice were considered free of infection. Furthermore, just like BALB/c mice,

DRAGA mice were able to sustain a PR8 i.n. lethal infection for 2 to 3 weeks (**Fig. 8C** & **8D**).

These experiments clearly demonstrated that the DRAGA mouse is a suitable model for

influenza infection, and thereby appropriate to assess the *in vivo* anti-flu effect of 16D11 hu-

mAb.

Testing the anti-flu effect of 16D11 hu-mAb in DRAGA mice.

Since 16D11 hu-mAb showed the highest *in vitro* neutralization capacity against

PR8A/34 virus among all four anti-HA$_{180-195}$ hu-mAbs, we tested its *in vivo* effect against lethal

infection with PR8 virus. Having established the DRAGA mouse model for PR8/A/34 virus

infection, we injected a single i.p. dose of 16D11 hu-mAb (600 µg/mouse) in these mice at the

time of i.n. lethal infection. Control groups were: (i) non-infected/untreated mice (control naïve

group), (ii) lethally-infected/untreated mice (control infection group), and (iii) lethally-infected

and treated with isotype control 25-3 hu-mAb. All DRAGA mice showed 15.1 to 35.6% CD19$^+$

B cells and 14.2 to 22.9% CD3$^+$ T cells in blood circulation on day 0 of this experiment.

DRAGA mice in the control infection group started to rapidly lose weight by day 2 post-

infection and survived 2 to 3 weeks post-lethal infection (**Fig. 9A & 9B**). Lung analysis at the

time of death in mice from control infection group showed massive damage to the lungs with

extensive lymphocyte infiltration, bleeding, and distorted alveolar architecture (**Fig. 9C,** lower

panels). In contrast, all treated DRAGA mice started to lose weight 10 days post-infection and

came close to the highest body-weight loss 2 weeks later than those in the control infection group. Interestingly, mice with the lowest number of B-cells (15.1% to 17.5% CD19$^+$ cells) accounted for the shortest survival, whereas those with higher number of B cells (28.4-35.6% CD19$^+$ cells) showed longer survival in both the infection control group and infection/treated group. In contrast, no correlation was found between the survival rates and number of CD3$^+$ T-cells in either group of mice. The most resilient DRAGA mouse to the infection in the infected/treated group showed diminished damage to the lungs, and fewer areas with distorted alveolar architecture and inter-alveolar infiltration with lymphocytes and blood, when compared with the control infection group (**Fig. 9C,** middle panels _vs_. lower panels). The isotype control group (n=3) that was lethally-infected with PR8 virus and treated i.p. with 600 µg/mouse of 25-3 isotope control hu-mAb at the time of infection showed a similar pattern of body-weight loss and rate of survival to that of control infection group (data not shown).

Together, these *in vivo* experiments demonstrated that the DRAGA mouse represents a new humanized mouse model for PR8/A/34 influenza virus infection, and that a single dose of 16D11 hu-mAb targeting a single HA epitope significantly delayed (by more than 2 weeks) death due to PR8/A/34 influenza virus infection.

2.4: Discussion

This study addressed several questions about the bio-applicability of a new humanized mouse strain (DRAGA: HLA-A2. HLA-DR4. Rag1 KO. IL-2Rγc KO. NOD). We first questioned whether DRAGA mice can be used to generate "fully" human monoclonal antibodies (hu-mAbs) targeting a homologous HA epitope among different influenza type A virus heterotypes (WSN-H1N1, Adachi-H3N2, Aichi-H3N2, Memphic-H3N2, VN1194-H5N1,

Hokkaido 67-H5N3, and W213-H9N2). The amino acid sequence ([180]WGIHHPPNSKEQQ NLY[195]) of the human B-cell epitope used to raise cross-reactive hu-mAbs in DRAGA mice was chosen from the HA of PR8/A/34 virus and is part of the immunogenic Sb site of HA1 chain[99].

Immunization of DRAGA mice with a KLH-HA$_{180-195}$ conjugate induced IgG and IgM hu-mAbs specific for PR8/A/34 influenza virus, and the hybridization process using K6/H6 human IgM myeloma cells rendered 4 stable, highly IgM/λ−secreting hybriboma cells with specificity for HA$_{180-195}$ epitope. Human anti-flu IgM antibodies can protect against influenza infection, as recent work demonstrated that human IgM$^+$ memory B cells induced upon influenza vaccination secreted cross-protective antibodies to human and avian viruses type A (H5N1 and H1N1 heterotypes)[65,91] and to the Sb antigenic site of HA protein[61]. Our IgM hu-mAbs specific for the HA$_{180-195}$ epitope showed structural integrity and were secreted by the hybriboma cells as pentameric molecules.

The antigen binding site of antibodies resides mostly in the CDR3 pocket of the heavy chain, and the nature of antigens can dictate unique CDR3 amino acid compositions aimed at establishing optimal interaction with the antigen[16,107]. Interestingly enough, although the same HA$_{180-195}$ epitope was used in this study for immunization, all selected hu-mAbs recognized this epitope found in HA and with 16D11 hu-mAb showing the highest amino acid diversity in the CDR3 VH region. The high CDR3 structural diversity of 16D11 hu-mAb was attributed to immunization-induced B-cell hypermutations in DRAGA mice. Similar observations were reported by Tsibane et al[47,108,109] showing that two different human monoclonal antibodies (1F1 and HC63) isolated from influenza-infected individuals and recognizing the same HA epitope shared by 1918, 1943, and 1977 influenza A-H1N1 heterotypes, displayed amino acid diversity with respect to the antigen binding site in CDR3 VH region. The authors showed that 1F1 and

HC63 hu-mAbs used similar germline V, D, and J regions to assemble the CDR3 region of the heavy chain. On the other hand, two human monoclonal antibodies using similar V, D, and J gene segments for the heavy chain but having different light chains, displayed different virus neutralization capacity, as one of them cross-neutralized three different H1N1 influenza heterotypes and the other one did not[47,110]. These data, together with our SPR sensograms, strongly suggest that amino acid composition in the HA receptor binding pocket of CDR3 VH region may affect not only the binding strength, but also the unique 3D folding of the antibody-HA binding site.

Among hu-mAbs specific for the $HA_{180-195}$ epitope generated in this study, the 16D11 hu-mAb showed the highest neutralization capacity *in vitro* against PR8/A/34 influenza virus, and cross-reacted with the HA viral protein from PR8, WSN, Aichi, Hokkaido and Vietnam influenza heterotypes. SPR sensograms revealed that 16D11 hu-mAb has relatively high binding affinity to the HA protein of PR8 and Hokkaido viruses, and it forms stable and long half-life 16D11-rHA complexes in solution. In contrast, the failure of 16D11 hu-mAb to recognize the HA proteins from Memphis and Hong Kong viruses was attributed to low binding affinity constants. A 100% homology of $HA_{180-195}$ epitope at the positions 181-186 in all studied virus strains except the Memphis virus, suggested that these residues are critical for the $HA_{180-195}$ helicoidally and/or interaction with our $HA_{180-195}$-specific hu-mAbs. In addition, the $HA_{180-195}$ epitope of Memphis and Hong Kong viruses lacks a conserved histidine at position 183 and a glutamic acid at position 191, and these substitutions could also be critical for maintaining the epitope helicoid structure required for the interaction with our $HA_{180-195}$-specific hu-mAbs.

Xenogeneic antibodies can significantly lower and even abolish an antibody-based therapy[77-83]. This was likely the case of our 16D11 hu-mAb, which showed a very short lifespan

and anti-flu effect in BALB/c mice. In contrast, a considerably longer lifespan of 16D11 hu-mAb (40x) was detected in DRAGA mice. Based on previous reports and our data, one may consider that "fully' human antibodies lacking xenogeneic reactions would be more efficient therapeutics when administered repeatedly in humans, though a number of "partially" humanized antibodies were quite successful in clinical trials for infectious disease, cancer, and autoimmune diseases. To rule out any possible murine xenogeneic interference with the *in vivo* effect of our 16D11 hu-mAb, and considering that DRAGA mice are suitable for sub-lethal and lethal infections with PR8A/34 virus, we used these mice to assess the *in vivo* anti-flu effect of 16D11 hu-mAb. PR8 lethally-infected DRAGA mice, treated with a single dose of 16D11 hu-mAb, showed a significant 2-week delay in body-weight loss and survival as compared with those infected and left untreated. Treated mice also showed less lung damage, which suggests delayed viral replication in the lungs. It remains to be further investigated whether repeated injections of 16D11 hu-mAb, or a cocktail of broadly cross-neutralizing hu-mAbs targeting several conserved HA epitopes, may provide better therapeutic efficacy than a single injection of a hu-mAb targeting a single conserved HA epitope. Cross-neutralization provided by a cocktail of antibodies targeting multiple HA viral epitopes may overcome seasonal mutations.

In summary, this work demonstrated first, that the DRAGA mouse is a reliable tool to generate heterotype cross-reactive, human anti-influenza monoclonal antibodies. Secondly, our results showed that the DRAGA mouse is the first humanized animal model for influenza infection. Since DRAGA mouse can sustain the malaria cycle of *Plasmodium falciparum*[37], as well as HIV[39] and Dengue infections (manuscripts in preparation), one may consider that this mouse can be used to establish humanized mouse models for various infectious diseases including those of potential biological threat or resistance to antibiotic therapy. Thirdly, our

results demonstrated that DRAGA mice can be used to assess the therapeutic effect of heterotype

cross-reactive, human anti-influenza monoclonal antibodies.

2.5: Materials and Methods

Mice

BALB/c female mice of 4 months of age were purchased from Jackson Labs. Humanized mice like DRAGA mice (HLA-A2.1. HLA-DR-0401. Rag1 KO. IL-2Rγc KO. NOD) are generated and reconstituted with human immune system in our laboratory as described below[31,36]. The humanized mice (DRAGA) were monitored twice a month by FACS for human T and B cell reconstitution and by ELISA kits for the amount of antibodies in sera, and used in experiments at the age of 5-6 months when full reconstitution was achieved. All animal procedures were conducted under IACUC protocols approved by USUHS (ID#MED-14-902) and WRAIR/ NMRC (ID#16-IDD-43) in compliance with the Animal Welfare Act and in accordance with the principles set forth in the "Guide for the Care and Use of Laboratory Animals," Institute of Laboratory Animals Resources, National Research Council, National Academy Press, 1996.

Generation of HA$_{180-195}$-specific hu-mAbs

We have recently reported the generation of a new humanized mouse strain (DRAGA mice, NOD/Rag1 KO/IL-2Rγc KO/HLA-DR*0401$^+$, HLA-A2.1$^+$) that can reconstitute functional human T and B cells upon infusion of CD34+ human hematopoietic stem cells (HSC)[42]. Briefly, HLA-DRB1*0401$^+$ umbilical cord bloods (UCB) purchased from AllCells and Promocell were enriched for CD34$^+$ stem cells to more than 60% when using EasySep, Human Progenitor Cell Enrichment kit (StemCell Technologies, Vancouver, BC). Three month-old female/male DRAGA mice were irradiated (350 rads) and then injected intravenously with 8x10^5 CD34$^+$-enriched stem cells. The extent of human T and B cell reconstitution was monitored weekly by

FACS using human CD3 Ab and respectively, human CD19 Ab. In parallel, mice were monitored for the levels of human IgM and IgG in sera by ELISA kits (Bethyl Laboratories) according to the manufacturer's instructions. Three HSC- reconstituted DRAGA mice (six months of age) showing between 1.0 and 1.5 mg/ml of human serum IgM and IgG were then immunized intraperitoneally (i.p.) with 100 μg/mouse of KLH-$HA_{180-195}$ conjugate in complete Freund's adjuvant (CFA) or poly (I:C),and boosted two weeks later with 100 μg/mouse of the same conjugate in incomplete Freund's adjuvant or poly (I:C), respectively. The levels of $HA_{180-195}$-specific and PR8-specific IgG and IgM hu-mAbs in sera were monitored weekly by ELISA using BSA-$HA_{180-195}$ coated plates (100 μg/ml) and PR8 virus (Charles Rivers) coated plates (50 μg/ml), and bound antibodies were revealed with goat anti-human IgM-HRP (Thermo Fisher Scientific) and respectively, goat anti-human IgG-HRP (Bethyl Laboratories) on a TMB (3,3', 5,5' tetramethylbenzidine, BD Biosciences) according to the manufacturer's instructions. To generate human hybridoma cells, spleen cells from immunized DRAGA mice were fused with K6H6/B5 myeloma cell partner (ATCC® CRL-1823™) using ClonaCell-HY Hybridoma kit (cat #03800, StemCell Technologies, Inc.) according to the manufacturer's instructions. Stable hypoxanthine-aminopterin-thymidine (HAT, Sigma Aldrich) hybrids were then cloned, and positive clones were re-cloned at 0.1 cell/well in 96-well plates in HAT-supplemented DMEM with 20% FCS. High and stable producers were confirmed by ELISA in plates coated with BSA-$HA_{180-195}$ conjugate or PR8 virus. Secreted IgM hu-mAbs specific for $HA_{180-195}$ were purified from the cell culture supernatants by affinity chromatography on Sepharose CL-4B (GE Healthcare Life Sciences) coupled to goat anti-human IgM Abs (Helena Labs), and dialyzed/concentrated on Amicon filter units (#UFC710008, Millipore) with 100 kDa molecular weight cut-off.

SDS-PAGE

Samples containing 1 µg of affinity-purified hu-mAbs were denatured at 100°C for 5 min in Laemmli sample buffer (Bio-Rad) containing 5% 2-mercaptoethanol, and subjected 1 h to 100 volts electrophoresis in 4-20% Mini-Protean TGX gels (Bio-Rad). Gels were silver stained and analyzed for hu-mAbs purity and the molecular weight of the hu-mAbs heavy and light chains.

Size exclusion chromatography

To determine whether the native hu-mAb molecules were properly assembled, we measured their molecular weight by a FPLC Superose 12 column coupled to an AKTA prime plus instrument (Amersham Biosciences, GE, Co). The samples, molecular markers, and column were equilibrated in PBS and samples were run at 1 ml/min flow-rate.

Immunoelectrophoresis

Isotyping and monoclonality of anti-HA hu-mAbs was carried out by visualization of hu-mAbs by immunoelectrophoresis (IEP kits, Helena Labs.). Some 5 µg of purified hu-mAbs in 5 µL barbital buffer were electrophoresed on pre-casted 1% agarose gels, and stained according to the manufacturer's instructions.

Titan-gel electrophoresis

Monoclonality of the anti-influenza hu-mAbs was also confirmed by protein electrophoresis in Titan agarose gels (Protein Titan gels, Helena Labs) according to the manufacturer's instructions.

Briefly, 15 μg of purified hu-mAbs in 5 μL barbital buffer were applied on the gel and electrophoresed for 60 min at 150 Volts. Gels were stained with Coomassie Brilliant Blue Stain for 30 min at room temperature, dried under hot air blower, and de-stained as per manufacturer's instructions.

Enzyme-Linked Immunosorbent Assays (ELISA)

ELISA was used to select positive hybridoma clones secreting anti-HA hu-mAbs and to isotype these antibodies, to determine the cross-reactivity of hu-mAbs to rHAs from various influenza virus heterotypes, to measure the BALB/c mouse Ab response to anti-HA hu-mAb treatment and to PR8 virus infection, and to determine the lifespan of 16D11 anti-HA hu-mAb in the circulation of BALB/c mice. Selection of stable hybridoma clones secreting anti-HA hu-mAbs in the cell culture supernatant and isotyping the affinity-purified hu-mAbs by these clones was carried out by semi-quantitative ELISA kits (Bethyl Laboratories) according to the manufacturer's instructions. Cross-reactivity of hu-mAbs to rHAs from various influenza virus heterotypes was measured in 96-well plates were coated overnight at 4°C with 20 μg/ml of recombinant HA proteins from A/Puerto Rico/8/1934 (Cat# 11684-V08H), A/WSN/1933 (Cat# 11692-V08H), A/Aichi/2/1968 (Cat# 11707-V08H), A/Memphis/1/1968 (Cat# 40101-V08H1), A/Vietnam/1194/2004 (Cat# 11062-V08H1), A/Hokkaido/167/2007 (Cat# 11696-V08H), and A/Hong Kong/2009 (Cat# 40174-V08H1) (Sino Biological) in 0.05M Bicarbonate buffer at pH 9.6. Coated plates were blocked with 5% BSA in 1X PBS overnight at 4°C, and hu-mAbs (5 μg /ml) were added to the plate and incubated for 2 h at room temperature. Plates were washed 3 times with 1X PBS containing 0.05% Tween, and secondary goat anti-human μ-chain-HRP

conjugate (ThermoFisher Scientific) was added at 1:2,000 dilution for 1 h at room temperature.

Plates were washed 3 times with 1X PBST, TMB substrate (BD Biosciences) was added to the

wells for 10 minutes followed by stop solution (0.18M H_2SO_4), and the optical density (OD) was

read at 450 nm in an ELISA reader (Molecular Devices). To measure the BALB/c mouse

xenogeneic response to anti-HA hu-mAbs, mice were injected i.p. with 250 μg of 16D11 hu-

mAb on days 1 and 2, and 7 days later harvested sera at 1:100 dilution was incubated overnight

at 4^0 C in 96-well plates coated with 16D11 hu-mAb (5 μg/well). Plate was blocked with 5%

BSA in 1X PBS for 2 h at room temperature, washed 3 times with 1X PBS containing 0.05%

Tween, and a secondary goat anti-IgM-HRP conjugate (Jackson Labs.) was added at 1:20,000

dilution for 2 h at room temperature. Plates were washed 3 times with 1X PBST, and TMB

substrate (BD Biosciences) was added to the wells for 10 minutes followed by stop solution

(0.18M H_2SO_4). Optical density (OD) was read at 450 nm in an ELISA reader (Molecular

Devices). To determine the lifespan of anti-HA hu-mAbs in the circulation of BALB/c mice, sera

from the same BALB/c mice treated with 16D11 hu-mAb described above was harvested and 7

days post-injection and the amount of remaining 16D11 hu-mAb was measured by semi-

quantitative ELISA kits (Bethyl Laboratories) according to the manufacturer's instructions.

Western Blot analysis

Isotype confirmation of hu-mAbs by ELISA kits (Bethyl Laboratories) was carried out by

Western blot analyses. Briefly, hu-mAbs separated in SDS-PAGE gels were transferred to

nitrocellulose (NC) membranes in semidry conditions using an semi-dry iBlot electro-transfer

equipment (ThermoFisher Scientific), and blocked overnight in 5% powdered milk plus 3% BSA

in 1X PBST. Triplicate NC membranes were then probed for 2 h at room temperature with goat

anti-human μ-chain-HRP conjugate (ThermoFisher Scientific), or goat anti-human λ-chain-HRP

conjugate (Southern Biotech.), or goat anti-human k-chain-HRP conjugate (Southern Biotech.)

followed by 3 washes in 1X PBST and exposed 10 min to SuperSignal West Pico

Chemiluminescent Substrate (ThermoFisher Scientific).

Rapid Amplification of cDNA Ends (RACE) for hu-mAbs sequencing

RACE procedure was used for amplification of heavy and light chain genes. Total RNA was

extracted from hybridoma cells using RNeasy Mini Kit (Qiagen), and cDNA synthesized using

our designed primers, IgM-Mu-R primer for heavy chain (5'-AACGGCCACGCTGCT

CGTATC 3'), and Lambda-new-R primer for light chain (5'-TATGAACATTCTGTAGGGGC-

3'). After the first strand of cDNA synthesis, the original mRNA template was removed by

treatment with the RNAse mix. Unincorporated dNTPs, primers, and other proteins were

separated from cDNA using the S.N.A.P. column. Terminal deoxynucleotidyl transferase (TdT)

was used to add homopolymeric tails to the 3' ends of cDNA, and tailed cDNA was then

amplified by PCR using 5' Abridged Anchor Primer (5'-GGCCACGCGTCGACTAGTACGGG

IIGGGIIGGGIIG-3') and a primer specific to IgM heavy chain (5'GGAGACGAGGGGGAA

AAG-3') or light chain primers (5'-TGGCTTGAAGCTCCTCAGAG-3'). PCR amplified

products were run in 1% LMP Agarose gel (ThermoFisher Scientific) using cyan/yellow tracker

dye (ThermoFisher Scientific). Bands corresponding to the molecular weights of expected

cDNA products were excised from the gel and extracted using QIAquick gel extraction kit

(Qiagen). Briefly, gel slices were weighed and three volumes of buffer QG were added to one

volume of gel, and then incubated at 50°C for 5 min. Samples were vortexed every 2-3 min to

help dissolve the gel. One gel volume of isopropanol was added to the sample and mixed.

Sample was applied to QIAquick column and centrifuged for 1 min at 13,000 rpm. Flow through was discarded, 500ul of Buffer QG was added to the QIAquick column and then centrifuged for 1 min at 13000 rpm. To wash column, 750ul of buffer PE was added to the QIAquick column, and then centrifuged for 1 minute. Flow through was discarded, and QIAquick column placed into a clean 1.5 ml microcentrifuge tube. To elute DNA, 50ul of DEPC-treated water was added to the column, and allow to incubate for 4 minutes, and then centrifuged. DNA sample for IgM heavy chain was sequenced at USUHS's Biomedical Instrumentation Center facility using primer (5'-GGAGACGAGGGGGAAAAG-3'), and for light lambda chain using primer (5'-TGGCTTGAAGCTCCTCAGAG-3'). Sequencing results were verified using forward primers for the IgM heavy chain (5'-ATGGAGTTTGGGCTGAGCTGG-3'), and light chain (5'-TGG CATGGATCCCTCTCTTC-3').

Evaluation of protective efficacy of hu-mAb 16D11 in DRAGA mice

DRAGA mice (n = 4 mice /group) were treated intraperitoneally with 40mg/kg of body weight of hu-mAb 16D11 (~600 µg per mouse) for two hours before intranasal inoculation with a LD100 dose of mouse-adapted A/PR/8/34 influenza virus (Charles River) under ketamine/xylazine anesthesia. For infection control group, DRAGA mice were infected by intranasal inoculation with a LD100 dose of mouse-adapted A/PR/8/34 influenza virus (Charles River) under ketamine/xylazine anesthesia. Mice were monitored every other 3rd or 4th dpi. Mice were monitored every two to three days for weight changes and survival. A weight loss exceeding 40% was used as experimental endpoint, and mice reaching this endpoint were euthanized.

Reverse Transcription-quantitative Polymerase Chain Reaction (RT-qPCR)

As a positive control for the expression of PR8 HA protein in the lungs, we used RNA extracted from live A/PR/8/34 (H1N1) (Charles River). Briefly, 200ug PR/8 virus was homogenized in RLT buffer using a syringe and a needle. Homogenized sample was used to purify total RNA using RNeasy Mini Kit (Qiagen) following the manufacture's protocol, and then quantitated by a NanoDrop-8000 instrument (ThermoFisher). Serial dilution of viral RNA from influenza virus was used as positive controls to establish limit of detection in gel in RT-qPCR.

To estimate the rate of virus clearance in PR8-infected and treated BALB/c with 16D11 hu-mAb, lungs from individual mice were sectioned, snap frozen, and stored in liquid nitrogen at $-196°C$. Some 30 mg snap-frozen lung tissue was lysed using lysing matrix D and FastPrep-24 instrument (MP Biomedicals) in RLT buffer as follows: 5 cycles at speed of 6 m/s with 5 min rest period in between cycles. Homogenized samples were spun at 14,000 rpm for 10 min at 4°C. Total lung RNA of individual mice was extracted using RNeasy Mini Kit (Qiagen) following the manufacturer's protocol, and then quantitated by a NanoDrop-8000 instrument (Thermo Fisher). 2.5 ug total RNA of each mouse sample was used for reverse transcription with SuperScript™ II Reverse Transcriptase (Fisher; Cat: 18064014). Quantitative PCR (Q-PCR) was performed using an ABI 7500 Real-Time PCR System and software SDS v1.4. Amplification of hemagglutinin (HA) cDNA of influenza virus Puerto Rico/8/A/34 (PR8) was carried out using our designed forward primer 5'- GACACTGTTGACACAGTACTC-3' and reverse primer 5'-AGAGCCATCCGGCGATGTTAC-3. Thermocycling parameters used were: 10 min at 95°C, 30 sec at 95°C followed by 1 min at 60°C. The threshold cycle (CT) is proportional to the number of target copies present in the sample, and is defined as the PCR cycle in which the gain in

51

fluorescence due to accumulating amplicon products exceeds 10 standard deviations of the mean baseline fluorescence. We have used CT data taken from cycles 10 to 28 with CT values higher than 28 considered below the sensitivity limit.

GAPDH was included as an internal control to make sure that a similar amount of starting PCR products were equally loaded in each agarose well. Amplification of cDNA GAPDH internal control from lung of individual corresponding mice was carried out using commercially available forward and reverse primers (Qiagen, Cat: QT01658692). Q-PCR reactions were performed in a total volume of 20 ul in SYBR Green Master Mix (ABI & Thermo Fisher; REF: 4309155) containing forward and reverse primers at 1.25 uM, respectively. The normalized signal level was calculated based on the ratio to the corresponding GAPDH signal. All RT-qPCR samples were electrophoresed at the same starting RNA concentration (before retro-transcription) on a 2% agarose gel containing 0.2% ethydium bromide.

To measure the level of AID expression in naïve and PR8-infected DRAGA mice, 5 ug total splenic RNA from individual mice was used for reverse transcription with SuperScript™ II Reverse Transcriptase using the same RT conditions described above for the HA of PR8 virus, and 45 cycles of PCR amplification. Our designed primers for human AID (forward: GGTTATCTTCGCAATAAGAAC, and reverse: TCGGGCTCAGCCTTGCGGTCC) revealed a 232 base pairs (bp) amplicon in 2% agarose gel electrophoresis.

3D Structural model of 16D11 hu-mAb

A structural model of the 16D11 hu-mAb was generated by using the Rosetta Antibody 3.0 software[111]. The best templates for the VL and VH scaffold identified by Rosetta based of

sequence homology were PDB ID 3mlr for the VL chain and PDB ID 3kdm for the VH chain. "De novo" modeling was requested for modeling the hyper variable CDR3 loop. The model with the best score was selected from the ten models generated by Rosetta antibody 3.0 software. N-terminal and one β-strand of the VL model generated by Rosseta Antibody software was miss folded and iTasser[111] was used to model the VL chain using the structure PDB ID 4aiz as a template. The VL model generated was superposed over the Fab model originally generated by Rosetta Antibody.

PROCHECK, a program to check the stereochemical quality of protein structures[112] was use to assess the quality of the 16D11 model. From the 189 non-glycine and non-proline residues contained in the VL-VH model, 81% are in the most favorable region of the Ramachandran plot. PDB files were visualized with UCSF Chimera software[113]. Chimera was also used for Coulomb surface coloring representation and to generate the 16D11 structure figures. Arrows to the encircled brown areas indicate the architecture of antibody combining site made between the CDR3 regions of VH and VL chains.

Surface Plasmon Resonance (SPR) analysis

SPR was used to measure the binding kinetics of hu-mAbs to HA protein of PR8/A/34 virus using a Biacore 3000 instrument (GE Healthcare). Briefly, rHA protein from several influenza A viral strains were coupled via amine-coupling procedure to the flow cells of CM5 sensor chip until levels of 2000, 1500 and 1000 resonance units were reached. Hu-mAbs at concentrations ranging between 200 to 1.25 nM diluted in 0.01 M HEPES buffer, pH 7.4, 0.15 M NaCl, 3mM EDTA, and 0.005% (v/v) Surfactant P20) (HBS-EP) were injected separately into the flow cells at 30 μL/min and 25°C during the 2 min association phase using HBS-EP as running buffer. The

dissociation phase, initiated by passage of HBS-EP buffer was carried out over a period of 4 min. Collected sensograms were aligned and fitted to a 1:1 Langmuir binding model using BIAevaluation software v4.1.1 to calculate the affinity and kinetics (K_D, ka and kd) constants between the 16D11 hu-mAb and rHAs from several influenza virus heterotypes. The kinetic constants were determined from fitting containing 6 concentration sensograms. Rmax values for the 16D11-Hokkaido and 16D11-PR8 interaction were 38.4± 0.1 and 44.7±0.4, respectively. All binding curves were corrected for background and bulk refractive index contribution by subtraction of the reference flow cells. To further validate the kinetics and affinity calculations, we tried to perform the SPR experiments by immobilizing the 16D11 hu-mAb on a CM5 chip surface and subsequently inject the rHA proteins, but immobilization of 16D11 by amine coupling was not possible, probably due to the low isoelectric point of the hu-mAb.

Hemagglutination inhibition assay (HIA)

Virus neutralization capacity of hu-mAbs was measured by hemagglutinin inhibition assay (HIA), as we previously described[114]. Briefly, 5 ml of fresh chicken red blood cells (RBC, Lampire Biologicals Labs) were first washed with 1X PBS at 1,200 rpm at 4°C until the supernatant was clear of hem lysate. To establish the hemagglutination titer of the virus, mixtures of 2 fold dilutions of PR8 virus (Charles River) in 1% chicken red blood cells (RBCs) were suspended 60 min at room temperature in 1X PBS in round-bottom 96 well plates. To determine the hemagglutination inhibition titer of hu-mAbs, the hu-mAbs at 200 μg/ml were serially diluted with 1X PBS in 96 well round bottom plates, and a standardized influenza virus concentration was added to the wells in the presence of 1% chicken RBCs for 2 h at room temperature. The HI

titer was defined as the minimum concentration of antibody that inhibit hemagglutination of 1% chicken RBCs.

Hematoxilin-Eosin (HE) staining of lung sections

Lungs from naive and infected mice with PR8 virus were fixed in formalin 10%, and 5 μ sections were stained with HE according to a standard technique to analyze the alveolar architecture and lymphocyte infiltration.

Biostatistics

Body-weight curves were compared by the Mantel-Cox log rank test, and for statistical significance by pairwise curves comparison by Gehan-Breslow-Wilcoxon test with Bonferroni's corrected threshold of significance for multiple groups. Statistical comparisons were made between PR8-infected *vs*. PR8-infected and treated groups of mice.

Disclosure of potential conflicts of interest. The authors declare no potential conflicts of interests.

work of the United States Government.' Title 17 U.S.C. §101 defines a U.S. Government work

as a work prepared by a military service member or employee of the U.S. Government as part of

that person's official duties. The views expressed in this paper are those of the authors and do not

necessarily represent the views of Uniformed Services University, Department of Defense, or

other Federal Agencies.

2.6: Figure and figure legends
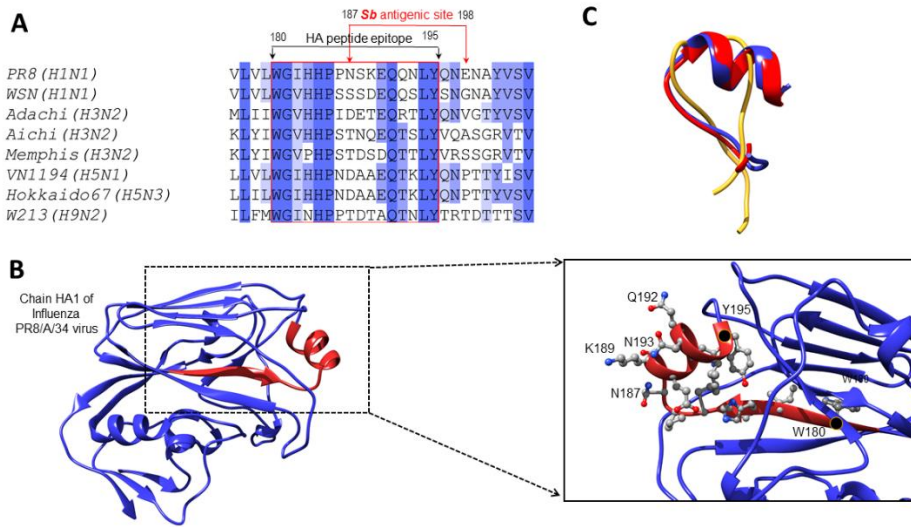
Figure 1. *HA$_{180-195}$ epitope homology among different influenza virus heterotypes.* (**A**) Sequence alignment of the HA proteins from several influenza virus strains and homologous residues 180-195 comprising part of the Sb antigenic site. (**B**) Ribbon representation of the HA protein (PDB ID 1ru7:A, residues 54-270) revealing the Sb antigenic site in red. Shown is a detailed view of the Sb antigenic site, the 180-195 residues side chains in ball and stick representation together with their carbon atoms colored in grey, nitrogen in blue and oxygen in red. The first and last residues of the Sb site are indicated with a black dot and labeled, and the highly exposed residues of the HA$_{180-195}$ epitope located within the α-helix are labeled. (**C**) Overlapped conformations of soluble HA$_{180-195}$ epitope from PR8/A/34 (red ribbon), Memphis (yellow ribbon) and Hokkaido (blue ribbon) viruses according to "de novo" modeling approach and PEP-FOLD server (described in materials and methods section).
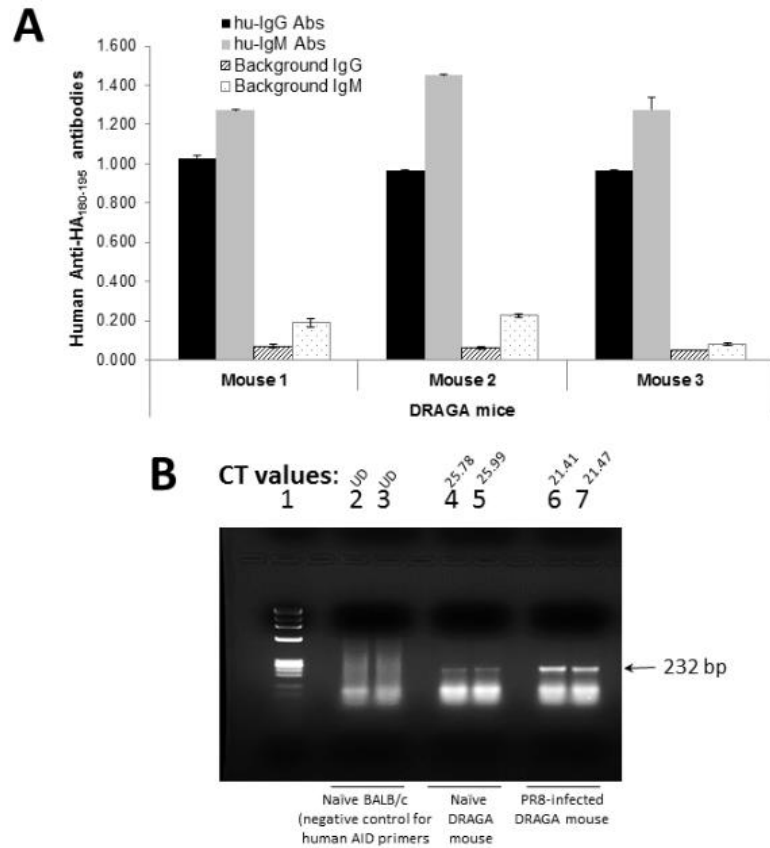
Figure 2. *HA$_{180-195}$ specific hu-Ab responses and human AID expression in DRAGA mice.* (**A**) DRAGA mice were immunized and boosted 2 weeks later with KLH-HA$_{180-195}$ conjugate. Two weeks after the boost, sera of immunized mice were assessed in ELISA plates coated with rHA of PR8 virus (2 μg/well) for titers of human anti-HA$_{180-195}$ IgM and IgG antibodies. Shown are the specific antibody titers for 3 representative mice and their corresponding signal-to-noise background of secondary antibody. (**B**) DRAGA mice (n=3) were infected or not by the intranasal route with a lethal dose of PR8 /A/34 virus (LD$_{100}$) and 7 days later the splenic RNA was extracted and analyzed by RT-qPCR using our designed primers for human AID (described in the Materials and Methods section). One representative DRAGA infected mouse (lanes 6 and 7) and naive DRAGA mouse (lanes 4 and 5) are shown. Negative control for human AID primer specificity was splenic RNA extracted from naive BALB/c mice (lanes 2 and 3). The CT values

for duplicate samples are shown for each mouse. Arrow indicates the size of human AID amplicon.
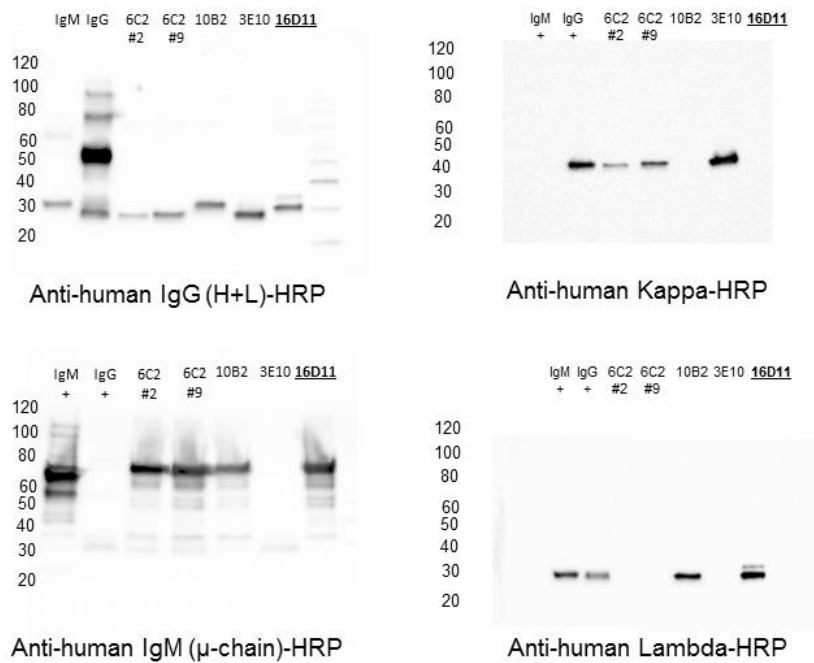
Figure 3. *Western Blot isotyping of HA$_{180-195}$ specific hu-mAbs.* Shown are the HA$_{180-195}$ specific hu-mAbs selected for this study as assessed by Western blot for the presence of IgG and IgM heavy and light chains. Affinity purified hu-mAbs were SDS-denatured and 2ME-reduced, applied at 5 µg/lane in 8-16% gradient gels of polyacrylamide, separated by SDS-PAGE, gels electro-transferred onto PVDF membranes, and the membranes were probed with specific antibodies for the µ, γ, κ, and λ chains followed by incubation with species-specific secondary Abs-HRP conjugates, as indicated in each panel.
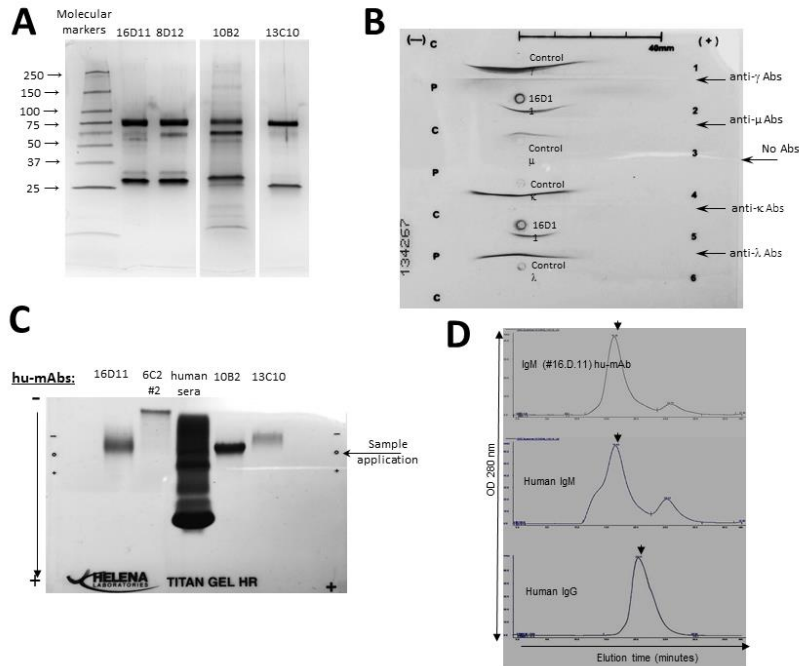
Figure 4. *Structural analyses of anti-HA$_{180-195}$ hu-mAbs*. (**A**) Silver stain of 8-16% gradient

SDS-PAGE gels ran under denaturing and reducing condition for four affinity purified, HA$_{180-195}$

specific hu-mAbs at 1 μg/lane. (**B**) Immunoelectrophoresis of 16D11 hu-mAb showing the

monoclonal bands of human μ heavy chain and human λ light chain as compared with the human

polyclonal μ heavy chain and λ light chain. (**C**) Agarose Titan gel analysis showing the

monoclonality and difference in the electrophoretic mobility of HA$_{180-195}$ specific hu-mAbs. (**D**)

Histograms of FPLC analysis showing intact pentameric molecules of 16D11 hu-mAb. Arrows

in each histogram indicates the earlier elution time for 16D11 IgM and control human IgM

pentameric molecules than for human control IgG monomeric molecules as detected at 280 nm.
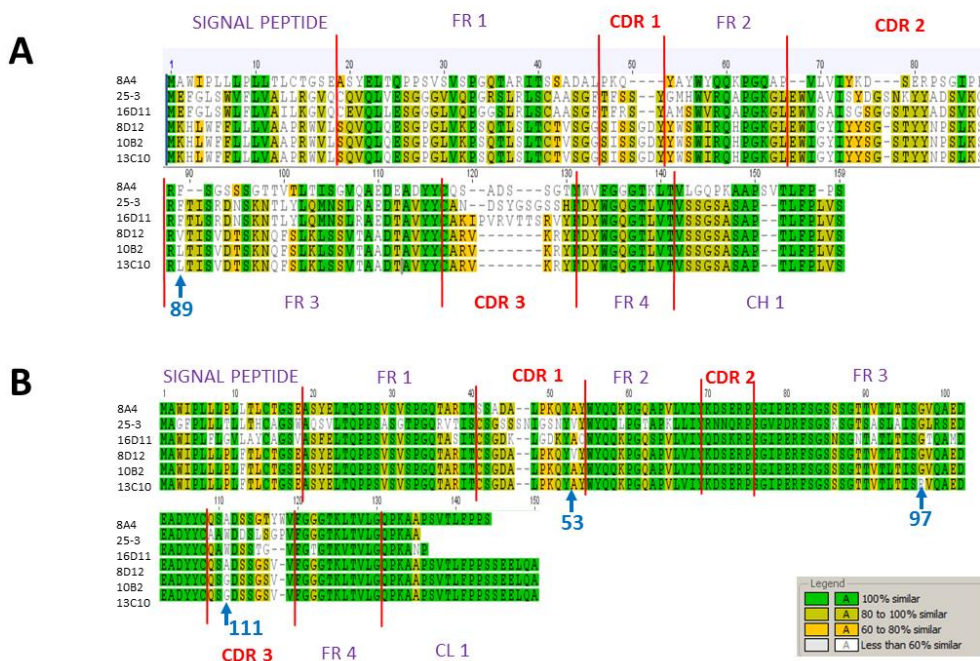
Figure 5. *Amino acid sequences of CDR3 VH and VL regions of hu-mAbs and their isotype controls.* (**A**) CDR3 VH sequences of four $HA_{180-195}$ specific IgM hu-mAbs (16D11, 10B2, 8D12, and 13C10) and two non-specific, isotype control IgM/lambda hu-mAbs (8A4 and 25-3 hu-mAbs). (**B**) CDR3 VL sequences of the same hu-mAbs as in panel A. Shown are the signal peptides for both the heavy and light chains, the flanking frame regions FR1 to FR4, the CDR3s, and 10 amino acids adjacent to constant regions CH1 and CL1. Similar amino acid residues among all hu-mAbs are highlighted in green, those with more than 80% similarity in light green, those between 60 to 80% similarity in yellow, and those with less than 60% similarity are left uncolored. Blue arrows indicate the position where amino acid differences occurred for 10B2, 8D12, and 13C10 hu-mAbs.

Figure 6. *Germline identification and 3D homology model for 16D11 hu-mAb.* (**A**) Sequence alignment of the VH and VL chain of 16D11 hu-mAb and their corresponding germline sequences. Sequence corresponding to the CDRs are colored, and those corresponding to the V, D and J genes are indicated at the top of each alignment. Protein sequence corresponding to the junction is highlighted in gray. Dots indicate sequence conservation, and dashes indicate gaps. (**B**) *Colliers de Perles* representation of the VH and VL protein chains. Residues corresponding to CDR loops are colored as in A, and square boxes represent the boundary residues between the framework and the CDR loops. Positions with red and bold letters indicate the five-conserved position of a V domain. (**C**) Ribbon and surface representation of the homology model of 16D11 Fab showing the VH and VL chains in dark, and respectively light grey. CDR loops are labeled

and colored as in B. (**D**) Coulomb surface coloring of 16D11 homology model. (**E**) Showed are the areas with no potential charges in red and positive charges in blue.
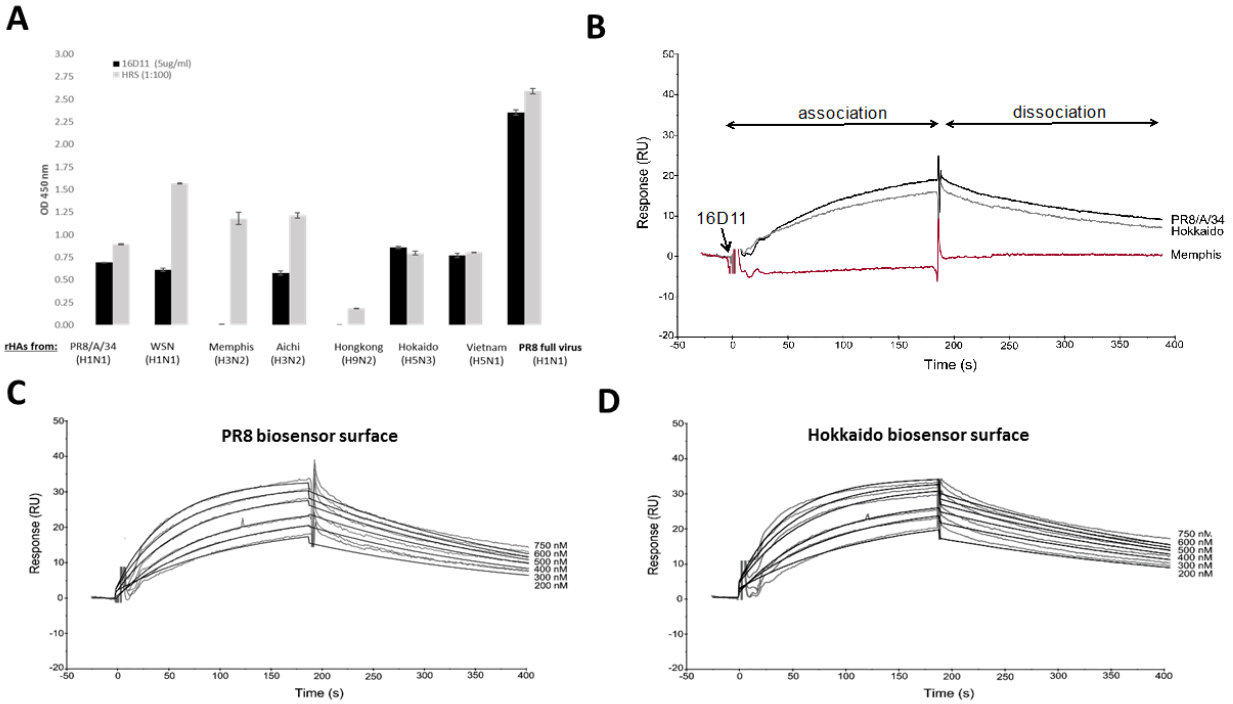
Figure 7. *HA cross-reactivity and binding affinity of 16D11 hu-mAb.* (**A**) Binding of 16D11 hu-mAb to rHA proteins from influenza virus heterotypes in ELISA. Shown are duplicate rHAs-coated wells and+/- SD for 99% confidence. Signal-to-noise background of the anti-human IgM-HRP secondary antibody (OD 450 nm = 0.045 average) has been subtracted from each sample. PR8 virus-coated wells and repository human sera (HRS) were used as controls. (**B**) SPR comparative binding of 16D11 hu-mAb at 200 nanoMoles to rHA proteins of PR8/A/34 virus (black), Hokkaido virus (grey) and Memphis virus (red). 16D11 injection point and association and dissociation phases are indicated. Representative Sensograms of different concentrations of 16D11 hu-mAbs across biosensor surfaces coupled to rHA protein of PR8 virus (**C**) and Hokkaido virus (**D**) at 30 µl/min and 25°C. Sensograms were analyzed using a simultaneous fit algorithm (BIAevaluation 3.1) to calculate the kinetic parameters and binding affinities (as shown in Table 1). SPR sensograms for each response are shown as gray lines whilst fit analyses are shown as black lines.
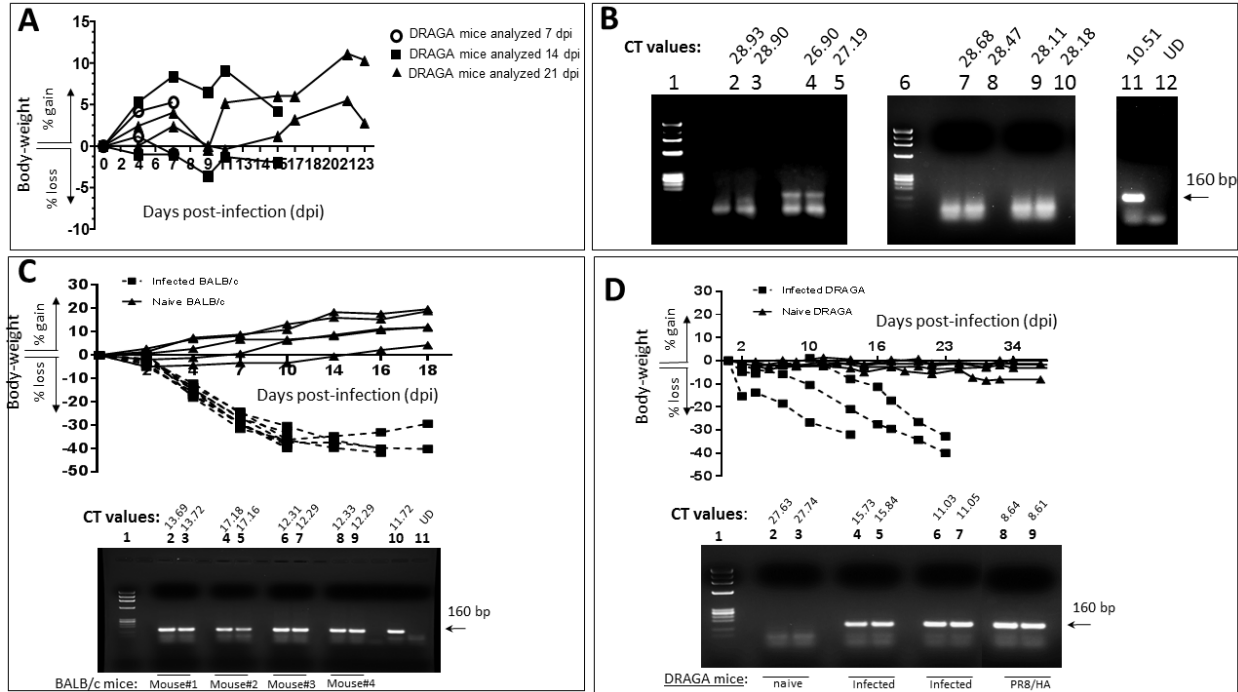
Figure 8. *Body-weights of PR8-infected DRAGA mice __vs.__ titers of viral HA expression in the lungs.* (**A**) Sub-lethal infection of DRAGA mice with PR8 virus. Body-weights of PR8 sub-lethally infected DRAGA mice (n =6) were monitored every other 3rd or 4th day post-infection (dpi). (**B**) Agarose gel electrophoresis of the HA amplicons obtained by RT-qPCR and corresponding CT values in the lungs of DRAGA mice from panel A (sub-lethal infection), as measured at 7, 14, and 21 dpi. Shown are duplicate samples from a naïve (not-infected) DRAGA mouse (lanes 2 and 3), and sublethally-infected 7 dpi (lanes 4-5) and 21 dpi (lanes 7-8 and 9-10). Arrow indicates the size (160 bp) amplicon of HA of PR8 virus (positive control, lane 11). Lane 1, molecular markers; Lane 12 distilled water (primer control). (**C**) Body-weights of PR8 lethally-infected (LD_{100}) BALB/c mice and naïve BALB/c mice (n =4 mice/group) monitored every other 3rd or 4th day post-infection (dpi). Lower panel, the agarose gel electrophoresis of HA amplicons in the lungs measured by RT-qPCR, and CT corresponding values in duplicate samples of lethally-infected BALB/c mice (lanes 2 to 9) at 18 dpi; Lane 1, molecular markers;

66

Lane 10, the 160 bp amplicon of HA of PR8 virus (positive control); Lane 11, a representative naïve (non-infected) BALB/c mouse. (**D**) Body-weights of PR8 lethally-infected (LD_{100}) DRAGA mice (n = 3 mice /group) versus naïve DRAGA mice (n=4 mice/group). Mice were monitored every other 3rd or 4th day post-infection. Lower panel, agarose gel electrophoresis of HA amplicons in the lungs measured by RT-qPCR, and CT corresponding values in duplicate samples. Lane 1, molecular markers; Lanes 2-3, a representative of naïve DRAGA mouse; Lanes 4-5 and 6-7, two representative DRAGA mice lethally infected, as measured at 14 dpi and 18 dpi; Lanes 8-9, 160 bp amplicon of HA of PR8 virus (positive control)
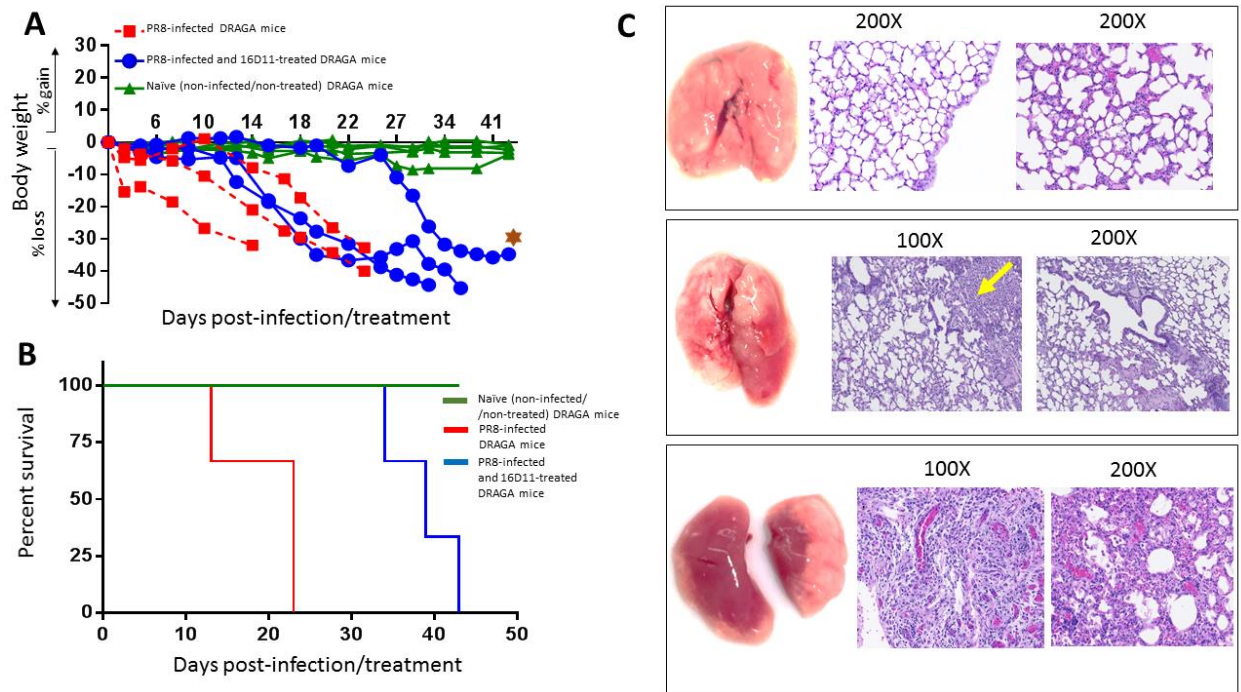
.**Figure 9.** *The effect of 16D11 hu-mAb in PR8 lethally-infected DRAGA mice.* (**A**) Body-weights of naïve (non-infected) DRAGA mice and PR8 lethally-infected (LD$_{100}$) DRAGA mice with and without 16D11 hu-mAb treatment. A single i.p. injection of 600 μg per mouse (n = 3-4 mice /group) was administered at the time of infection. Mice were monitored every other 3rd or 4th dpi. Brown star indicates the most resilient mouse in the treatment group. (**B**) Survival rates for groups of DRAGA mice described in panel A. Of note, the most resilient DRAGA mouse in the PR8-infected/treated group showed 40% less loss in body-weight at day 43 post-infection when sacrificed for analysis, which is significant when compared with the average loss in body-weight for the control infection group ($p = 0.026$ according to Mantel-Cox test, and $p = 0.016$ according to pairwise curves comparisons of Gehan-Breslow-Wilcoxon test). (**C**) Lung analysis of DRAGA mice described in panel A. *Upper panels*, lungs and Hematoxilin-Eosin (HE) staining of lung sections from a representative naïve DRAGA mouse; *Middle panels*, lungs and HE staining of lung sections from the most resilient DRAGA mouse to PR8 lethal infection upon

68

16D11 hu-mAb treatment as analyzed 40 days post-infection. Shown is a mild lung damage in the lower lobe of the right lung (diffuse grayish area) with slightly distorted alveolar architecture and scattered lymphocyte infiltrates (yellow arrow); *Lower panels*, lungs and HE staining of lung sections from a representative PR8-lethally DRAGA mouse left untreated, and analyzed 20 days post-infection. Shown is massive pneumonia in both lungs (dark reddish areas) with heavily distorted alveolar architecture, and interstitial and intra-alveolar lymphocyte infiltration.

2.7: Tables:

Table 1. *Kinetic analysis of 16D11 hu-mAb interaction with rHAs from PR8, Hokkaido and Memphis influenza viruses*

	Ka (mean ± SD) $M^{-1} s^{-1}$	Kd (mean ± SD) s^{-1}	KD nM	t ½ min
PR8/A/34	$(22.4 \pm 0.2) \times 10^3$	$(4.39 \pm 0.03) \times 10^{-3}$	199	2.62
Hokaido	$(25.8 \pm 0.2) \times 10^3$	$(3.32 \pm 0.03) \times 10^{-3}$	130	3.46
Memphis	n.b.d*	n.b.d	n.b.d	N/A

SPR sensograms for the interaction of 16D11 with rHA proteins as shown in figure 7. The kinetic data were fit using a 1:1 Langmuir binding model for the estimation of the association (ka) and dissociation (kd) rates and affinity (KD=ka/kd). No binding was detected (*nbd.) for the interaction of 16D11 with rHA of Memphis virus. The complex half-life was calculated as $t^{1/2}$=Ln/kd.

Table 2. *HIA for PR8 virus neutralization by anti-HA$_{180-195}$ hu-mAbs.*

anti-HA$_{180-195}$ hu-mAbs

#16D11	#6C2 (#2)	#13C10	#10B2	#25-3 (hu-IgM control)	human sera (dilution factor)
12.5	100	100	50	> 300	1/160

First row indicates the denomination for hu-mAbs used in HIA ; Second row indicates the amount of hu-mAbs required to induce virus neutralization (RBC hemagglutination) (µg/ml) in HIA

2.8: Supplemental material:
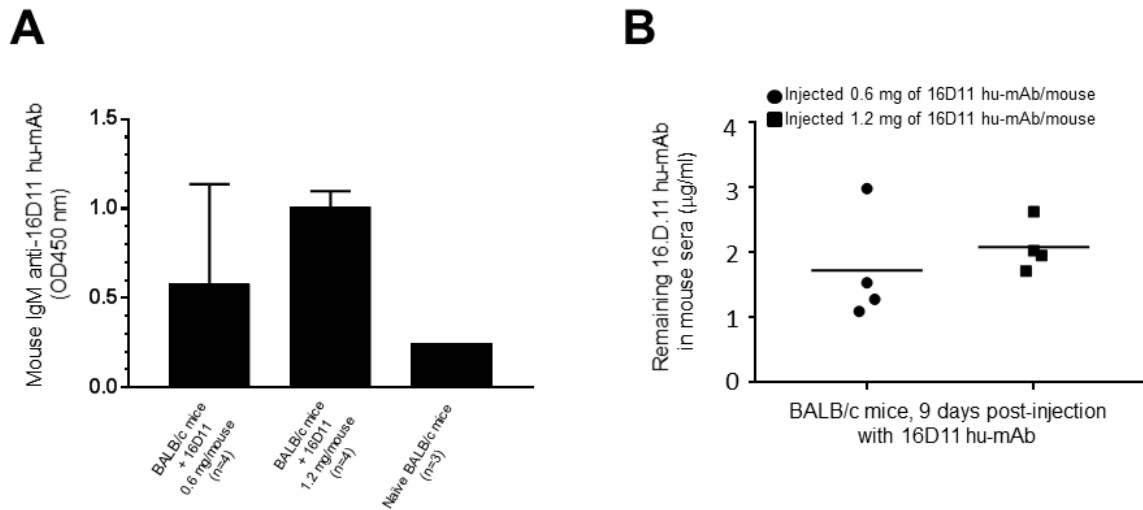
Figure 1S. *In vivo lifespan of 16D11 hu-mAb and murine antibody response to 16D11 hu-mAb.* (**A**) Murine IgM xenogeneic serum antibodies to 16D11 hu-mAb in BALB/c mice upon i.p. injection of 600 μg or 1,200 μg of 16D11 hu-mAb as measured by ELISA in individual mice. (**B**) Lifespan of 16D11 hu-mAb in BALB/c mice upon i.p. injection of 600 μg or 1,200 μg of 16D11 hu-mAb (n = 4/group). The amount of remaining 16D11 hu-mAb in BALB/c sera was measured by ELISA 9 days post-injection.
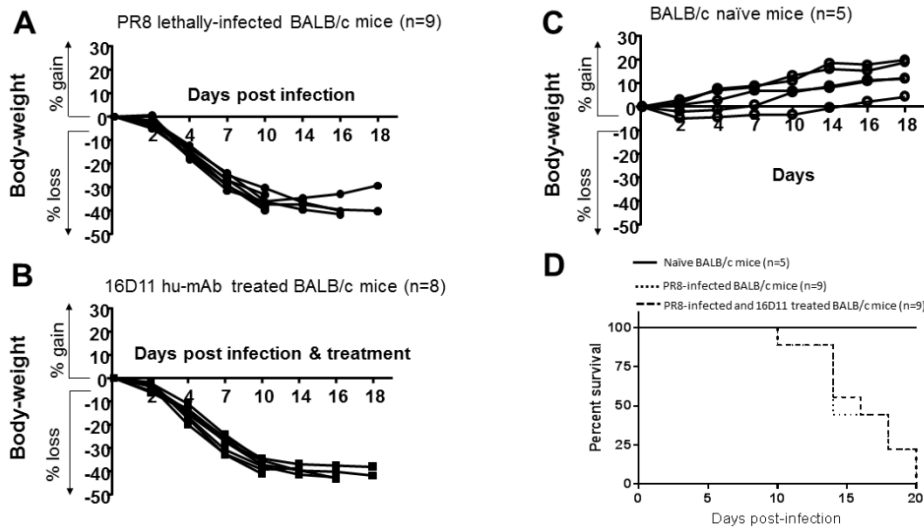
Figure 2S. *Lack of effect of 16D11 hu-mAb in PR8 lethally-infected BALB/c mice.* (**A**) Body-weights of lethally-infected BALB/c mice with PR8/A/34 virus (n=9). (**B**) Body-weights of lethally-infected BALB/c mice with PR8/A/34 virus and treated i.p. with 600 μg of 16D11 hu-mAb at the time of infection (n=8). (**C**) Body-weights of BALB/c naïve mice (n=5). Body weight of 4 month-old BALB/c female mice in all groups was monitored at 3 to 4 day interval of time. (**D**) Survival rates of BALB/c mice described in panels A, B, and C.

Chapter 3:
DISSERTATION DISCUSSION

Ongoing research to develop and improve current immunodeficient mouse strains for human cell reconstitution over the last 25 years has led to the generation of a robust human immune system in humanized mice[115 26,116,117]. Key genetic breakthroughs, such as disruption of the IL2Rγc and the RAG1 or RAG2 genes, have allowed for superior human cell engraftment. Moreover, the introduction of HLA class I and II genes allow human T cells to be educated in the mouse thymus resulting in improved T cell reconstitution. Engraftment of different human cells (HSC and PBMC) and tissues (bone marrow, liver, and thymus) into immunodeficient mouse strains has created a variety of functional humanized mouse models. These improved models are currently used to study human biological responses and diseases[117]. They are also becoming an attractive new tool to assess drugs and identify mechanisms in various types of infectious diseases. However, very few studies have utilized this new version of humanized mice in influenza studies[117]. Our goal in this project was to assess the ability of a new humanized mouse model to model influenza infection, generate antibodies against influenza, and test the therapeutic potential of human anti-flu mAbs.

Only a couple of studies have used humanized mice harboring certain key features of the human immune system to evaluate influenza infection. Our newly developed humanized mouse model, DRAGA, is distinguished from previous used models by its expression of HLA class I and II genes[36]. The RT-qPCR of lungs harvested from DRAGA mice, and clinical manifestation of up to 40% weight loss seen in Chapter 2, demonstrates their ability to model lethal and sub-lethal influenza infections. The expression of HLA class I and II likely does not have an effect on DRAGA's susceptibility to influenza infection; rather DRAGA mice represent a new model of infection that mimics a particular human population carrying these HLA alleles. Furthermore, establishing this new humanized model of infection, introduces novel opportunities to evaluate

the human immune response to influenza infection, restricted to HLA-DR4 and HLA-A2 expression. DRAG mice, the predecessor of DRAGA mice, were previously shown to sustain infections with the malaria parasite *Plasmodium falciparum*[37] and HIV [33,39]. Our findings therefore continue to expand the abilities of DRAG/DRAGA mice for studies involving infection to human pathogens.

Perhaps it is expected that DRAGA mice can model influenza infection since the strain of influenza virus used is mouse adapted. Influenza viruses mediate infection by binding HA protein to cell surface molecules (glycoprotein and glycolipids) that contain sialic acid chains linked by α2,3 or α2,6 glycosidic bonds[118-120]. Avian influenza viruses will bind primarily to glycan receptors linked by α2,3 SA bonds, while the human influenza will bind primarily to glycan receptors linked by α2,6 SA bonds[121,122]. Thus, receptor-binding specificity is an important determinant of host transmission. The human upper respiratory system, such as the nasal mucosa and nasopharynx, is mostly composed of α2,6 SA bonds, while the lower respiratory system, the lungs, contains both α2,3 and α2,6 SA bonds[118,123,124]. On the other hand, the mouse respiratory tract predominately contains α2,3 SA bonds and little α2,6 SA bonds[125,126]. Since the majority of human influenza virus isolates produce mild infection in mice, the human strains have to be adapted to the mouse through serial passage[5]. The respiratory tract of DRAGA mice predominately contains α2,3 SA bonds as opposed to α2,6 SA bonds, and the PR8/A/34 (H1N1) strain that we used to model influenza infection is a well-known mouse and lab adapted strain[5]. Thus, infection of DRAGA mice with PR8/A/34 (H1N1) strain is not surprising. However, we should be mindful that DRAGA mice, like other humanized mice used for influenza research, lack a murine immune response. Even though the murine immune system is absent, DRAGA has reconstituted key features of the human immune response, such as human

B and T cells, allowing it to sustain the infection and not perish rapidly after inoculation with the virus.

In the future, we aim to examine the ability of DRAGA mice to sustain infection with human strains of influenza viruses. As mentioned previously, human strains of influenza virus predominately bind to $\alpha2,6$ SA bonds present on the surface of epithelial cells lining the respiratory tract. Studies have shown that HSC can differentiate into multiple lineages within the blood and lymphoid tissues, but more recent studies revealed that HSC can also differentiate into non-hematopoietic cells such as hepatocytes, cardiac myocytes, vascular endothelial cells, gastrointestinal epithelial cells, and renal tubular epithelial cells[127-132]. Therefore it is possible that human HSC engrafted into DRAGA mice can generate human epithelial cells lining the respiratory tract and lungs. In fact, DRAG mice have previously been shown to possess human-derived non-hematopoietic cells such as hepatocytes and liver endothelial cells[37]. In that study, we were interested in detecting CD36, a glycoprotein expressed in various epithelial and endothelial cells and in erythrocytes. We stained lung sections from DRAGA mice and observed a small number of cells positive for human CD36, suggesting that DRAGA mice can also reconstitute human lung endothelial and epithelial cells. As shown in Figure 1(A), human lung alveolar cells moderately express human CD36[133,134] and in figure 1(B) we observe a positive staining for CD36 expression in the lungs of DRAGA mice. These preliminary findings suggest that DRAGA mice reconstitute epithelial/endothelial cells in their lungs. Since DRAGA mice appear able to reconstitute human epithelial cells, we believe these human cells could be potentially susceptible to infection with human influenza strains that have not undergone the process of mouse adaptation. However, further studies are necessary to confirm whether human

epithelial cells present in the lungs of DRAGA mice express α2,6 SA bonds, an important

requirement for human influenza mediated infection.
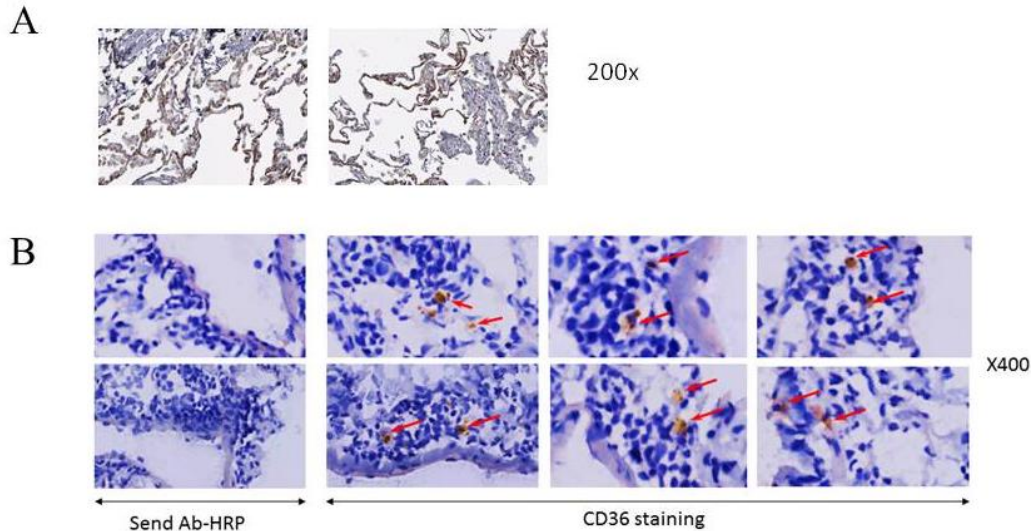
Figure 1: Expression of CD36 in both human lungs and DRAGA mouse lungs. A)
Immunohistochemistry data from The Human Protein Atlas (http://www.proteinatlas.org/)
shows positive staining of CD36 in human lungs. B) Positive IHC staining of CD36 in
lungs of DRAGA mice. The secondary Ab-HRP sections represent lungs incubated with
HRP labeled antibody in the absence of anti-human CD36 antibody.

Our second goal was to utilize DRAGA mice as a new source of monoclonal antibody

development and generation. In Chapter 2, we demonstrated that upon immunization with a 16

amino acid HA peptide conserved among 7 influenza strains, DRAGA mice mount an antibody

response comprised of both human IgM and IgG composition specific to the HA peptide or the

viruses themselves. Furthermore, we previously showed that DRAG mice can generate specific

IgG antibodies to tetanus toxoid[31] and malaria *Plasmodium falciparum*[37], which in addition to

our current findings, confirm the capacity of DRAGA mice to mount a specific human antibody

response to antigens. Next, we proposed to isolate these antibody producing B cells specific to

the HA peptide or virus, and immortalize them for continuous antibody production using

hybridoma technology. DRAGA mice generated IgM antibodies specific to the virus, but had no

success in producing a stable IgG hybridoma with specificity to the virus. Out of all the IgM

mAbs generated using DRAGA mice, the one that showed the most diversity in terms of CDR3

region and neutralization capacity by HIA, was hu-mAb 16D11. It is well known that IgMs are

the first line of defense during an initial acute phase of microbial and viral infections[14]. Even

though IgMs tend to be have lower affinity, their pentameric nature compensates by conferring

greater valency, i.e. number of arms available to bind antigen, and therefore higher avidity for

the antigen. ELISA and SPR analysis confirmed that hu-mAb 16D11 binds to the rHA protein of

PR8/A/34, and is able to cross-react with rHAs derived from other strains of influenza virus. We

have also shown that hu-mAb 16D11 is a pentamer, suggesting a higher avidity for PR8/A/34

influenza virus, as well as for WSN, Aichi, Hokkaido and Vietnam influenza strains. HAI

experiments showed that 16D11 hu-IgM is able to inhibit RBC agglutination mediated by the

virus demonstrating its ability to neutralize virus activity. Therefore, we should not

underestimate the protective properties of IgM such as 16D11 against viral infections.

Previous studies have shown that IgM antibodies can confer protection against influenza

infection. For example, Harada et al. used AID-knockout mice unable to switch IgMs to IgGs

demonstrating that unmutated IgMs protect against both primary and secondary infections with

PR8/A/34, but with higher morbidity[135]. Even though, high affinity IgG plays an important role

in influenza immunity, the level of protection of IgM was remarkable[135]. Additionally, IgM Abs

have been evaluated in host defense and protection against other viral infections. For example,

Diamond et al. assessed the role of IgMs in protection against West Nile Virus infection[136].

They demonstrated that specific and neutralizing IgMs protected mice infected with WNV by

limiting viremia and viral dissemination into the CNS[136]. Furthermore, other studies involving

Ag-specific IgM antibodies demonstrated their role in protection against polyoma virus[137], herpes simplex virus[138], enteroviruses[139], yellow fever virus[140], and vesicular stomatitis infections[141,142]. The most significant study with relevance to our project described the generation of human monoclonal antibodies from human IgM[+] memory B cells of volunteers who were vaccinated with seasonal influenza vaccine. The IgM mAb CR621 protected against viral infection with lethal H1N1 and H5N1 influenza strains[65]. Furthermore, Kim et al. demonstrated that influenza-specific IgM memory B cells exhibited broad cross-reactivity against contemporary seasonal strains and pandemic strains. Cross-reactivity of IgM-secreting cells appeared to be broader than their IgG counterparts; the authors concluded that upon vaccination, a portion of the IgM memory B cells directly differentiated into highly cross-reactive IgM-secreting plasmablast cells able to confer protection[143]. Both of these studies demonstrate a critical role for IgM in protective immunity to influenza viral infection.

Lastly, we proposed to evaluate the therapeutic potential of our anti-flu hu-mAb 16D11 in preventing influenza infection. After determining that DRAGA mice can sustain influenza infection, we assessed the neutralizing anti-flu capacity of hu-mAb 16D11 in these DRAGA mice. Our results demonstrated that DRAGA mice receiving hu-mAb 16D11 at the time of infection survived longer than DRAGA mice who did not receive 16D11. Given the nature of 16D11 being an IgM antibody, we speculate that its reduced half-life in comparison to IgG antibodies is responsible for incomplete clearance of the influenza virus. We believe that if 16D11 had a half-life comparable to IgGs, then it would have stayed in circulation for more days and could have prevented influenza infection in DRAGA mice. Future studies involving the re-engineering of 16D11 as an IgG could confer complete protection from flu infection with PR8/A/34 due to an increase in half-life and the additional effects of more effector functions.

We also showed that DRAGA's humanized immune system can be utilized as new model to test therapeutics. Even though we generated multiple IgM clones able to bind to PR/8/34 virus, we did not assess their combined capacity to neutralize the virus *in vivo*. It would be interesting to also assess whether a cocktail of anti-flu mAbs could confer complete protection against influenza virus and be beneficial over administration of a single mAb. Even though we introduced human antibodies into a mouse model, we noticed that DRAGA mice did not produce a xenogeneic response to hu-mAb 16D11 which could have hampered its therapeutic potential against viral infection demonstrating that the humanized immune system of DRAGA did not interfere with purified human antibodies.

Even though it is unknown how hu-mAb 16D11 delayed infection with influenza virus strain PR8/A/34, we can propose a mechanism responsible for the observed delay of influenza infection in the DRAGA mouse model. This model is based on the distribution and distinct effector functions of IgM antibodies. DRAGA mice were inoculated intranasally with a lethal dose (LD100) of influenza virus strain A/PR8/34 strain. The influenza virus then traveled down the respiratory tract and bound to epithelial cells lining the lung airways. The virus infected the epithelial cells, replicated, and released more virus particles to infect adjacent cells within the lower respiratory tract. Infection with these viral particles resulted in lung lesions characteristic of pneumonia, such as pulmonary edema and inflammatory infiltrates in DRAGA mice. HE staining of lung sections from a representative PR8-lethally DRAGA mouse left untreated and analyzed 20 days post-infection revealed massive pneumonia in both lungs with heavily distorted alveolar architecture, and interstitial and intra-alveolar lymphocyte infiltration.

Pentameric IgM antibodies are normally found in the bloodstream rather than in intercellular spaces within tissues; their large molecular size hinders their distribution from the

bloodstream into the intracellular spaces of tissues (e.g. lungs) [14]. Hu-mAb 16D11 was

administered into the peritoneal cavity of DRAGA mice two hours prior to influenza virus

exposure. The distribution of 16D11 from the peritoneal cavity to the lungs most likely

depended on transvascular transportation. Studies on biological activity of IgM antibodies

support the idea that IgM monoclonal antibodies such as 16D11 most likely entered circulation

from the peritoneum and remained there in sufficient amounts over at least a 24 hr period[144]. In

the same manner, human monoclonal 16D11 antibodies once present in the bloodstream were

also transported through the tissues of the organs such as the lungs. However, it is also possible

that human 16D11 antibodies left the peritoneum cavity at slower rate than IgG antibodies; once

in circulation these antibodies could not reach the lungs rapidly enough to provide complete

protection. This observation is supported by a previous study that showed a decrease in

transcapillary escape rate from plasma to the interstitial space, as the molecular weight increased

between albumin, IgG, and IgM molecules[145]. Therefore, passive diffusion of 16D11 antibodies

to and from the bloodstream may have been restricted due to their pentameric structure validated

by size exclusion chromatography assessment in Chapter 2.

Even though the pentameric structure of hu-mAb 16D11 may have hampered its ability to

move across interstitial tissue spaces, it could have also benefited its transportation across

epithelial barriers. Polymeric immunoglobulin receptor (pIgR) is present on basolateral surfaces

of the overlying epithelial cells, and serves to facilitate the transcytosis of dimeric IgA and

pentameric IgM to the apical surface of epithelial cells. The overall amino acid homology

between human pIgR and mouse, rat, mouse, and bovine pIgR is 66% [146]. Furthermore, the

functionally important sequence such as the putative Ig contact site in domain 1 shares an

average homology of 93% between human and mouse pIgR[147]. Therefore, hu-mAb 16D11 could

potentially interact with the mouse pIgR receptors of DRAGA mouse, allowing its transportation through the epithelium cells until reaching the respiratory tract.

Once human monoclonal16D11 antibodies have localized to the lungs, they will come into contact with influenza virus and initiate their effector functions to hinder the spread of the virus. Studies have shown that IgM antibodies confer protection by activation of complement, enhancement of phagocytosis of pathogens, and direct neutralization of some bacteria and viruses in circulation. We speculate that hu-mAb 16D11 delayed infection with influenza virus strain PR8/A/34 by using these protective mechanisms to prevent and hinder the lethal and infectious effect of the virus. It is well known that the major effector function of IgM antibodies is activation of the complement system[14]. Once complement is activated, it will promote the uptake and destruction of pathogens by phagocytes. Theoretically, hu-mAb 16D11 bound to the HA protein of influenza virus forming a complex, and initiated the classical pathway of complement activation by binding to C1 via C1q, CR3, and CR4 receptors, resulting in enhanced phagocytosis, a process also known as opsonization, and clearance of the virus. Even though, 16D11 antibodies are of human origin they are still capable of activating mouse complement system of DRAGA mice. The interaction between human antibodies and mouse complement system has been previously observed in a different study which demonstrated that purified human IgM antibodies can synergize with mouse complement to neutralize adenovirus vectors[148]. Furthermore, IgM antibodies such as 16D11 are also capable of opsonizing pathogens and play a role in phagocytosis by specifically binding to the Fc receptor known as Fcα/μR which recognizes IgM and IgA antibodies[149-151]. Fcα/μR is a type 1 transmembrane with an extracellular Ig-like domain expressed on B cells and macrophages, where it can mediate phagocytosis of IgM-antigen immune complexes[149,150]. Lastly, IgM antibodies bind to viruses

and neutralize them by preventing the viruses from infecting cells[14]. We demonstrated in Chapter 2 that hu-mAb 16D11 prevented the A/PR8/34 influenza virus from agglutinating red blood cells, and therefore confirmed that these antibodies can neutralize the ability of the virus from biding to other cells *in vitro*. Therefore, we believe that neutralization by 16D11 may be the most important mechanism at play against A/PR8/34 influenza virus in influenza-infected DRAGA mice.

Understanding the factors associated with bio distribution of antibody-based therapeutics are important for development of future and better therapeutic candidates. Although, the distribution and effector mechanisms of Hu-mAb 16D11 were not characterized in this project, we hope to carry out future experiments that could help us understand the anti-influenza viral effects of hu-mAb 16D11 *in vivo*.
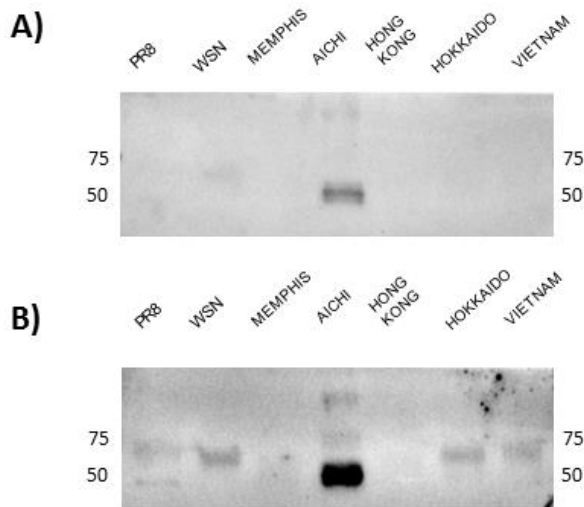
Figure 2: Human antibodies from DRAGA mice bind to rHA of different influenza strains.

(A) Anti-flu IgM and (B) IgG binding to rHA proteins.

Studies evaluating the immune response of DRAGA mice upon infection with PR8/A/34 influenza virus strain should be pursued. Preliminary data from our influenza infections performed in Chapter 2 demonstrates that DRAGA mice are able to generate human antibodies in response to influenza infection using sera collected upon death. We evaluated the cross-reactivity of anti-flu antibodies to rHAs from different

influenza strains by using serum collected from a DRAGA mouse that was infected with PR8/A/34. In Fig. 2 panel (A), we see a low reactivity of human IgM to rHAs derived from three of the seven rHAs used. On the other hand, panel (B) shows binding of human IgG to PR8, WSN, Aichi, Hokkaido, and Vietnam rHAs. These results demonstrate that DRAGA mice can mount an immune response specific to PR8/A/34 with cross-reactivity to other strains of influenza. However, we need to repeat these experiments and evaluate a larger number of PR8/A/34-infected DRAGA mice to see if they all respond to immunization with similar cross-reactivity and IgM levels to these rHAs. Furthermore, we would like to assess the involvement of T and B cells in mediating a specific immune response to influenza infection in DRAGA mice.

In conclusion, our findings demonstrate valuable new opportunities to use DRAGA mice as a novel model of influenza infection.   Furthermore, DRAGA mice represent a new mouse model to study human T and B cell development and function, vaccine development, and generation of human monoclonal antibodies for therapeutic use.

REFERENCES

1   CDC. *Seasonal Influenza: Flu Basics. 2015*,
        <http://www.cdc.gov/flu/about/disease/index.htm.> (2015).
2   Treanor, J. J. in *Infectious Diseases*   (ed John Bennett Gerald Mandell, Raphael Dolin)
        Ch. Influenza viruses, including avian influenza and swine influenza 2265-2288
        (Churchill Livinstone Elsevier).
3   Nelson, M. I. & Holmes, E. C. The evolution of epidemic influenza. *Nat Rev Genet* **8**,
        196-205 (2007).
4   Flu.gov. *Pandemic Flu History*, <http://www.flu.gov/pandemic/history/.htm. > (2015).
5   Bouvier, N. M. & Lowen, A. C. Animal Models for Influenza Virus Pathogenesis and
        Transmission. *Viruses* **2**, 1530-1563, doi:10.3390/v20801530 (2010).
6   CDC. Vaccine Effectiveness - How Well Does the Flu Vaccine Work? (2017).
7   Moscona, A. Medical management of influenza infection. *Annual review of medicine* **59**,
        397-413, doi:10.1146/annurev.med.59.061506.213121 (2008).
8   Fleming, D. M. Managing influenza: amantadine, rimantadine and beyond. *International
        journal of clinical practice* **55**, 189-195 (2001).
9   Koudstaal W., UytdeHaag F.G., Friesen R.H. & J., G. in *Influenza vaccines for the future*
        (eds Rappuoli R. & Del Giudice G.) 383-398 (Spinger Basel AG, 2011).
10   Ma, C. *et al.* Identification of the pore-lining residues of the BM2 ion channel protein of
        influenza B virus. *The Journal of biological chemistry* **283**, 15921-15931,
        doi:10.1074/jbc.M710302200 (2008).
11   Diseases, N. I. o. A. a. I. *New Vaccine Technologies*,
        <http://www.niaid.nih.gov/topics/Flu/Research/vaccineResearch/pages/technologies.aspx
        .htm> (2011).
12   CDC. *Key Facts About Seasonal Flu Vaccine*,
        <https://www.cdc.gov/flu/protect/keyfacts.htm> (2017).
13   CDC. *Frequently Asked Flu Questions 2017-2018 Influenza Season*,
        <https://www.cdc.gov/flu/about/season/flu-season-2017-2018.htm> (2017).
14   Murphy, K. *Janeway's Immunobiology*. 8th edn, (Garland Science Taylor & Francis
        Group, 2012).
15   P., P. *The immune system.* Third

        edn, (Garland Sicence, Taylor & Francis Group, LLC 2009).
16   Xu, J. L. & Davis, M. M. Diversity in the CDR3 region of V(H) is sufficient for most
        antibody specificities. *Immunity* **13**, 37-45 (2000).
17   Skountzou, I. *et al.* Influenza virus-specific neutralizing IgM antibodies persist for a
        lifetime. *Clinical and vaccine immunology : CVI* **21**, 1481-1489, doi:10.1128/CVI.00374-
        14 (2014).
18   Casadevall, A. & Scharff, M. D. Serum therapy revisited: animal models of infection and
        development of passive antibody therapy. *Antimicrobial agents and chemotherapy* **38**,
        1695-1702 (1994).
19   KÖHler, G. & Milstein, C. Continuous cultures of fused cells secreting antibody of
        predefined specificity. *Nature* **256**, 495, doi:10.1038/256495a0 (1975).
20   E., G. in *Antibodies: A laboratory manual*

        (ed Greenfiel E.) 201-301 (Cold Spring Harbor Laboratory Press, 2014).

21   Yamashita, M., Katakura, Y. & Shirahata, S. Recent advances in the generation of human monoclonal antibody. *Cytotechnology* **55**, 55-60, doi:10.1007/s10616-007-9072-5 (2007).

22   McConnell, A. D. *et al.* High affinity humanized antibodies without making hybridomas; immunization paired with mammalian cell display and in vitro somatic hypermutation. *PloS one* **7**, e49458, doi:10.1371/journal.pone.0049458 (2012).

23   Sawyer, L. A. Antibodies for the prevention and treatment of viral diseases. *Antiviral research* **47**, 57-77 (2000).

24   Harding, F. A., Stickler, M. M., Razo, J. & DuBridge, R. B. The immunogenicity of humanized and fully human antibodies: residual immunogenicity resides in the CDR regions. *mAbs* **2**, 256-265 (2010).

25   Ito, M. *et al.* NOD/SCID/gamma(c)(null) mouse: an excellent recipient mouse model for engraftment of human cells. *Blood* **100**, 3175-3182, doi:10.1182/blood-2001-12-0207 (2002).

26   Shultz, L. D., Brehm, M. A., Garcia-Martinez, J. V. & Greiner, D. L. Humanized mice for immune system investigation: progress, promise and challenges. *Nature reviews. Immunology* **12**, 786-798, doi:10.1038/nri3311 (2012).

27   Bosma, G. C., Custer, R. P. & Bosma, M. J. A severe combined immunodeficiency mutation in the mouse. *Nature* **301**, 527-530 (1983).

28   McCune, J. M. *et al.* The SCID-hu mouse: murine model for the analysis of human hematolymphoid differentiation and function. *Science* **241**, 1632-1639 (1988).

29   M., I. in *Humanized mice for HIV research*   (ed Larisa Y. Poluektova J. Victor Garcia Yoshio Koyanagi Markus G. Manz Andrew M. Tager) 1-12 (Spring Science, 2014).

30   Shultz, L. D. *et al.* Human lymphoid and myeloid cell development in NOD/LtSz-scid IL2R gamma null mice engrafted with mobilized human hemopoietic stem cells. *Journal of immunology* **174**, 6477-6489 (2005).

31   Danner, R. *et al.* Expression of HLA class II molecules in humanized NOD.Rag1KO.IL2RgcKO mice is critical for development and function of human T and B cells. *PloS one* **6**, e19826, doi:10.1371/journal.pone.0019826 (2011).

32   Brehm, M. A. *et al.* Parameters for establishing humanized mouse models to study human immunity: analysis of human hematopoietic stem cell engraftment in three immunodeficient strains of mice bearing the IL2rgamma(null) mutation. *Clinical immunology* **135**, 84-98, doi:10.1016/j.clim.2009.12.008 (2010).

33   Allam, A. *et al.* TFH cells accumulate in mucosal tissues of humanized-DRAG mice and are highly permissive to HIV-1. *Scientific reports* **5**, 10443, doi:10.1038/srep10443 (2015).

34   Strowig, T. *et al.* Priming of protective T cell responses against virus-induced tumors in mice with human immune system components. *The Journal of experimental medicine* **206**, 1423-1434, doi:10.1084/jem.20081720 (2009).

35   Shultz, L. D. *et al.* Generation of functional human T-cell subsets with HLA-restricted immune responses in HLA class I expressing NOD/SCID/IL2r gamma(null) humanized mice. *Proceedings of the National Academy of Sciences of the United States of America* **107**, 13022-13027, doi:10.1073/pnas.1000475107 (2010).

36   Majji, S. *et al.* Differential effect of HLA class-I versus class-II transgenes on human T and B cell reconstitution and function in NRG mice. *Scientific reports* **6**, 28093, doi:10.1038/srep28093 (2016).

37   Wijayalath, W. *et al.* Humanized HLA-DR4.RagKO.IL2RgammacKO.NOD (DRAG) mice sustain the complex vertebrate life cycle of Plasmodium falciparum malaria. *Malaria journal* **13**, 386, doi:10.1186/1475-2875-13-386 (2014).

38   Yi, G. *et al.* A DNA Vaccine Protects Human Immune Cells against Zika Virus Infection in Humanized Mice. *EBioMedicine*, doi:10.1016/j.ebiom.2017.10.006.

39   Kim, J. *et al.* Tracking Human Immunodeficiency Virus-1 Infection in the Humanized DRAG Mouse Model. *Front. Immunol.* **8** (2017).

40   Yu, C. I. *et al.* Broad influenza-specific CD8+ T-cell responses in humanized mice vaccinated with influenza virus vaccines. *Blood* **112**, 3671-3678, doi:10.1182/blood-2008-05-157016 (2008).

41   Wada, Y. *et al.* A humanized mouse model identifies key amino acids for low immunogenicity of H7N9 vaccines. *Scientific Reports* **7**, 1283, doi:10.1038/s41598-017-01372-5 (2017).

42   Yu, C. I. *et al.* Human CD1c+ dendritic cells drive the differentiation of CD103+ CD8+ mucosal effector T cells via the cytokine TGF-beta. *Immunity* **38**, 818-830, doi:10.1016/j.immuni.2013.03.004 (2013).

43   Willinger, T. *et al.* Human IL-3/GM-CSF knock-in mice support human alveolar macrophage development and human immune responses in the lung. *Proceedings of the National Academy of Sciences of the United States of America* **108**, 2390-2395, doi:10.1073/pnas.1019682108 (2011).

44   Li, Y. *et al.* Induction of functional human macrophages from bone marrow promonocytes by M-CSF in humanized mice. *Journal of immunology* **191**, 3192-3199, doi:10.4049/jimmunol.1300742 (2013).

45   Corti, D. *et al.* A neutralizing antibody selected from plasma cells that binds to group 1 and group 2 influenza A hemagglutinins. *Science* **333**, 850-856, doi:10.1126/science.1205669 (2011).

46   Dreyfus, C. *et al.* Highly conserved protective epitopes on influenza B viruses. *Science* **337**, 1343-1348, doi:10.1126/science.1222908 (2012).

47   Ekiert, D. C. *et al.* Antibody recognition of a highly conserved influenza virus epitope. *Science* **324**, 246-251, doi:10.1126/science.1171491 (2009).

48   Tan, G. S. *et al.* A pan-H1 anti-hemagglutinin monoclonal antibody with potent broad-spectrum efficacy in vivo. *Journal of virology* **86**, 6179-6188, doi:10.1128/JVI.00469-12 (2012).

49   Hu, H. *et al.* A human antibody recognizing a conserved epitope of H5 hemagglutinin broadly neutralizes highly pathogenic avian influenza H5N1 viruses. *Journal of virology* **86**, 2978-2989, doi:10.1128/JVI.06665-11 (2012).

50   Hu, W. *et al.* Fully human broadly neutralizing monoclonal antibodies against influenza A viruses generated from the memory B cells of a 2009 pandemic H1N1 influenza vaccine recipient. *Virology* **435**, 320-328, doi:10.1016/j.virol.2012.09.034 (2013).

51   Casares, S., Brumeanu, T. D., Bot, A. & Bona, C. A. Protective immunity elicited by vaccination with DNA encoding for a B cell and a T cell epitope of the A/PR/8/34 influenza virus. *Viral immunology* **10**, 129-136, doi:10.1089/vim.1997.10.129 (1997).

52   Wang, T. T. *et al.* Vaccination with a synthetic peptide from the influenza virus hemagglutinin provides protection against distinct viral subtypes. *Proceedings of the National Academy of Sciences of the United States of America* **107**, 18979-18984, doi:10.1073/pnas.1013387107 (2010).

53   Kilbourne, E. *Influenza*. (Plenum Medical Book Company, 1987).

54   Li, O. T. & Poon, L. L. One step closer to universal influenza epitopes. *Expert review of anti-infective therapy* **7**, 687-690, doi:10.1586/eri.09.48 (2009).

55   Velkov, T. *et al.* The antigenic architecture of the hemagglutinin of influenza H5N1 viruses. *Molecular immunology* **56**, 705-719, doi:10.1016/j.molimm.2013.07.010 (2013).

56   Osterholm, M. T. Preparing for the next pandemic. *The New England journal of medicine* **352**, 1839-1842, doi:10.1056/NEJMp058068 (2005).

57   Cassetti, M. C., Couch, R., Wood, J. & Pervikov, Y. Report of meeting on the development of influenza vaccines with broad spectrum and long-lasting immune responses, World Health Organization, Geneva, Switzerland, 26-27 February 2004. *Vaccine* **23**, 1529-1533 (2005).

58   McMurry, J. A., Johansson, B. E. & De Groot, A. S. A call to cellular & humoral arms: enlisting cognate T cell help to develop broad-spectrum vaccines against influenza A. *Human vaccines* **4**, 148-157 (2008).

59   Epstein, S. L. Control of influenza virus infection by immunity to conserved viral features. *Expert review of anti-infective therapy* **1**, 627-638 (2003).

60   Nilvebrant, J. *et al.* IBC's 22nd Annual Antibody Engineering and 9th Annual Antibody Therapeutics International Conferences and the 2011 Annual Meeting of The Antibody Society, December 5-8, 2011, San Diego, CA. *mAbs* **4**, 153-181, doi:10.4161/mabs.4.2.19495 (2012).

61   Yoshida, R. *et al.* Cross-protective potential of a novel monoclonal antibody directed against antigenic site B of the hemagglutinin of influenza A viruses. *PLoS pathogens* **5**, e1000350, doi:10.1371/journal.ppat.1000350 (2009).

62   Lambkin, R., McLain, L., Jones, S. E., Aldridge, S. L. & Dimmock, N. J. Neutralization escape mutants of type A influenza virus are readily selected by antisera from mice immunized with whole virus: a possible mechanism for antigenic drift. *The Journal of general virology* **75 (Pt 12)**, 3493-3502, doi:10.1099/0022-1317-75-12-3493 (1994).

63   Murphy, B. R. *et al.* Secretory and systemic immunological response in children infected with live attenuated influenza A virus vaccines. *Infection and immunity* **36**, 1102-1108 (1982).

64   Burlington, D. B., Clements, M. L., Meiklejohn, G., Phelan, M. & Murphy, B. R. Hemagglutinin-specific antibody responses in immunoglobulin G, A, and M isotypes as measured by enzyme-linked immunosorbent assay after primary or secondary infection of humans with influenza A virus. *Infection and immunity* **41**, 540-545 (1983).

65   Throsby, M. *et al.* Heterosubtypic neutralizing monoclonal antibodies cross-protective against H5N1 and H1N1 recovered from human IgM+ memory B cells. *PloS one* **3**, e3942, doi:10.1371/journal.pone.0003942 (2008).

66   Oh, H. L. *et al.* An antibody against a novel and conserved epitope in the hemagglutinin 1 subunit neutralizes numerous H5N1 influenza viruses. *Journal of virology* **84**, 8275-8286, doi:10.1128/JVI.02593-09 (2010).

67   Chen, Y. *et al.* Humanized antibodies with broad-spectrum neutralization to avian influenza virus H5N1. *Antiviral research* **87**, 81-84, doi:10.1016/j.antiviral.2010.04.012 (2010).

68   Zheng, Q. *et al.* Properties and therapeutic efficacy of broadly reactive chimeric and humanized H5-specific monoclonal antibodies against H5N1 influenza viruses.

Antimicrobial agents and chemotherapy **55**, 1349-1357, doi:10.1128/AAC.01436-10 (2011).

69   Wang, T. T. *et al.* Broadly protective monoclonal antibodies against H3 influenza viruses following sequential immunization with different hemagglutinins. *PLoS pathogens* **6**, e1000796, doi:10.1371/journal.ppat.1000796 (2010).

70   Hanson, B. J. *et al.* Passive immunoprophylaxis and therapy with humanized monoclonal antibody specific for influenza A H5 hemagglutinin in mice. *Respiratory research* **7**, 126, doi:10.1186/1465-9921-7-126 (2006).

71   Du, L. *et al.* Identification and structural characterization of a broadly neutralizing antibody targeting a novel conserved epitope on the influenza virus H5N1 hemagglutinin. *Journal of virology* **87**, 2215-2225, doi:10.1128/JVI.02344-12 (2013).

72   Fujimoto, Y. *et al.* Cross-protective potential of anti-nucleoprotein human monoclonal antibodies against lethal influenza A virus infection. *The Journal of general virology* **97**, 2104-2116, doi:10.1099/jgv.0.000518 (2016).

73   Wrammert, J. *et al.* Broadly cross-reactive antibodies dominate the human B cell response against 2009 pandemic H1N1 influenza virus infection. *The Journal of experimental medicine* **208**, 181-193, doi:10.1084/jem.20101352 (2011).

74   Klausberger, M. *et al.* Globular Head-Displayed Conserved Influenza H1 Hemagglutinin Stalk Epitopes Confer Protection against Heterologous H1N1 Virus. *PloS one* **11**, e0153579, doi:10.1371/journal.pone.0153579 (2016).

75   Clementi, N. *et al.* Influenza B-cells protective epitope characterization: a passkey for the rational design of new broad-range anti-influenza vaccines. *Viruses* **4**, 3090-3108, doi:10.3390/v4113090 (2012).

76   Nguyen, H. H. *et al.* Prophylactic and therapeutic efficacy of avian antibodies against influenza virus H5N1 and H1N1 in mice. *PloS one* **5**, e10152, doi:10.1371/journal.pone.0010152 (2010).

77   Tjandra, J. J., Ramadi, L. & McKenzie, I. F. Development of human anti-murine antibody (HAMA) response in patients. *Immunology and cell biology* **68** (**Pt 6**), 367-376, doi:10.1038/icb.1990.50 (1990).

78   Collins, A. M., Roberton, D. M., Hosking, C. S. & Flannery, G. R. Oral immunization with xenogeneic antibodies stimulates the production of systemic and mucosal anti-idiotypic antibodies. *Immunology* **73**, 388-393 (1991).

79   Clark, J. I. *et al.* Induction of multiple anti-c-erbB-2 specificities accompanies a classical idiotypic cascade following 2B1 bispecific monoclonal antibody treatment. *Cancer immunology, immunotherapy : CII* **44**, 265-272 (1997).

80   Kimball, J. A. *et al.* The OKT3 Antibody Response Study: a multicentre study of human anti-mouse antibody (HAMA) production following OKT3 use in solid organ transplantation. *Transplant immunology* **3**, 212-221 (1995).

81   Schroff, R. W., Foon, K. A., Beatty, S. M., Oldham, R. K. & Morgan, A. C., Jr. Human anti-murine immunoglobulin responses in patients receiving monoclonal antibody therapy. *Cancer research* **45**, 879-885 (1985).

82   Reynolds, J. C. *et al.* Anti-murine antibody response to mouse monoclonal antibodies: clinical findings and implications. *International journal of radiation applications and instrumentation. Part B, Nuclear medicine and biology* **16**, 121-125 (1989).

83   Baudouin, V. *et al.* Anaphylactic shock caused by immunoglobulin E sensitization after retreatment with the chimeric anti-interleukin-2 receptor monoclonal antibody

basiliximab. *Transplantation* **76**, 459-463, doi:10.1097/01.TP.0000073809.65502.8F (2003).

84   Gonzales, N. R. *et al.* Minimizing immunogenicity of the SDR-grafted humanized antibody CC49 by genetic manipulation of the framework residues. *Molecular immunology* **40**, 337-349 (2003).

85   Hosono, M. *et al.* Human/mouse chimeric antibodies show low reactivity with human anti-murine antibodies (HAMA). *British journal of cancer* **65**, 197-200 (1992).

86   Luiten, R. M. *et al.* Chimeric bispecific OC/TR monoclonal antibody mediates lysis of tumor cells expressing the folate-binding protein (MOv18) and displays decreased immunogenicity in patients. *Journal of immunotherapy* **20**, 496-504 (1997).

87   Chan, K. T., Cheng, S. C., Xie, H. & Xie, Y. A humanized monoclonal antibody constructed from intronless expression vectors targets human hepatocellular carcinoma cells. *Biochemical and biophysical research communications* **284**, 157-167, doi:10.1006/bbrc.2001.4837 (2001).

88   Slavin-Chiorini, D. C. *et al.* A CDR-grafted (humanized) domain-deleted antitumor antibody. *Cancer biotherapy & radiopharmaceuticals* **12**, 305-316, doi:10.1089/cbr.1997.12.305 (1997).

89   Bitoh, S., Lang, G. M., Kierek-Jaszczuk, D., Fujimoto, S. & Sehon, A. H. Specific immunosuppression of human anti-murine antibody responses in hu-PBL-SCID mice. *Human antibodies and hybridomas* **4**, 134-143 (1993).

90   Sivolapenko, G. B., Kanariou, M., Edwards, R. J., Epenetos, A. A. & Ritter, M. A. Immunosuppression by immunoglobulin deaggregation is not effective in reducing the anti-xenogeneic immunoglobulin response: experimental and clinical studies. *British journal of cancer* **60**, 511-516 (1989).

91   Simmons, C. P. *et al.* Prophylactic and therapeutic efficacy of human monoclonal antibodies against H5N1 influenza. *PLoS medicine* **4**, e178, doi:10.1371/journal.pmed.0040178 (2007).

92   Traggiai, E. *et al.* Development of a human adaptive immune system in cord blood cell-transplanted mice. *Science* **304**, 104-107, doi:10.1126/science.1093933 (2004).

93   Watanabe, Y. *et al.* The analysis of the functions of human B and T cells in humanized NOD/shi-scid/gammac(null) (NOG) mice (hu-HSC NOG mice). *International immunology* **21**, 843-858, doi:10.1093/intimm/dxp050 (2009).

94   Matsumura, T. *et al.* Functional CD5+ B cells develop predominantly in the spleen of NOD/SCID/gammac(null) (NOG) mice transplanted either with human umbilical cord blood, bone marrow, or mobilized peripheral blood CD34+ cells. *Experimental hematology* **31**, 789-797 (2003).

95   Baenziger, S. *et al.* Disseminated and sustained HIV infection in CD34+ cord blood cell-transplanted Rag2-/-gamma c-/- mice. *Proceedings of the National Academy of Sciences of the United States of America* **103**, 15951-15956, doi:10.1073/pnas.0604493103 (2006).

96   Rajesh, D. *et al.* Th1 and Th17 immunocompetence in humanized NOD/SCID/IL2rgammanull mice. *Human immunology* **71**, 551-559, doi:10.1016/j.humimm.2010.02.019 (2010).

97   Jaiswal, S. *et al.* Dengue virus infection and virus-specific HLA-A2 restricted immune responses in humanized NOD-scid IL2rgammanull mice. *PLoS one* **4**, e7251, doi:10.1371/journal.pone.0007251 (2009).

98   Akkina, R. New generation humanized mice for virus research: comparative aspects and future prospects. *Virology* **435**, 14-28, doi:10.1016/j.virol.2012.10.007 (2013).

99   Soundararajan, V. *et al.* Networks link antigenic and receptor-binding sites of influenza hemagglutinin: mechanistic insight into fitter strain propagation. *Scientific reports* **1**, 200, doi:10.1038/srep00200 (2011).

100   Shen, Y., Maupetit, J., Derreumaux, P. & Tuffery, P. Improved PEP-FOLD Approach for Peptide and Miniprotein Structure Prediction. *Journal of chemical theory and computation* **10**, 4745-4758, doi:10.1021/ct500592m (2014).

101   Thevenet, P. *et al.* PEP-FOLD: an updated de novo structure prediction server for both linear and disulfide bonded cyclic peptides. *Nucleic acids research* **40**, W288-293, doi:10.1093/nar/gks419 (2012).

102   Yang, J. *et al.* The I-TASSER Suite: protein structure and function prediction. *Nature methods* **12**, 7-8, doi:10.1038/nmeth.3213 (2015).

103   Roy, A., Kucukural, A. & Zhang, Y. I-TASSER: a unified platform for automated protein structure and function prediction. *Nature protocols* **5**, 725-738, doi:10.1038/nprot.2010.5 (2010).

104   Zhang, Y. I-TASSER server for protein 3D structure prediction. *BMC bioinformatics* **9**, 40, doi:10.1186/1471-2105-9-40 (2008).

105   Brochet, X., Lefranc, M. P. & Giudicelli, V. IMGT/V-QUEST: the highly customized and integrated system for IG and TR standardized V-J and V-D-J sequence analysis. *Nucleic acids research* **36**, W503-508, doi:10.1093/nar/gkn316 (2008).

106   Ruiz, M. & Lefranc, M. P. IMGT gene identification and Colliers de Perles of human immunoglobulins with known 3D structures. *Immunogenetics* **53**, 857-883, doi:10.1007/s00251-001-0408-6 (2002).

107   Barrios, Y., Jirholt, P. & Ohlin, M. Length of the antibody heavy chain complementarity determining region 3 as a specificity-determining factor. *Journal of molecular recognition : JMR* **17**, 332-338, doi:10.1002/jmr.679 (2004).

108   Barbey-Martin, C. *et al.* An antibody that prevents the hemagglutinin low pH fusogenic transition. *Virology* **294**, 70-74, doi:10.1006/viro.2001.1320 (2002).

109   Daniels, P. S. *et al.* The receptor-binding and membrane-fusion properties of influenza virus variants selected using anti-haemagglutinin monoclonal antibodies. *The EMBO journal* **6**, 1459-1465 (1987).

110   Yu, X. *et al.* Neutralizing antibodies derived from the B cells of 1918 influenza pandemic survivors. *Nature* **455**, 532-536, doi:10.1038/nature07231 (2008).

111   Weitzner, B. D., Kuroda, D., Marze, N., Xu, J. & Gray, J. J. Blind prediction performance of RosettaAntibody 3.0: grafting, relaxation, kinematic loop modeling, and full CDR optimization. *Proteins* **82**, 1611-1623, doi:10.1002/prot.24534 (2014).

112   Laskowski, R. A., Moss, D. S. & Thornton, J. M. Main-chain bond lengths and bond angles in protein structures. *Journal of molecular biology* **231**, 1049-1067, doi:10.1006/jmbi.1993.1351 (1993).

113   Pettersen, E. F. *et al.* UCSF Chimera--a visualization system for exploratory research and analysis. *Journal of computational chemistry* **25**, 1605-1612, doi:10.1002/jcc.20084 (2004).

114   Brumeanu, T. D., Casares, S., Bot, A., Bot, S. & Bona, C. A. Immunogenicity of a contiguous T-B synthetic epitope of the A/PR/8/34 influenza virus. *Journal of virology* **71**, 5473-5480 (1997).

115   Brehm, M. A., Bortell, R., Verma, M., Shultz, L. D. & Greiner, D. L.   285-326 (2015).

116   Shultz, L. D., Ishikawa, F. & Greiner, D. L. Humanized mice in translational biomedical research. *Nature reviews. Immunology* **7**, 118-130, doi:10.1038/nri2017 (2007).

117   Walsh, N. C. *et al.* Humanized Mouse Models of Clinical Disease. *Annu Rev Pathol* **12**, 187-215, doi:10.1146/annurev-pathol-052016-100332 (2017).

118   Lakdawala, S. S. *et al.* Receptor specificity does not affect replication or virulence of the 2009 pandemic H1N1 influenza virus in mice and ferrets. *Virology* **446**, 349-356, doi:10.1016/j.virol.2013.08.011 (2013).

119   Rogers, G. N. & Paulson, J. C. Receptor determinants of human and animal influenza virus isolates: differences in receptor specificity of the H3 hemagglutinin based on species of origin. *Virology* **127**, 361-373 (1983).

120   Rogers, G. N. & D'Souza, B. L. Receptor binding properties of human and animal H1 influenza virus isolates. *Virology* **173**, 317-322 (1989).

121   Matrosovich, M. *et al.* Early alterations of the receptor-binding properties of H1, H2, and H3 avian influenza virus hemagglutinins after their introduction into mammals. *Journal of virology* **74**, 8502-8512 (2000).

122   Connor, R. J., Kawaoka, Y., Webster, R. G. & Paulson, J. C. Receptor specificity in human, avian, and equine H2 and H3 influenza virus isolates. *Virology* **205**, 17-23, doi:10.1006/viro.1994.1615 (1994).

123   Shinya, K. *et al.* Avian flu: influenza virus receptors in the human airway. *Nature* **440**, 435-436, doi:10.1038/440435a (2006).

124   van Riel, D. *et al.* H5N1 Virus Attachment to Lower Respiratory Tract. *Science* **312**, 399, doi:10.1126/science.1125548 (2006).

125   Ibricevic, A. *et al.* Influenza virus receptor specificity and cell tropism in mouse and human airway epithelial cells. *Journal of virology* **80**, 7469-7480, doi:10.1128/JVI.02677-05 (2006).

126   Jayaraman, A. *et al.* Decoding the distribution of glycan receptors for human-adapted influenza A viruses in ferret respiratory tract. *PloS one* **7**, e27517, doi:10.1371/journal.pone.0027517 (2012).

127   Lagasse, E. *et al.* Purified hematopoietic stem cells can differentiate into hepatocytes in vivo. *Nature medicine* **6**, 1229-1234, doi:10.1038/81326 (2000).

128   Orlic, D. *et al.* Bone marrow cells regenerate infarcted myocardium. *Nature* **410**, 701-705, doi:10.1038/35070587 (2001).

129   Okamoto, R. *et al.* Damaged epithelia regenerated by bone marrow-derived cells in the human gastrointestinal tract. *Nature medicine* **8**, 1011-1017, doi:10.1038/nm755 (2002).

130   Shimizu, K. *et al.* Host bone-marrow cells are a source of donor intimal smooth- muscle-like cells in murine aortic transplant arteriopathy. *Nature medicine* **7**, 738-741, doi:10.1038/89121 (2001).

131   Takahashi, T. *et al.* Ischemia- and cytokine-induced mobilization of bone marrow-derived endothelial progenitor cells for neovascularization. *Nature medicine* **5**, 434-438, doi:10.1038/7434 (1999).

132   Lin, F. *et al.* Hematopoietic stem cells contribute to the regeneration of renal tubules after renal ischemia-reperfusion injury in mice. *J Am Soc Nephrol* **14**, 1188-1199 (2003).

133   Uhlen, M. *et al.* Proteomics. Tissue-based map of the human proteome. *Science* **347**, 1260419, doi:10.1126/science.1260419 (2015).

134   *Human Protein Atlas*, <www.proteinatlas.org>

135   Harada, Y., Muramatsu, M., Shibata, T., Honjo, T. & Kuroda, K. Unmutated immunoglobulin M can protect mice from death by influenza virus infection. *The Journal of experimental medicine* **197**, 1779-1785, doi:10.1084/jem.20021457 (2003).

136   Diamond, M. S. *et al.* A critical role for induced IgM in the protection against West Nile virus infection. *The Journal of experimental medicine* **198**, 1853-1862, doi:10.1084/jem.20031223 (2003).

137   Szomolanyi-Tsuda, E. *et al.* Antiviral T-cell-independent type 2 antibody responses induced in vivo in the absence of T and NK cells. *Virology* **280**, 160-168, doi:10.1006/viro.2000.0766 (2001).

138   Doerr, H. W., Gross, G. & Schmitz, H. Neutralizing serum IgM antibodies in infections with Herpes simplex virus hominis. *Med Microbiol Immunol* **162**, 183-192 (1976).

139   Lim, X. F. *et al.* Characterization of an isotype-dependent monoclonal antibody against linear neutralizing epitope effective for prophylaxis of enterovirus 71 infection. *PloS one* **7**, e29751, doi:10.1371/journal.pone.0029751 (2012).

140   Niedrig, M., Kursteiner, O., Herzog, C. & Sonnenberg, K. Evaluation of an indirect immunofluorescence assay for detection of immunoglobulin M (IgM) and IgG antibodies against yellow fever virus. *Clinical and vaccine immunology : CVI* **15**, 177-181, doi:10.1128/CVI.00078-07 (2008).

141   Fehr, T. *et al.* T-cell independent IgM and enduring protective IgG antibodies induced by chimeric measles viruses. *Nature medicine* **4**, 945-948 (1998).

142   Bachmann, M. F., Hengartner, H. & Zinkernagel, R. M. T helper cell-independent neutralizing B cell response against vesicular stomatitis virus: role of antigen patterns in B cell induction? *Eur J Immunol* **25**, 3445-3451, doi:10.1002/eji.1830251236 (1995).

143   Kim JH, R. A., Biber R, Cao W, Chirkova T, Katz J, Sambhara S. Role of human IgM memory B cells in influenza vaccine response (P4401). *J. Immunol.* (2013).

144   Bjornson, A. B. & Michael, J. G. Biological Activities of Rabbit Immunoglobulin M and Immunoglobulin G Antibodies to Pseudomonas aeruginosa. *Infection and immunity* **2**, 453-461 (1970).

145   Parving, H. H., Rossing, N., Nielsen, S. L. & Lassen, N. A. Increased transcapillary escape rate of albumin, IgG, and IgM after plasma volume expansion. *Am J Physiol* **227**, 245-250, doi:10.1152/ajplegacy.1974.227.2.245 (1974).

146   Lu, L., Lamm, M. E., Li, H., Corthesy, B. & Zhang, J. R. The human polymeric immunoglobulin receptor binds to Streptococcus pneumoniae via domains 3 and 4. *The Journal of biological chemistry* **278**, 48178-48187, doi:10.1074/jbc.M306906200 (2003).

147   Brandtzaeg P., J. F.-E., Krajci P., Natvig I. in *Encyclopedia of Immunology* (ed Roitt D.P.) 2152–2158 (Academic Press, London, 1998).

148   Harmon, A. W., Moitra, R., Xu, Z. & Byrnes, A. P. Hexons from adenovirus serotypes 5 and 48 differentially protect adenovirus vectors from neutralization by mouse and human serum. *PloS one* **13**, e0192353, doi:10.1371/journal.pone.0192353 (2018).

149   Shibuya, A. *et al.* Fc alpha/mu receptor mediates endocytosis of IgM-coated microbes. *Nature immunology* **1**, 441-446, doi:10.1038/80886 (2000).

150   Shibuya, A. & Honda, S. Molecular and functional characteristics of the Fcalpha/muR, a novel Fc receptor for IgM and IgA. *Springer Semin Immunopathol* **28**, 377-382, doi:10.1007/s00281-006-0050-3 (2006).

151   Honda, S. *et al.* Enhanced humoral immune responses against T-independent antigens in Fc alpha/muR-deficient mice. *Proceedings of the National Academy of Sciences of the United States of America* **106**, 11230-11235, doi:10.1073/pnas.0809917106 (2009).

152   Murray, C. J. *et al.* Global malaria mortality between 1980 and 2010: a systematic analysis. *Lancet* **379**, 413-431, doi:10.1016/S0140-6736(12)60034-8 (2012).

153   Garamszegi, L. Z. Global distribution of malaria-resistant MHC-HLA alleles: the number and frequencies of alleles and malaria risk. *Malaria journal* **13**, 349, doi:10.1186/1475-2875-13-349 (2014).

154   May, J. *et al.* HLA class II factors associated with Plasmodium falciparum merozoite surface antigen allele families. *The Journal of infectious diseases* **179**, 1042-1045, doi:10.1086/314661 (1999).

155   Osafo-Addo, A. D. *et al.* HLA-DRB1*04 allele is associated with severe malaria in northern Ghana. *The American journal of tropical medicine and hygiene* **78**, 251-255 (2008).

156   Hill, A. V. *et al.* Common west African HLA antigens are associated with protection from severe malaria. *Nature* **352**, 595-600, doi:10.1038/352595a0 (1991).

157   Hill, A. V. The immunogenetics of human infectious diseases. *Annual review of immunology* **16**, 593-617, doi:10.1146/annurev.immunol.16.1.593 (1998).

158   May, J., Lell, B., Luty, A. J., Meyer, C. G. & Kremsner, P. G. HLA-DQB1*0501-restricted Th1 type immune responses to Plasmodium falciparum liver stage antigen 1 protect against malaria anemia and reinfections. *The Journal of infectious diseases* **183**, 168-172, doi:10.1086/317642 (2001).

159   Busson, M. *et al.* HLA-DRB1 and DQB1 allele distribution in the Muong population exposed to malaria in Vietnam. *Tissue antigens* **59**, 470-474 (2002).

160   Wijayalath, W. *et al.* HLA class II (DR0401) molecules induce Foxp3+ regulatory T cell suppression of B cells in Plasmodium yoelii strain 17XNL malaria. *Infection and immunity* **82**, 286-297, doi:10.1128/IAI.00272-13 (2014).

161   Arnold, L. *et al.* Further improvements of the P. falciparum humanized mouse model. *PloS one* **6**, e18045, doi:10.1371/journal.pone.0018045 (2011).

162   Arnold, L. *et al.* Analysis of innate defences against Plasmodium falciparum in immunodeficient mice. *Malaria journal* **9**, 197, doi:10.1186/1475-2875-9-197 (2010).

163   Delovitch, T. L. & Singh, B. The nonobese diabetic mouse as a model of autoimmune diabetes: immune dysregulation gets the NOD. *Immunity* **7**, 727-738 (1997).

164   Anderson, M. S. & Bluestone, J. A. The NOD mouse: a model of immune dysregulation. *Annual review of immunology* **23**, 447-485, doi:10.1146/annurev.immunol.23.021704.115643 (2005).

165   van Belle, T. L., Coppieters, K. T. & von Herrath, M. G. Type 1 diabetes: etiology, immunology, and therapeutic strategies. *Physiological reviews* **91**, 79-118, doi:10.1152/physrev.00003.2010 (2011).

166   Coppieters, K. T., Wiberg, A. & von Herrath, M. G. Viral infections and molecular mimicry in type 1 diabetes. *APMIS : acta pathologica, microbiologica, et immunologica Scandinavica* **120**, 941-949, doi:10.1111/apm.12011 (2012).

167   Pane, J. A. *et al.* Rotavirus acceleration of murine type 1 diabetes is associated with a T helper 1-dependent specific serum antibody response and virus effects in regional lymph nodes. *Diabetologia* **56**, 573-582, doi:10.1007/s00125-012-2798-4 (2013).

168   Pane, J. A. & Coulson, B. S. Lessons from the mouse: potential contribution of bystander lymphocyte activation by viruses to human type 1 diabetes. *Diabetologia* **58**, 1149-1159, doi:10.1007/s00125-015-3562-3 (2015).

169   Knip, M. & Simell, O. Environmental triggers of type 1 diabetes. *Cold Spring Harbor perspectives in medicine* **2**, a007690, doi:10.1101/cshperspect.a007690 (2012).

170   Wen, L. *et al.* Innate immunity and intestinal microbiota in the development of Type 1 diabetes. *Nature* **455**, 1109-1113, doi:10.1038/nature07336 (2008).

171   Valdes, C. *et al.* Is there a link between influenza and type I diabetes? Increased incidence of TID during the pandemic H1N1 influenza of 2009 in Chile. *Pediatric endocrinology reviews : PER* **11**, 161-166 (2013).

172   Drescher, K. M., Kono, K., Bopegamage, S., Carson, S. D. & Tracy, S. Coxsackievirus B3 infection and type 1 diabetes development in NOD mice: insulitis determines susceptibility of pancreatic islets to virus infection. *Virology* **329**, 381-394, doi:10.1016/j.virol.2004.06.049 (2004).

173   Serreze, D. V. *et al.* Diabetes acceleration or prevention by a coxsackievirus B4 infection: critical requirements for both interleukin-4 and gamma interferon. *Journal of virology* **79**, 1045-1052, doi:10.1128/JVI.79.2.1045-1052.2005 (2005).

174   Jaidane, H. & Hober, D. Role of coxsackievirus B4 in the pathogenesis of type 1 diabetes. *Diabetes & metabolism* **34**, 537-548, doi:10.1016/j.diabet.2008.05.008 (2008).

175   Farnsworth, C. W. *et al.* A humoral immune defect distinguishes the response to Staphylococcus aureus infections in mice with obesity and type 2 diabetes from that in mice with type 1 diabetes. *Infection and immunity* **83**, 2264-2274, doi:10.1128/IAI.03074-14 (2015).

176   Petzold, A., Solimena, M. & Knoch, K. P. Mechanisms of Beta Cell Dysfunction Associated With Viral Infection. *Current diabetes reports* **15**, 73, doi:10.1007/s11892-015-0654-x (2015).

177   Jaidane, H. *et al.* Enteroviruses and type 1 diabetes: towards a better understanding of the relationship. *Reviews in medical virology* **20**, 265-280, doi:10.1002/rmv.647 (2010).

178   Hober, D. & Alidjinou, E. K. Enteroviral pathogenesis of type 1 diabetes: queries and answers. *Current opinion in infectious diseases* **26**, 263-269, doi:10.1097/QCO.0b013e3283608300 (2013).

179   Morgan, N. G. & Richardson, S. J. Enteroviruses as causative agents in type 1 diabetes: loose ends or lost cause? *Trends in endocrinology and metabolism: TEM* **25**, 611-619, doi:10.1016/j.tem.2014.08.002 (2014).

180   Tai, N. *et al.* Microbial antigen mimics activate diabetogenic CD8 T cells in NOD mice. *The Journal of experimental medicine* **213**, 2129-2146, doi:10.1084/jem.20160526 (2016).

181   Pow Sang, L., Majji, S., Casares, S. & Brumeanu, T. D. Long-term silencing of autoimmune diabetes and improved life expectancy by a soluble pHLA-DR4 chimera in a newly-humanized NOD/DR4/B7 mouse. *Human vaccines & immunotherapeutics* **10**, 693-699 (2014).

182   Weinbaum, F. I., Evans, C. B. & Tigelaar, R. E. Immunity to Plasmodium Berghei yoelii in mice. I. The course of infection in T cell and B cell deficient mice. *Journal of immunology* **117**, 1999-2005 (1976).

183   Morgado, M. G., Cam, P., Gris-Liebe, C., Cazenave, P. A. & Jouvin-Marche, E. Further evidence that BALB/c and C57BL/6 gamma 2a genes originate from two distinct isotypes. *The EMBO journal* **8**, 3245-3251 (1989).

184   Pow Sang, L., Surls, J., Mendoza, M., Casares, S. & Brumeanu, T. HLA-DR*0401 expression in the NOD mice prevents the development of autoimmune diabetes by multiple alterations in the T-cell compartment. *Cellular immunology* **298**, 54-65, doi:10.1016/j.cellimm.2015.09.003 (2015).

185   Kreuzer, D. *et al.* Reduced interferon-alpha production by dendritic cells in type 1 diabetes does not impair immunity to influenza virus. *Clinical and experimental immunology* **179**, 245-255, doi:10.1111/cei.12462 (2015).

186   Kondrashova, A. *et al.* Influenza A virus antibodies show no association with pancreatic islet autoantibodies in children genetically predisposed to type 1 diabetes. *Diabetologia* **58**, 2592-2595, doi:10.1007/s00125-015-3723-4 (2015).

187   Casares, S. & Richie, T. L. Immune evasion by malaria parasites: a challenge for vaccine development. *Current opinion in immunology* **21**, 321-330, doi:10.1016/j.coi.2009.05.015 (2009).

188   D'Alise, A. M. *et al.* The defect in T-cell regulation in NOD mice is an effect on the T-cell effectors. *Proceedings of the National Academy of Sciences of the United States of America* **105**, 19857-19862, doi:10.1073/pnas.0810713105 (2008).

189   Lee, K. H., Wucherpfennig, K. W. & Wiley, D. C. Structure of a human insulin peptide-HLA-DQ8 complex and susceptibility to type 1 diabetes. *Nature immunology* **2**, 501-507, doi:10.1038/88694 (2001).

Appendix A:
MANUSCRIPT

APPENDIX A: Nonobese Diabetic (NOD) Mice Lack a Protective B-Cell Response against the "Nonlethal" Plasmodium yoelii 17XNL Malaria Protozoan

Published as: **Mirian Mendoza[1],* Luis Pow Sang[1],* [2], Qi Qiu[1], Sofia Casares[1],[3], and Teodor-D. Brumeanu[1]**

1Department of Medicine, Division of Immunology, Uniformed Services University of the Health Sciences, Bethesda, MD 20814, USA

2Benaroya Research Institute at Virginia Mason, 1201 Ninth Avenue, Seattle, WA 98101, USA

3Infectious Diseases Directorate, Division of Malaria, Naval Medical Research Center/Walter Reed Army Institute of Research, Silver Spring, MD 20910, USA

* These authors contributed equally to this work.

APPENDIX OVERVIEW:

In addition to studying the humoral immune system to influenza virus in the humanized mouse model DRAGA, we were also interested in evaluating the humoral immune response to malaria infection in a different mouse model termed Nonobese Diabetic Mice (NOD). At present, there is no correlation between the trends of malaria infection and autoimmune diabetes, since it is unknown whether type 1 diabetes (T1D) could exacerbate malaria infection or, contrarily, benefit the same disease. Therefore, the main question in the present study was whether a predisposing T1D background may interfere with the sensitivity or resistance to malaria infection. NOD mice prone to T1D, and C57/BL/6 mice not prone to T1D were infected with the nonlethal murine strain of P. yoelii 17XNL malaria parasite. We assessed the antibody response between these two mouse strains to malaria infection, and found that NOD mice cannot mount a protective antibody response to P. yoelii 17XNL infection. Previous studies have suggested that parasite-specific Foxp3+ Treg cells suppress B cell function in mice. Our results suggest that an increased pool of Foxp3+ Tregs in P. yoelii 17XNL-infected NOD mice could be responsible for suppression in B cell response to malaria infection.

ABSTRACT:

Plasmodium yoelii 17XNL is a nonlethal malaria strain in mice of different genetic backgrounds including the C57BL/6 mice (I-Ab/I-E^{null}) used in this study as a control strain. We have compared the trends of blood stage infection with the nonlethal murine strain of P. yoelii 17XNL malaria protozoan in immunocompetent Nonobese Diabetic (NOD) mice prone to type 1 diabetes (T1D) and C57BL/6 mice (control mice) that are not prone to T1D and self-cure the P. yoelii 17XNL infection. Prediabetic NOD mice could not mount a protective antibody response to the P. yoelii 17XNL-infected red blood cells (iRBCs), and they all succumbed shortly after infection. Our data suggest that the lack of anti-P. yoelii 17XNL-iRBCs protective antibodies in NOD mice is a result of parasite-induced, Foxp3+ T regulatory (Treg) cells able to suppress the parasite-specific antibody secretion. Conclusions. The NOD mouse model may help in identifying new mechanisms of B-cell evasion by malaria parasites. It may also serve as a more accurate tool for testing antimalaria therapeutics due to the lack of interference with a preexistent self-curing mechanism present in other mouse strains.

INTRODUCTION:

At present, there are no correlates between the trends of malaria infection and autoimmune diabetes, as it is not known whether one disease can worsen the other or, contrarily, may benefit the other disease. Therefore, the main question raised in the present study was whether a predisposing T1D background may interfere with the sensitivity or resistance to malaria infection.

Malaria is an Anopheles mosquito-borne infectious disease caused in humans by five different members of the protozoan genus Plasmodium (i.e., falciparum, vivax, malariae, ovale, and knowlesi). P. falciparum is the most virulent and deadly human malaria parasite that annually infects 1 to 2 billion people[152]. In humans, variations in the non-HLA genetic background as well as in the HLA haplotype observed in different ethnic groups were correlated to the sensitivity versus resistance to malaria infection[153]. Expression of HLA-DRB1∗04 alleles has been linked in particular to severe malaria in Gabon and Northern Ghana[154,155], while the HLA-DRB1∗1302, HLA-DRB1*0101, and HLA-DQB1*0501 suballeles have been associated with resistance to severe malaria in The Gambia, Western Kenya, Gabon, and Vietnam[156-159]. In agreement with human studies, we found that, indeed, humanized HLA-DR4 (DRB1*0401) mouse lacking murine MHC class II molecules (EA0) have impaired production of protective antibodies to nonlethal P. yoelii 17XNL strain of malaria, and they succumbed shortly after infection[160].

Plasmodium yoelii 17XNL is a nonlethal malaria strain in mice of different genetic backgrounds and MHC class II haplotypes including the C57BL/6 mice (I-Ab/I-E^{null}) used in this study as a control group. Mice show parasitemia shortly upon sporozoites challenge; they gradually develop high titers of antibodies to infected red blood cells (iRBCs) and, as a consequence, they are able to self-cure the blood stage infection within 4 to 7 weeks, depending on the sporozoites

load and genetic background[160]. In contrast, the NOD mice were unable to mount an antibody response to iRBCs, and they all succumbed shortly after infection.

Several immunodeficient NOD-based models like the NSG model (NOD/Scid mouse) were shown to sustain the Plasmodium falciparum blood infection upon infusion with human infected RBCs[161,162]. However, these models cannot explore a full malaria cycle *in vivo*, as the liver stage of infection is being bypassed. We have reported that a new humanized HLA-DR4 transgenic NRG mouse was able to sustain a complete vertebrate life cycle of P. falciparum malaria[37].

The NOD wild type mouse is a well-known model for spontaneous autoimmune diabetes (Type 1 Diabetes, T1D) in context of several types of immune dysregulation such as impaired macrophage function, reduced Natural Killer (NK) cells and Natural Killer T (NKT) cells, and reduced Treg function[163,164]. Few weeks after birth, the NOD mice develop prediabetic pancreatic lesions characterized by progressive lymphocyte infiltration of the pancreatic Langerhans (β)-islets. Later on, the NOD mice develop high titers of autoantibodies specific for several self-proteins including Insulin and GAD65 protein[165]. Hyperglycemia onset occurs in 60–90% of female NOD mice sometimes between 4 and 6 months of age when the pancreatic islets are heavily infiltrated with lymphocytes and more than 80% of the insulin-secreting β-cells in the islets are apoptotic. Like in humans, T1D in the NOD mice is an organ-specific autoimmune disease triggered by an unusual high number of self-reactive T cells to the pancreatic antigens that bypass the physiological mechanisms of immune tolerance[164].

The NOD wild type mice have been also used to investigate the role of viral infections and trends of autoimmune diabetes[166]. Reports showed that acceleration of T1D in NOD mice and humans is associated with infections with rotaviruses, influenza type A[161[Lee, 2010 #78,167-171]], and Coxsackie viruses[172-174]. Since T1D not only has a genetic predisposition but is also linked to

environmental factors, a number of reports pointed out to environmental infections with bacteria and enteroviruses[168,175]. While several studies describe the likelihood of EV infections and T1D progression, the results on EVs infection and T1D remain inconclusive and in some instances are even against it[174,176-179]. Recently, the role of gut microbiota in antigen mimicry of the islet-specific glucose 6-phosphatase catalytic subunit-related protein (IGRP)-reactive CD8^{+} cytolytic T cells is believed to play a role in T1D progression in NOD mice[180]. To our knowledge, there are no reports on how a prediabetic or diabetic autoimmune disease can affect the trends of malaria infection in humans or NOD mice.

Herein we investigated the trends of blood stage infection with a "nonlethal" strain of murine malaria (P. yoelii 17XNL) in immunocompetent, genetically nonmanipulated NOD mice. We report for the first time that the previously denominated "nonlethal" murine strain of P. yoelii 17XNL malaria is lethal in NOD mice. Lack of protection and parasite clearance from the blood in the NOD mice was paralleled by the lack of antibody response to P. yoelii 17XNL-iRBCs. Our data suggest that the CD4+Foxp3+ T regulatory cells (Treg) may be responsible for a deficient B-cell antibody production specific for P. yoelii 17XNL-iRBCs in the NOD mice.

MATERIALS AND METHODS:

Mice

Two-month-old, prediabetic NOD female mice that are prone to the development of autoimmune diabetes and control C57BL/6 female mice that do not develop the disease and are known to self-cure the blood stage infection with P. yoelii 17XNL parasite were used in the experiments. Mice were purchased from Jackson Labs and housed in a pathogen-free facility at USUHS. The experimental protocol was approved in compliance with Federal and local regulations by the IACUC committee at USUHS.

Blood Stage Infection with P. yoelii 17XNL Sporozoites

Live sporozoites were obtained from the salivary glands of P. yoelii-infected Anopheles stephensi mosquitoes as we previously described [9]. NOD mice and C57BL/6 mice were challenged retroorbitally with 100 P. yoelii 17XNL live sporozoites per mouse. P. yoelii 17XNL-infected NOD mice and C57BL/6 mice were followed weekly for the trends of blood stage infection based on parasitemia measurements. Parasitemia was monitored 7, 14, 21, 28, and 35 days after challenge by counting 3,000 red blood cells (RBCs) in Giemsa-stained thin blood smears from individual mice and expressed as percentage of infected RBCs (iRBCs), as we previously described [9]. Briefly, Teflon printed slides (12-well; Electron Microscopy Sciences, Hatfield, PA) were coated with iRBCs (104/well) harvested from infected BALB/c, Rag KO mice with parasitemia higher than 30%, and slides were blocked for 30 min at 37°C with phosphate-buffered saline (PBS) containing 1% bovine serum albumin (BSA). Twenty μL of serial dilutions of sera from individual P. yoelii-infected mice in each group were added to the wells. Slide smears from these preparations were incubated for 1 h at 37°C, washed three times

with PBS, and incubated for 30 min at 37°C with fluorescein isothiocyanate- (FITC-) labeled F(ab′)2 goat anti-mouse total IgG, or IgG1, or IgG2b, or IgG2c, or IgG3 (Southern Biotechnologies, Birmingham, AL).

Diabetes Follow-Up

To find whether the P. yoelii 17XNL sporozoites are sequestered in the pancreatic parenchyma or in β-islets of the NOD-infected mice and may thus interfere with the early diabetogenic process in pancreas, 5 μm frozen pancreatic sections was incubated for 2 h at 37°C with 1/10 dilution of pooled sera from self-cured C57BL/6 mice with high titers of anti-iRBCs IgG2c antibodies. Binding of IgG2c Abs to the pancreatic sections was revealed with an F(ab)′2 goat anti-mouse IgG2c-FITC conjugate, and binding of rabbit anti-insulin Ab was revealed by a goat anti-rabbit IgG-Alexa Fluor 594 conjugate (Life Technologies). Slides were then washed and mounted with Vectashield-DAPI (4′,6-diamidino-2-phenylindole) (Vector Laboratories, Burlingame, CA). Slide preparations were analyzed by fluorescence microscopy, as we previously described[181].

The NOD and C57BL/6 mice challenged with P. yoelii 17XNL parasites were monitored weekly for glycemia and development of early pancreatic lesions characteristic of the onset of autoimmune diabetes such as intra- and peri-islet infiltration with lymphocytes. Glycemia was monitored starting 20 days after infection by using an Accu-Check glucose meter and glucose test strips (Roche Co). To identify pancreatic infiltration with lymphocytes and to estimate the amount of intraislet secretion of insulin, 5 μm paraffin-embedded pancreatic sections was doubly stained with hematoxylin-eosin (HE) and with a rabbit anti-insulin Ab revealed by a goat anti-rabbit IgG-HRP (Life Technologies). Some 50 β-islets per group of mice were analyzed by

fluorescence microscopy for preceding diabetic lesions such as lymphocyte infiltration in the pancreatic β-islets.

Analysis of Foxp3+ T Regulatory Cells

Single cell suspensions from the spleen of NOD and C57BL/6 mice that were infected or not with P. yoelii 17XNL parasites were prepared 20 days after infection. Cells were double-stained with anti-mouse Foxp3 Ab-FITC and anti-mouse CD4-PE conjugates (BD PharMingen, San Jose, CA). Some 2×105 cell events were acquired from individual mice in each group and analyzed by a LSR instrument for the frequency of Foxp3+ CD4+ T cells (Tregs).

Biostatistics

Survival rate of NOD mice and C57Bl/6 mice infected with P. yoelii 17XNL parasites was determined by the nonparametric Kaplan-Meier test for which values (log-rank Mantel Cox test) of less than 0.05 were considered significant. Significant differences in antibody titers against Py17XNL-iRBCs between the groups of NOD and C57BL/6 mice were measured by the nonparametric test of Mann–Whitney and data were presented as medians with interquartile ranges.

RESULTS:

The NOD Mice Do Not Survive the Blood Stage Infection with the "Nonlethal" P. yoelii 17XNL Parasite

P. yoelii 17XNL strain of malaria is nonlethal in various mouse strains including the C57BL/6 mouse strain. Mice infected with P. yoelii 17XNL go through a transitory stage of infection, as they totally clear the parasites and self-cure within 4 to 6 weeks, depending the parasite load and genetic background. The NOD wild type mouse is a mouse model for spontaneous autoimmune diabetes (T1D) in which the outcome of infection with the nonlethal P. yoelii 17XNL strain after infection has not been investigated yet. Herein, we tested for the first time whether the NOD mouse self-cures the infection with nonlethal P. yoelii 17XNL malaria parasite. Two large groups of 2-month-old NOD female mice (MHC class II haplotype I-Ag7/I-E^{null}) and C57BL/6 female mice (MHC class II haplotype I-Ab/I-E^{null}) were challenged with 100 infectious P. yoelii 17XNL sporozoites per mouse. Both groups of mice started to show blood stage parasitemia within 14 days after challenge (Figures 1(a) and 1(b)). The reproducibility of results within the same group of mice was statistically significant, and the degree of variability among individual mice within the same group was insignificant according to the nonparametric Kaplan-Meier test.

C57BL/6 mice have been chosen as a control group that self-cure the blood stage infection with nonlethal strain of P. yoelii 17XNL protozoan. The rate of survival in C57BL/6 group was significantly higher than in the NOD group 14 days after challenge (∗p = 0.0002, Figure 1(b)). In contrast to the C57BL/6 mice that self-cured the blood stage infection with P. yoelii 17XNL by day 35 after infection, the NOD mice did not. The NOD-infected mice started to succumb by day 14 after challenge when parasitemia reached 10% to 30% (Figure 1(a)). No NOD-infected mouse survived longer than 21 days after challenge when parasitemia was close to 50%. In contrast, all

C57BL/6 mice with similar levels of parasitemia 21 days after challenge survived, and they were able to completely clear the parasites by day 35 after challenge (Figure 1(b)).

P. yoelii 17XNL-Infected NOD Mice Cannot Mount an Anti-iRBCs Antibody Response

In most mouse strains including the C57BL/6 mice (control mice in these experiments) the specific antibodies are critical for clearing the P. yoelii 17XNL malaria parasites from the blood[160,182]. We previously showed that the process of self-curing the blood stage infection with P. yoelii 17XNL parasite by C57BL/6 mice is strongly dependent on the IgG2c antibody titer to the P. yoelii-iRBCs[160]. In contrast to the C57BL/6 mice, none of the NOD mice was able to mount a specific antibody response against the P. yoelii 17XNL-iRBCs, and they all succumbed to the parasite infection. Thus, 14 days after challenge the titer of antibodies specific for iRBCs was significantly higher in P. yoelii 17XNL-infected C57BL/6 mice than in P. yoelii 17XNL-infected NOD mice according to the Mann–Whitney test ($*p = 0.0001$) (Figure 2(a)). The predominant class of antibodies specific for P. yoelii 17XNL-iRBCs in C57BL/6 mice was IgG2c (Figure 2(b)).

P. yoelii 17XNL-Infected NOD Mice Upregulate the Size of Foxp3+ CD4+ T Regulatory Cell Pool

FACS measurement of Foxp3+ Tregs frequency in the blood of infected NOD mice at day 14 after infection showed a 50% to 65% increase as compared to their own controls prior to infection. Some 20 days after infection the size of Foxp3+ Tregs pool in P. yoelii 17XNL-infected NOD mice was significantly increased by almost 100% ($*p = 0.045$, Figure 3(b)). In agreement with our previous study [9], the P. yoelii 17XNL-infected C57BL/6 mice showed no significant increase in the size of Foxp3+ Tregs pool ($*p = 0.99$) (Figure 3(a)). Accordingly, a

significant increase in the number of Foxp3+ Tregs strongly suggests that these cells may well account for the suppression of antibody response to P. yoelii 17XNL-iRBCs, which in turn explains the lack of protection in NOD mice.

P. yoelii 17XNL Infection Does Not Accelerate the Prediabetogenic Process in the NOD Mice

Infection of NOD mice with P. yoelii 17XNL did not accelerate the T1D development in the prediabetic stage, as the P. yoelii 17XNL infection did not show an earlier onset of pancreatic infiltration with lymphocytes (pancreatic insulitis, Figure 4(a)). With the exception of few P. yoelii 17XNL-infected RBCs (iRBCs) found in the pancreatic vessels, there was no sequestration of iRBCs in the pancreatic parenchyma or β-islets (Figure 4(b)). Pancreatic β-islet infiltration with lymphocytes in humans as well as in NOD mice is an early prediabetic lesion mediated by autoreactive T cells that precedes the onset of hyperglycemia. Also, pancreatic β-islet infiltration with lymphocytes in the NOD mice with high parasitemia (30–50% parasitemia) at day 20 after infection has not been detected (Figure 4(c), left panel). These results indicated that the P. yoelii 17XNL-infected NOD mice did not show an accelerated onset of pancreatic insulitis.

DISCUSSION:

In our knowledge, there are no reports describing the outcomes of malaria infection in mice or in humans predisposed to autoimmune diabetes. Herein, we have investigated prediabetic NOD mice as the most appropriate model for human autoimmune diabetes (type 1 diabetes, T1D)[165]. Our data showed for the first time that NOD mice prone to autoimmune diabetes cannot self-cure the blood stage infection with a "nonlethal" strain of murine malaria (P. yoelii 17XNL), as they cannot mount a protective antibody response to the parasite. The results of this study suggest that several immune evasion mechanisms may operate alone or together in P. yoelii 17XNL-infected NOD mice.

Different murine genetic backgrounds respond to different strains of malaria infection with different antiparasite antibody classes, which depends in part on the degree of T cell involvement. Thus, the IgG1 isotype is sustained by CD4 Th2 cells, while the IgG2a is sustained by CD4 Th1 cells. As we previously reported[160], the C57BL/6 mouse responds to P. yoelii infection with an IgG2a-like isotype (IgG2c)[183]that is a Th1-biased response. Since the NOD mice share much of the C57BL/6 genetic background, they can also secrete an IgG2a-like isotype (IgG2c). The IgG2c antibodies to P. yoelii 17XNL-iRBCs are known to play critical role in clearing the parasite and self-curing the infection by mice with different genetic backgrounds[160]. The inability of NOD mice to surpass the blood stage infection and self-cure the P. yoelii 17XNL infection was strongly associated with the lack of a specific antibody response to the parasite-iRBCs. Lack of a specific antibody response in the NOD mice is not a consequence of deficient B-cell function, since during the diabetes development these mice develop high titers of autoantibodies to a large number of self-antigens including Glutamic Acid Decarboxylase of 65 KDa (GAD65) and Insulin[165]. In addition, we have reported that

immunization of prediabetic NOD mice with a preparation of UV-inactivated influenza virus PR8/A/34 induced a robust titer of neutralizing anti-viral antibodies[184]. Recently, it has been shown that the influenza virus infection does not impair the antiviral immune response in NOD mice[185]. Also, human studies showed no significant difference in the titers of anti-influenza viral antibodies between nonvaccinated, genetically predisposed children to T1D and control children[186]. Our study showed that in the case of P. yoelii 17XNL infection, the NOD mice are unable to mount an anti-parasite antibody response, which infers our previous hypothesis that a major mechanism of immune evasion by malaria parasites relies on suppression of B-cell function throughout induction of parasite-specific Foxp3+ Treg cells[187].

We recently reported that specific B-cell responses to the P. yoelii 17XNL-iRBCs are efficiently suppressed by Foxp3+ Treg cells in a C57BL/6 mouse coexpressing a human MHC class II molecule (HLA-DR∗0401 transgene), but not in C57BL/6 mice coexpressing other HLA transgenes[160]. Obviously, induction of Tregs by the P. yoelii 17XNL parasite is tightly controlled by some MHC class II haplotypes. The inability of NOD mice to develop anti-P. yoelii 17XNL-iRBCs antibodies occurred in the context of a significant increase (almost 100%) in the number of splenic Foxp3+ Treg cells. Quite interestingly, the Treg compartment known to control the T cell homeostasis including the diabetogenic CD4$^+$ T cells, is deficient in the NOD mice[163,188] as compared with mouse strains not prone to autoimmune diabetes. This strongly suggests that the increase size in the pool of Foxp3+ Tregs in P. yoelii 17XNL-infected NOD mice was mainly induced by the parasite. It thus remains to define what parasite antigens at what stage of infection are responsible for upregulation of parasite-specific Foxp3+ Tregs. This is a difficult task to achieve if taking into account the large number of antigens expressed by the parasite during its life cycle. Theoretically, adoptive cell transfer of Tregs from P. yoelii 17XNL-infected NOD

mice to C57BL/6 mice prior to infection with P. yoelii 17XNL is expected to lower the resistance of C57BL/6 mice to the infection, and it would provide direct evidence of Tregs suppression of anti-P. yoelii protective antibodies. However, technically, an adoptive cell transfer is not be feasible due to the development of host versus graft reaction. Using an alternative approach, we showed that depletion of Foxp3+ Treg cells with an anti-CD25 antibody in HLA-DR transgenic C57BL/6 mice (unable to raise IgG2c anti-P. yoelii-iRBCs antibodies and could not self-cure the infection) enables these mice to raise anti-parasite antibodies and to self-cure the blood stage infection[160].

The MHC class II molecules on antigen presenting cells bind peptide antigens and present them to various T cell subsets, a process leading to cell activation and expansion depending on the structure of peptide and MHC class II molecules. The MHC class II haplotype in NOD mice and C57BL/6 control mice used in this study is quite different: I-Ag7/I-E^{null} versus I-Ab/I-E^{null}. Likewise, the MHC class II I-Ag7 molecules in NOD mice and MHC class II HLA-DQ8 molecules in humans have the same single-point mutation at Asparagine 56 in the variable region of I-A β-chain, and both molecules are associated with high predisposition to T1D[189]. The Asp56 amino acid residue has been considered to provide unusual binding and presentation of self-peptides like some pancreatic self-peptides to the CD4 T helper cells, which in turn may trigger expansion of pancreatic self-reactive (diabetogenic) CD4 Th1-cells and ultimately the development of autoimmune diabetes[189]. It remains to further investigate if the unique structure of the I-Ag7 molecules expressed by the NOD mice may present P. yoelii 17XNL-derived peptides able to expand the population of P. yoelii 17XNL-specific Foxp3+ Tregs that can lead to suppression of the antiparasite specific B-cell response. The MHC class II (I-Ag7) haplotype in the NOD mouse is unique, and there is no other mouse MHC class II haplotype that develops

spontaneous diabetes. However, the I-Ag7 haplotype NOD mouse cannot be completely ruled in as the main cause for lack of resistance to P. yoelii infection as long as the gene polymorphism in more than 22 genes associated with diabetes is ruled out.

CONCLUSION:

Prediabetic P. yoelii 17XNL-infected NOD mice were unable to mount an anti-parasite antibody response and could not self-cure the blood stage infection. Accordingly, one may reconsider the terminology of "nonlethal" for the P. yoelii 17XNL strain of murine malaria. Our data suggest that the immune evasion by P. yoelii 17XNL parasite in the NOD mice may well be the parasite-induced Foxp3+ CD4+ Treg cells able to suppress the parasite-specific B-cell responses. On the autoimmune side of this study, the P. yoelii 17XNL infection did not seem to accelerate the early diabetogenic process in pancreas. The NOD mouse model may help in identifying new mechanisms of B-cell evasion by malaria parasites. The NOD mouse may also serve as a more accurate tool for testing antimalaria therapeutics due to the lack of interference with a preexistent self-curing mechanism present in other mouse strains.

FIGURES AND FIGURE LEGENDS:
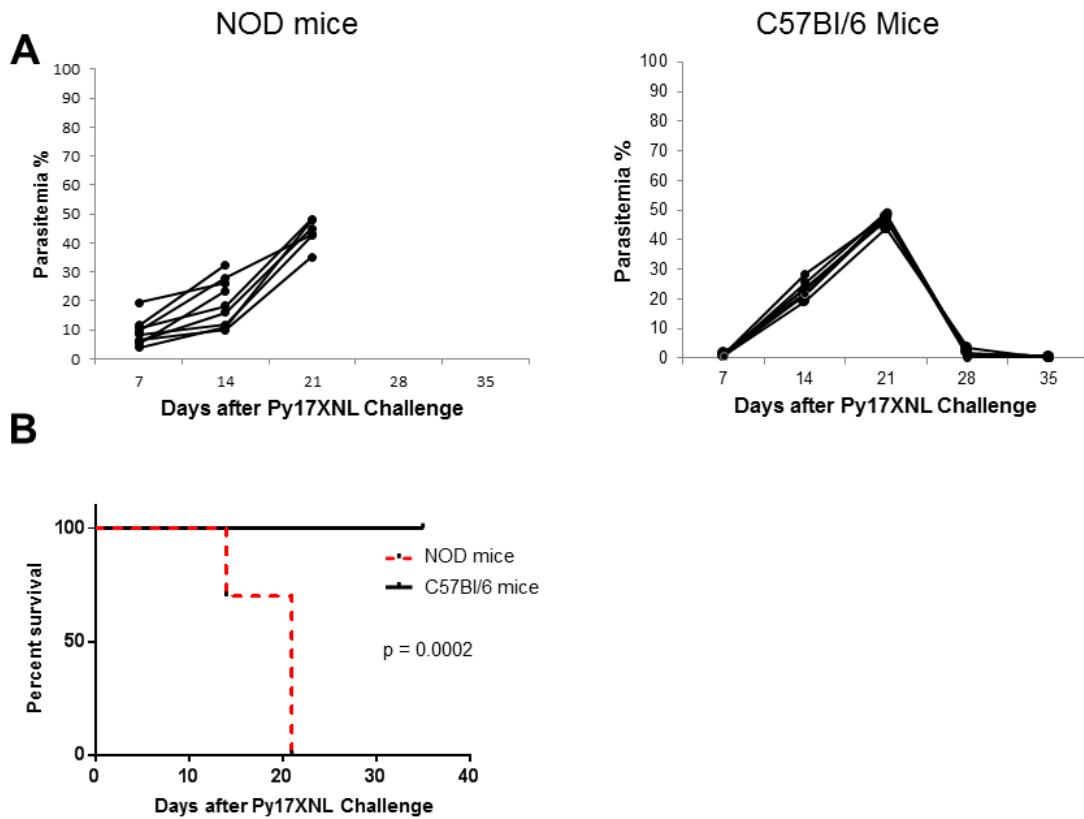
Figure 1

Figure 1: Outcome of P. yoelii 17XNL infection in the NOD and C57BL/6 mice. (a) Parasitemia

values in 10 NOD mice and 10 C57BL/6 mice after P. yoelii infection. The results were collected

from two groups of each strain of mice (n=5 mice/group/strain) and represented together on the

same graph. Of note, the complete clearance of P. yoelii parasites in C57BL/6 mice occurred by

day 35 after infection. The degree of variability between the analyzed groups was null, since all

NOD mice succumbed to the infection and all C57BL/6 mice self-cured the infection regardless

of the time when the experiments were carried out. (b) The percentage of survival in NOD and

C57BL/6 groups challenged with P. yoelii 17XNL sporozoites.
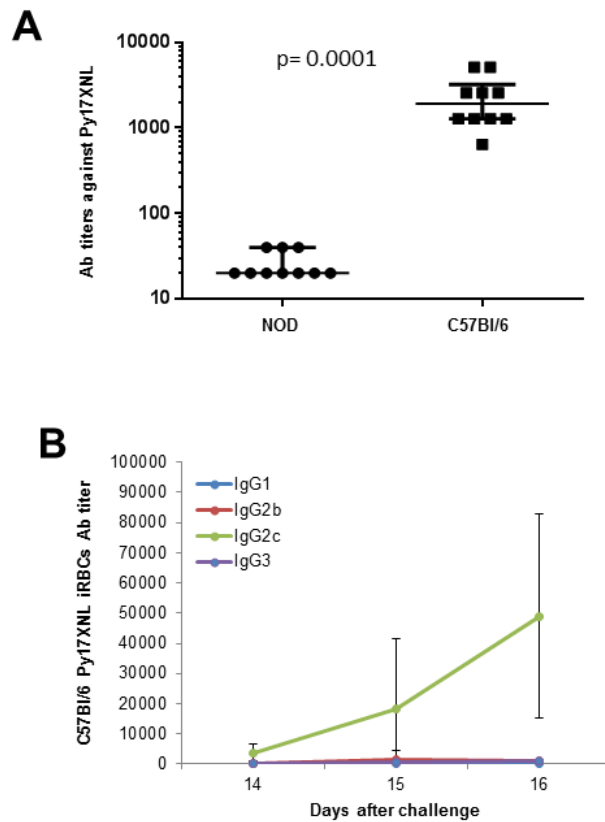
Figure 2: Anti-iRBCs B-cell responses in the P. yoelii 17XNL-infected NOD and C57BL/6 mice. (a) Antibody titers in individual mice from P. yoelii-infected NOD mice and C57BL mice by immunofluorescence (IFA) 14 days after infection; (b) sera from the same individual mice analyzed at the same time points as in (a) for the IgG1, or IgG2b, or IgG2c, or IgG3 titers specific for iRBCs. y-axis shown in both (a) and (b) represents the serum serial dilutions tested in IFA. Of note, only specific IgG2c antibodies were detected in the blood of C57BL/6 mice, but not in NOD-infected mice. The results were collected from each strain of mice (n=5 mice/group/strain).
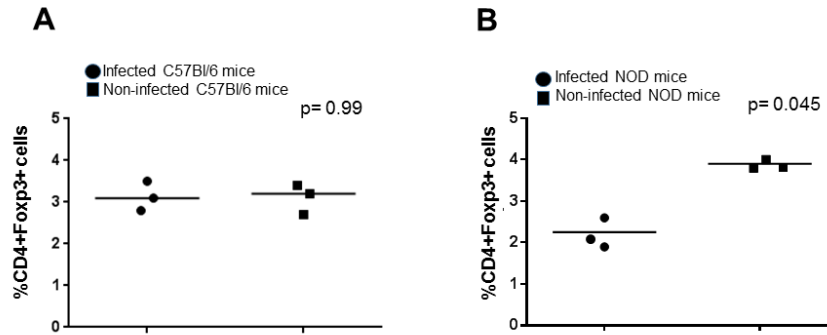
Figure 3

Figure 3: Frequency of Foxp3+ CD4+ T regulatory cells (Tregs) in P. yoelii 17XNL-infected NOD mice. Cytofluorimetric analysis of Tregs was determined by FACS in the spleen cells from individual mice from both groups (n=3 mice/group) that were not infected or infected with P. yoelii 17XNL live sporozoites. FACS measurements were carried out 20 days after infection. (a) Percent of peripheral (splenic) Tregs in 3 individual mice from C57Bl/6 control mice (n=3) before and after each P. yoelii 17XNL challenge; group; (b) percent of peripheral (splenic) Tregs in the spleen of NOD mice (n=3) before and after P. yoelii 17XNL challenge. Shown are the significant *P values between the groups of infected and noninfected mice.
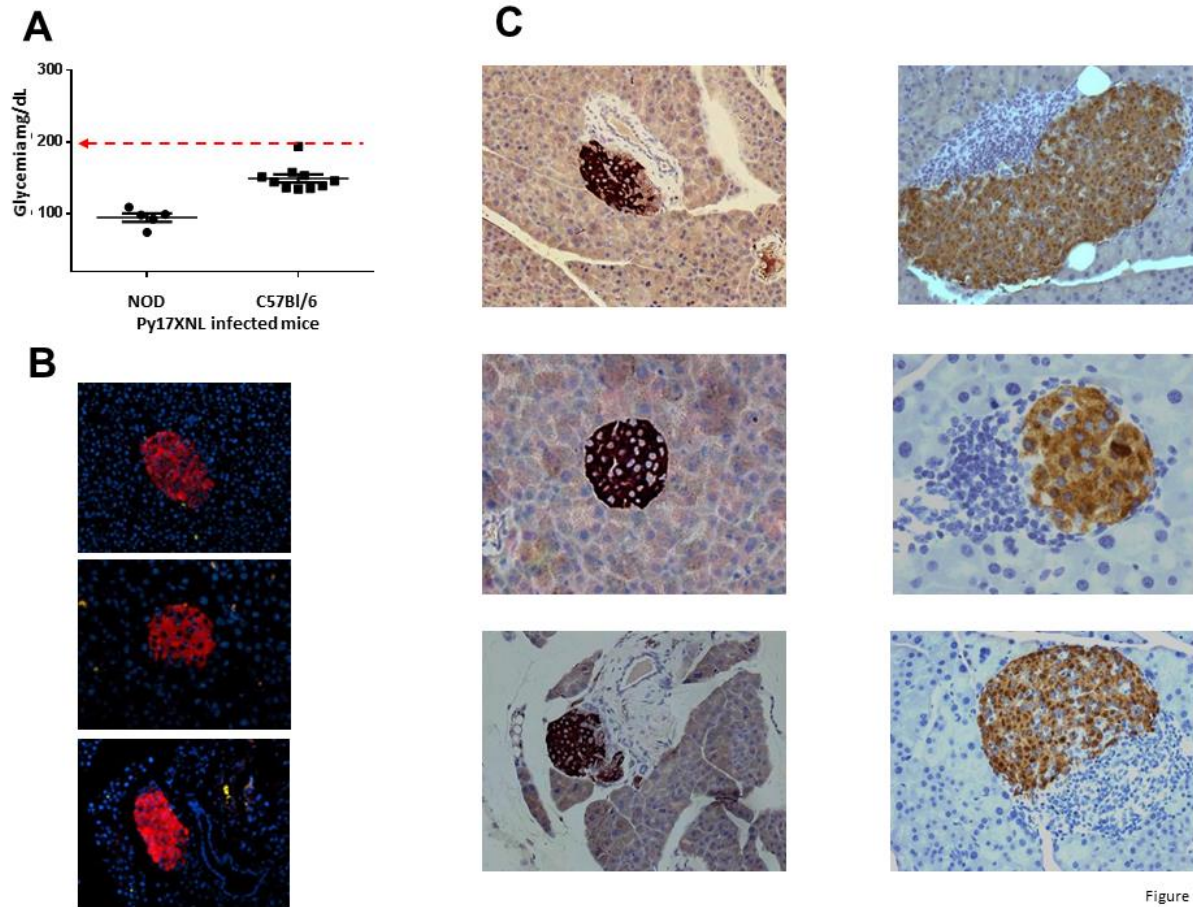
Figure 2

Figure 4: Pancreatic analysis of NOD mice infected with P. yoelii 17XNL sporozoites. (a) Glycemia values in P. yoelii 17XNL-infected mice as monitored 20 days after infection. Dotted line indicates the upper limit of normoglycemia (200 mg/dL) as determined in a cohort of 25 untouched, 2-month-old C57Bl/6 mice and 20 untouched, 2-month-old NOD mice; (b) pancreatic β-islets from P. yoelii-infected NOD mice at day 20 after infection. Shown are scattered P. yoelii 17XNL-iRBCs (green spots) in the pancreatic parenchyma. The β-islets are shown in fluorescent red and cell nuclei in blue. (c) Three representative pancreatic β-islets from a P. yoelii-infected NOD mouse that succumbed 21 days after infection (left panels). Note the lack of lymphocyte infiltration and normal intraislet insulin secretion (dark-brown color) in

contrast to heavy lymphocyte infiltration (dark cyan cells) and reduced intraislet insulin secretion

in a 5-month-old, diabetic NOD control mouse (3 right panels).

Appendix B:
COPYRIGHT CLEARANCE

Copyright clearance of Figure 1:

Copyright clearance of Figure 2.